

Automated Local Fourier Analysis (aLFA) and geometric multigrid for graphene



Dissertation

Bergische Universität Wuppertal
Fakultät für Mathematik und Naturwissenschaften

eingereicht von
Nils Kintscher
zur Erlangung des Grades eines Doktors der Naturwissenschaften

Betreut durch Priv.-Doz. Dr. Karsten Kahl

Wuppertal, 29. Juli 2019

The PhD thesis can be quoted as follows:

urn:nbn:de:hbz:468-20191209-112655-0

[<http://nbn-resolving.de/urn/resolver.pl?urn=urn%3Anbn%3Ade%3Ahbz%3A468-20191209-112655-0>]

DOI: 10.25926/0jm4-6y25

[<https://doi.org/10.25926/0jm4-6y25>]

Acknowledgments

At this point I would like to thank all the people who contributed to the success of this thesis and supported me in some way or another.

First of all, I would like to thank Karsten Kahl for raising my interest in iterative methods and your great commitment in supervising this thesis. It is remarkable that you were always available to discuss and answer my — even if not always meaningful — questions. Without these countless hours of cooperation, your clarity and confidence, this work would be unthinkable.

Furthermore, I wish to thank Andreas Frommer for enabling me to do my doctorate in the working group “Applied Computer Science” at the University of Wuppertal in such a pleasant working environment. Thanks to all former and current colleagues, especially my long-term office mates Marcel and Jan. The cooperation with you, but also the time together at conferences and away from work have always given me a lot of joy and will remain in my special memory.

Finally, I would like to thank my family and friends who accompanied me during the recent years. In particular, I thank my parents for making it possible for me to study mathematics in the first place. Last but not least a special *thank you* to Björn and Michaela for your continuous support. I’m glad I have you.

Contents

1. Introduction	1
2. Normal forms of integer matrices	9
2.1. The Hermite normal form	10
2.2. The Smith normal form	11
3. Crystalline structures	15
3.1. Lattices	15
3.2. Primitive cells	18
3.3. Crystals	20
3.4. Quotient spaces	20
3.5. The dual lattice	25
4. Operators on lattices and crystals	27
4.1. Function spaces	27
4.2. Operators	33
4.3. Automated Local Fourier Analysis (aLFA)	40
5. Linear iterative methods	51
5.1. Convergence theory	53
5.2. Splitting methods	55
5.3. Multigrid methods	63
5.4. Symmetries in colored smoothers	69
5.5. Smoothing analysis	73
6. Graphene	79
6.1. Crystal structure of graphene	79
6.2. Tight-binding Hamiltonian	80
6.3. Components of the geometric multigrid method	83
6.4. Analysis of the coarse grid correction	91

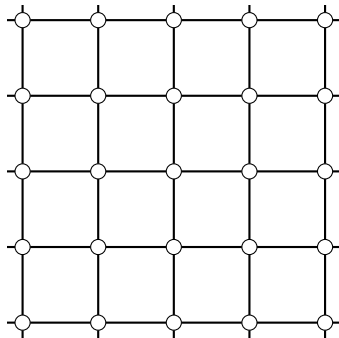
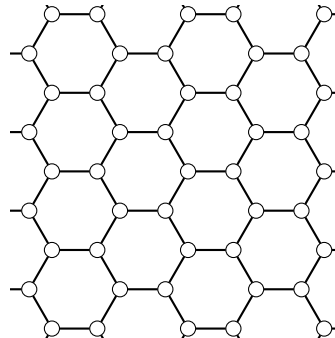
6.5. Convergence rates of the multigrid method	95
6.5.1. Open boundaries	100
7. Conclusion	107
A. Algorithms	109
Nomenclature	113

Introduction

Many physical phenomena, such as fluid dynamics, electrodynamics, heat transfer (and many more) can be modeled by partial differential equations (PDEs). As these equations generally cannot be solved analytically, we rely on numerical simulations. To this end, the problem needs to be discretized which is the process of transferring the continuous problem, the PDE, to a discrete counterpart, i.e., the problem is described only approximately on a discrete set of points in space (and time). This discrete set is often the result of a simple equidistant segmentation of the space of interest as illustrated in Figure 1.1. Often we end up with linear systems of equations where every point only interacts with its nearest neighbors. The solutions of these discrete problems are then approximations to the original continuous problems. In Example 1.1 we demonstrate this construction for the Poisson equation.

In the research of phenomena resulting from atomic-scale properties, scientists do face problems with a predefined underlying structure. For example in solid state physics, the basic research of solid materials, a tight-binding method is used which models the interaction of each atom with its nearest neighbors [2]. In simulations to investigate material properties, linear systems of equations need to be solved which are inherently formulated on the occurring geometric arrangement of its atoms [13, 48]. For example, in Figure 1.2 the atomic structure of graphene is illustrated where every circle represents one carbon atom.

As all these linear systems tend to be very large and sparse, direct methods to solve these problems become prohibitively expensive and unsuitable. With a suitable iterative method, however, such systems can be solved fast and efficiently. Among the most efficient iterative solvers are (geometric) multigrid methods, which make use of the underlying structure in a way that the computational cost grows only linearly with increasing problem size [47]. Due to

**Figure 1.1.:** A rectangular tiling.**Figure 1.2.:** Atomic structure of graphene.

this optimal scaling, multigrid methods can outperform other methods from a certain problem size onwards. Nevertheless, in contrast to many other direct and iterative methods, multigrid methods usually do not work out of the box. Its components need to be constructed with respect to certain parameters of the problem and finely tuned. In order to do so, one requires a deeper understanding of the underlying problem.

Local Fourier analysis (LFA) is a powerful tool used in the construction and analysis of multigrid methods first introduced in [10]. The fundamental idea of LFA is to leverage the connection between position space and frequency space via the Fourier transform. That is, in case the involved operators can be described by stencils in position space, meaning that they are translationally invariant, their Fourier transform yields so-called symbols, which can be handled much more easily. In the context of multigrid methods LFA can be used to obtain precise approximations of the asymptotic convergence rate by assessing the spectral radius of the corresponding error propagation operator [40]. This approximation of the convergence rate is (asymptotically) still valid if the translational invariance is slightly violated, as for example when lexicographic Gauss-Seidel type smoothers are used, or in the case of certain non-periodic boundary conditions [11, 38, 45]. In other cases a similar convergence rate can usually be obtained by additional processing [23, 47]. Due to these facts, LFA is one of the main tools in the quantitative analysis of two- and multigrid methods.

An introduction to LFA including several examples can be found in [47, 51]. Multigrid methods have first been considered for the solution of the linear systems of equations originating from the discretization of (elliptic) PDEs [47]. Due to the fact that the simplest tiling of space is rectangular and discretizations are particularly simple to carry out on such tilings, the usual multigrid components and the LFA have originally been designed and tailored for such discretizations (cf. [47, 51]). Several other geometries, including systems of PDEs, have been considered in the past as well. LFA has been carried out for

operators defined on triangular tilings in [17] and on hexagonal tilings in [53]. Further, it has been applied to edge-based quadrilateral discretizations [7], regular Voronoi meshes associated with acute triangular grids [37], edge-based discretizations on triangular grids [39] and jumping coefficients on rectangular grids [6]. These papers do a complete two-grid analysis, and in some cases even a three-grid analysis, which was first introduced in [50].

While the concept of LFA is well understood, its application quickly becomes complex and involved the more frequencies get intermixed, e.g., by block smoothers, in a three-grid analysis, or in higher dimensional problems ($n > 2$). Thus, there exists software that automates the application of LFA [36, 51]. In contrast to the software described in [51], which basically consists of a collection of templates corresponding to certain smoother and restriction/prolongation strategies for specific problems, the software [36], freely available on GitHub,¹ can be used to analyze arbitrary translationally invariant operators on rectangular grids. This software has for example been used to analyze colored block Jacobi methods in combination with aggressive coarsening applied to PDEs with jumping coefficients in [6, 35]. As the number of frequencies which get intermixed increases with the block-size of the smoother and the growing coarsening rate, a manual analysis of this problem would be laborious.

The bulk of the analysis in the previously mentioned references is mainly carried out in frequency space. LFA with an emphasize on position space is rare in the literature. In [21] a position space oriented LFA is introduced under the name *compact Fourier analysis* where block Toeplitz matrices are used in order to capture the different classes of unknowns.

This thesis consists of two major parts with different objectives. In the first part of this thesis we present an approach to LFA which unifies the position space oriented approaches and allows the treatment of operators on arbitrary repetitive structures. To do so, we introduce a mathematical framework for the analysis of translationally invariant operators which alter value distributions on lattices and crystals [2, 41]. These structures can be based on arbitrary sets of primitive vectors, including non-orthogonal ones, i.e., non-rectangular structures. These crystal structures, which naturally occur in the tight-binding descriptions of solid-state physics [2] or discretizations of systems of PDEs, enable the convenient and concise description of the resulting operators and allow for the automatic generation of their representations when enlarging their translational invariance, e.g., coarsening in the context of multigrid methods. Furthermore, they are very helpful in the representation of overlapping and non-overlapping block smoothers. This framework is developed to such an extent that the only task required of the user is to provide a description of the occurring operators with respect to (potentially non-matching) descriptions of the underlying repetitive structures, i.e., each operator can be supplied in

¹github.com/hrittich/lfa-lab

the simplest or most convenient representation. The remainder of the analysis can then be carried out automatically. In contrast to previously developed LFA, this is achieved by explicitly including a connection of the operator to its underlying structure. On the one hand, this allows us to automate the transformation of operators in position space, e.g., by finding a least common lattice of translational invariance of two operators and to rewrite their representations accordingly. On the other hand, this focus on structure yields a natural representation and discretization of the dual space that enables the automation of the frequency space part of the analysis as well. All these tasks can be carried out using basic principles and normal forms of integer linear algebra [41]. In combination, these developments alleviate the use of LFA by removing any manual calculations. That is, neither a mixing analysis nor transformations of operators to common (and rectangular) translational invariances have to be carried out by hand. While the automated LFA does not necessarily enlarge the set of methods that are analyzable by conventional LFA, it enables the reliable and easy-to-use analysis of complex methods on complicated structures (e.g., overlapping block smoothers and discretizations of systems of PDEs). An open-source Python implementation of the automated LFA framework [24] is freely available on GitLab.²

The automation does have some limitation in terms of the smoothers that can be analyzed. Any sequential, i.e., lexicographic, smoother with overlapping update regions changes values in the overlap multiple times in one application. This cannot be easily translated to the structures introduced in this paper. While such smoothers have been analyzed in frequency space before (cf. [26, 27, 43]), this particular treatment of sequential overlap is momentarily not covered in this framework.

The second part of this thesis contains a derivation of a geometric multigrid method for the tight-binding Hamiltonian of graphene. The obtained method, i.e., the coarse-grid correction in combination with a simple sequential smoother, along with a proof via local Fourier analysis regarding its robustness and efficiency has already been published in [23]. In addition to these results, we present an in-depth analysis of the coarse grid correction as well as alternative smoothers which show better performance and can be parallelized. The special characteristic of the tight-binding Hamiltonian of graphene is two-fold. Besides the already mentioned unusual geometric structure, the resulting linear system of equations is maximally *indefinite*, i.e., it has an equal number of positive and negative eigenvalues. Multigrid methods for *indefinite* problems have been considered mainly in the context of the indefinite Helmholtz equation or other second order elliptic boundary value problems. Typically, convergence of a multigrid method for these problems can only be guaranteed if particular conditions are fulfilled; cf. [4, 5, 8, 9, 42, 52]. The most prominent

²gitlab.com/NilsKintscher/alfa

restriction oftentimes requires that the coarsest grid needs to be sufficiently fine/large. This means that there is no such method with the typical multigrid advantage—an asymptotic convergence rate independent of the grid size. Recently, in the context of Lattice Gauge Theory algebraic multigrid methods have experimentally been shown to be efficient for indefinite spin systems in [3, 15, 25, 31]. However, no theoretical proof of convergence is available for these methods.

In addition to these two major topics, we present a general symmetry analysis of block smoothers, i.e., domain decomposition methods. Due to increasingly parallel computing environments such smoothers have become more and more important to achieve high efficiency in multigrid solvers as they can be easily parallelized and possess nice data locality. In order to realize the full potential of these block smoothers one has to color the blocks such that any two blocks of the same color decouple and thus can be processed in parallel. We show that the ordering in which the colors are processed can have a large influence on the convergence rate of the resulting two- and multigrid method. As the number of different orderings to be considered grows factorial with the number of colors, we demonstrate how to determine orderings which yield the same convergence rate due to algebraic and geometric symmetries of the underlying crystal structure.

The thesis is organized as follows. We first introduce normal forms for integer matrices in Chapter 2 which play an important role in Chapter 3, where we present basic notation to describe the underlying structures of the operators we want to analyze: lattices and crystals. In the context of LFA we are interested in translationally invariant operators which alter value distributions on crystals. These kinds of operators and their properties are specified in Chapter 4. In particular, we present similarity transformations of these operators referring to the non-unique representation of the underlying crystal structure which make an automated analysis of compositions of operators possible. The similarity transformations make up a large part of the algorithms listed in Appendix A used in the automated local Fourier analysis (aLFA). In Chapter 5, we introduce some main principles of iterative methods. *Splitting methods*, which are a sub-class of iterative methods, are then brought into the context of Chapter 4 in Section 5.2. Afterwards, we study (*geometric multigrid methods*) in Section 5.3. Throughout Chapter 5 we show several examples, including multicolored block smoother, applied to the (discretized) Laplacian to illustrate the application of the algorithms of aLFA and also validate the developed theory. Based on the determined convergence rates of a multicolored block smoother, we then use this example to study how equivalent orderings can be determined using underlying algebraic and geometric symmetries. Furthermore, we show a general approach to *smoothing analysis* within the aLFA framework in Section 5.5. Finally, Chapter 6 deals with the tight-binding Hamiltonian of graphene and the developed multigrid method.

Several of the presented results are obtained using the previously developed automated local Fourier analysis. Note that a list of frequently used symbols can be found at the end this thesis.

Due to the importance for the first few chapters of this thesis we introduce the following model problem.

Example 1.1. *The Laplacian Δ is an operator used to model several physical phenomena. For example, it describes the heat flow in solid materials as a result of temperature differences. We consider this operator*

$$\Delta : \mathcal{L}(\Omega, \mathbb{C}) := \{f : \Omega \rightarrow \mathbb{C}\} \rightarrow \mathcal{L}(\Omega, \mathbb{C}), \quad u \mapsto \frac{\partial^2 u}{\partial x_1^2} + \frac{\partial^2 u}{\partial x_2^2}$$

on the unit square $[0, 1]^2$ with periodic boundaries, i.e., the domain of interest resembles the surface of a torus. We can define this domain as

$$\Omega := \{[x] : x \in \mathbb{R}^2\},$$

where its elements $[x], [y] \in \Omega$ are defined by

$$[x] = [\tilde{x}] \Leftrightarrow \text{there exist } i, j \in \mathbb{Z} \text{ such that } x = \tilde{x} + ia_1 + ja_2,$$

where $a_1 := (1, 0)$ and $a_2 := (0, 1)$. A function $f \in \mathcal{L}(\Omega, \mathbb{C})$ may describe the heat-flux density applied to the torus. Then, the solution u of the Poisson equation

$$-\Delta u = f \text{ in } \Omega,$$

corresponds to the equilibrium the system will eventually end up in.

In order to calculate u numerically, we consider a simple tiling of the space of interest:

$$\Omega_{1/N} = \{[x] : x = \frac{i}{N} \cdot a_1 + \frac{j}{N} \cdot a_2, \ i, j \in \mathbb{Z}\} \subset \Omega.$$

The definition of the elements carries over as

$$[x] = [y] \in \Omega_{1/N} \text{ if } [x] = [y] \in \Omega.$$

Using the finite central differences scheme on $\Omega_{1/N}$ we get a second order approximation

$$\Delta_h : \mathcal{L}(\Omega_{1/N}, \mathbb{C}) \rightarrow \mathcal{L}(\Omega_{1/N}, \mathbb{C})$$

of the Laplacian Δ with

$$-\Delta_h u_{i,j} := \frac{1}{h^2} (4u_{i,j} - u_{i+1,j} - u_{i-1,j} - u_{i,j+1} - u_{i,j-1}) \stackrel{!}{=} f_{i,j}$$

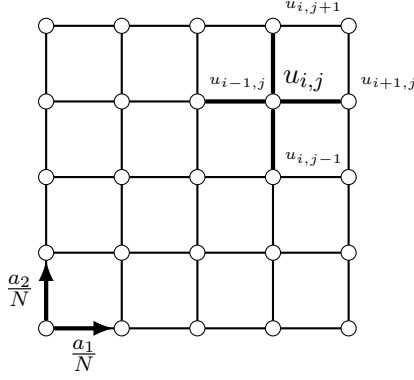


Figure 1.3.: Section of the discretized unit cell Ω_h as well as the connections of one unknown with its neighbors corresponding to the discretized Laplacian.

where $u_{i,j}$ and $f_{i,j}$ correspond to the value of u and f at $[x] = [i\frac{1}{N}a_1 + j\frac{1}{N}a_2]$ respectively. Due to the periodicity we restrict ourselves to $i, j \in \{0, 1, \dots, N-1\}$. Introducing the notation

$$u_i = (u_{i,0}, \dots, u_{i,N-1})^T \text{ and } f_i = (f_{i,0}, \dots, f_{i,N-1})^T,$$

these equations can be written in matrix notation by

$$\frac{1}{h^2} \begin{bmatrix} B & -I & & -I \\ -I & B & \ddots & \\ & \ddots & \ddots & -I \\ -I & & -I & B \end{bmatrix} \begin{bmatrix} u_0 \\ \vdots \\ u_{N-1} \end{bmatrix} = \begin{bmatrix} f_0 \\ \vdots \\ f_{N-1} \end{bmatrix}, \quad B = \begin{bmatrix} 4 & -1 & & \\ -1 & 4 & \ddots & \\ & \ddots & \ddots & -1 \\ & & -1 & 4 \end{bmatrix}.$$

The underlying structure of this problem is illustrated in Figure 1.3.

Normal forms of integer matrices

In this chapter we briefly review two normal forms of integer matrices which play an important role in Chapter 3 in the classification of lattices. We introduce them beforehand separated from this context. The presented results can for example be found in more detail in [30, 41].

Definition 2.1. A matrix $U \in \mathbb{Z}^{n \times n}$ is called unimodular if $\det(U) \in \{\pm 1\}$.

Lemma 2.2. The following elementary (column) operations are unimodular:

- (i) exchanging two columns,
- (ii) multiplying a column with -1 and
- (iii) adding an integral multiple of one column to another.

Proof. Let us denote these column manipulations by $A \mapsto AU$. Then the matrix $U \in \mathbb{Z}^{n \times n}$ fulfilling the mentioned operations has to be the identity matrix with the following modifications respectively:

- (i) two columns of U are exchanged,
- (ii) one diagonal entry is -1 instead of 1 and
- (iii) one off-diagonal entry is changed to some $\alpha \in \mathbb{Z}$ from 0 .

These matrices are obviously unimodular. □

Lemma 2.3. If $U \in \mathbb{Z}^{n \times n}$ is unimodular, then U^{-1} is unimodular. Thus, $U : \mathbb{Z}^n \rightarrow \mathbb{Z}^n$ is a bijection.

Proof. Due to Cramer's rule we have the equality

$$U^{-1} = \text{cof}(U)^T \cdot \frac{1}{\det(U)} = \text{cof}(U)^T,$$

where $\text{cof}(U)$ denotes the cofactor matrix of U , which is integral. □

2.1. The Hermite normal form

Unimodular matrices define an equivalence relation on the set of matrices via

$$A \sim B \iff \text{there exists an unimodular } U, \text{ such that } AU = B.$$

The first normal form we present is the *Hermite normal form*, a unique triangular representation of integral matrices in the equivalence class induced by \sim . The *Hermite normal form* answers for example whether two lattices are equivalent.

Definition 2.4. We say $H = (h_{i,j})_{i,j} \in \mathbb{R}^{n \times n}$ is in Hermite normal form (HNF) if

- H is upper triangular, i.e., $h_{i,j} = 0$, $i > j$.
- non-negative, i.e., $h_{i,j} \geq 0$, and
- its unique row-wise maximum is located on the diagonal, i.e., $h_{i,i} > h_{i,j}$, $j > i$.

Theorem 2.5. Every nonsingular matrix $A \in \mathbb{Q}^{n \times n}$ can be brought into Hermite normal form by an unimodular transformation, i.e., there is an unimodular matrix $U \in \mathbb{Z}^{n \times n}$, such that $H = AU$ is in Hermite normal form.

Proof. The following constructive proof is split into two steps and uses elementary column operations only. We assume without loss of generality that $A = (a_{ij})_{ij}$ is integral. First, we show that A can be brought into upper triangular form by eliminating nonzero entries below the diagonal row-wise. We start with the last row $\left[a_{n,1} \mid a_{n,2} \mid \dots \mid a_{n,n} \right]$ and perform the following steps.

1. For each negative row-entry below the diagonal $a_{n,j}$, we multiply column a_j by -1 , such that $a_{n,j} \geq 0$ for all $j \leq n$.
2. Due to A being nonsingular, there is at least one nonzero entry $a_{n,j}$, $j \leq n$. If the diagonal element is zero, we exchange columns a_j and a_n such that $a_{n,n}$ is now nonzero.
3. Finally, we eliminate the nonzero entries of row n below the diagonal elementwise. Let $a_{n,j}$, $j < n$, be a nonzero element. The Euclidean algorithm applied to $a_{n,j}$ and $a_{n,n}$ generates a sequence $(q_k)_k$ of quotients and a sequence $(r_k)_k$ of remainders with $r_0 = a_{n,n}$, $r_1 = a_{n,j}$ and

$$r_{k-2} = q_{k-1}r_{k-1} + r_k \iff r_k = r_{k-2} - q_{k-1}r_{k-1}, \quad (2.1)$$

with $|r_{k+1}| < |r_k|$, $r_{\hat{k}} = 0$ and $r_{\hat{k}-1} = \gcd(a_{n,j}, a_{n,n})$. We apply these steps of the Euclidean algorithm to column j for each $k = 2, \dots, \hat{k}$ as follows:

- a) Exchange columns a_j and a_n , such that $a_{n,j} = r_{k-2}$ and $a_{n,n} = r_{k-1}$.
- b) Add an integral multiple of column a_n to a_j , i.e., $a_j \leftarrow a_j - q_{k-1}a_n$, such that $a_{n,j} = r_{k-2} - q_{k-1}r_{k-1} = r_k$, cf. equation (2.1).

After this procedure the diagonal element $a_{n,n}$ is equal to the greatest common divisor of all original row entries $a_{n,1}, a_{n,2}, \dots, a_{n,n}$.

It follows by induction, that these steps can be applied row-wise from bottom to top to obtain an upper triangular matrix as these operations only change entries in the the upper left matrix block of size $i \times i$.

The second step brings the upper triangular matrix into the desired shape, that is, we reduce or increase the off-diagonal entries such that the maximum is then located on the diagonal and all entries are non-negative. We again work row-wise from bottom to top. Let $a_{i,j}$, $j > i$, be an element with $a_{i,j} < 0$ or $a_{i,j} \geq a_{i,i}$. We apply division by the diagonal entry with remainder, i.e., $a_{i,j} = qa_{i,i} + r$, to column a_j . That is, $a_j \leftarrow a_j - qa_i$, such that $a_{i,j} = a_{i,j} - qa_{i,i} = r$ with $0 \leq r < a_{i,i}$. As this operation does not alter the entries below row i , we can hereby bring all the off diagonal entries into the desired form when successively working from bottom to top to obtain the HNF H . \square

Theorem 2.6. *The Hermite normal form H of a matrix $A \in \mathbb{Q}^{n \times n}$ is unique.*

Proof. Without loss of generality we can restrict ourselves to integral matrices. Let us assume that $H = AU, H' = AU' \in \mathbb{Z}^{n \times n}$ are two Hermite normal forms of A with $H \neq H'$. The matrices differ in at least one column j , i.e., $H_j \neq H'_j$. Let us denote the difference by $d := H_j - H'_j$. Due to the fact that any column H'_k of H' can be expressed as an integral linear combination of the columns of H , the same is true for d . Let i be the largest index of a nonzero entry in d , i.e., $d_i \neq 0$ and $d_j = 0$ for $j = i + 1, \dots, n$. As H is upper triangular, we can rewrite d as an integral linear combination of the columns H_k , $k \leq i$. In particular, d_i has to be an integral multiple of h_{ii} . Thus, we have $0 \neq |h_{ij} - h'_{ij}| = |d_i| \geq h_{ii}$. On the other hand, as $0 \leq h_{ij} < h_{ii}$ as well as $0 \leq h'_{ij} < h_{ii}$, we have $|h_{ij} - h'_{ij}| = |d_i| < h_{ii}$. Thus our assumption is incorrect, and the matrices H and H' are equal. \square

Remark 2.7. *In consequence of Theorems 2.5 and 2.6, every unimodular matrix U can be split into a sequence of the elementary operations introduced in Lemma 2.2.*

2.2. The Smith normal form

In case we additionally allow also elementary row operations, we can bring each integral matrix into *Smith normal form*, a unique diagonal matrix representation.

Definition 2.8. We say $S \in \mathbb{R}^{n \times n}$ is in Smith normal form (SNF) if

- S is diagonal, i.e., $S = \text{diag}(\sigma_1, \dots, \sigma_n)$, and
- the diagonal entries satisfy $\sigma_i \mid \sigma_{i+1}$ for all $i = 1, \dots, n - 1$. These entries are called the elementary divisors.

Theorem 2.9. Every nonsingular matrix $A \in \mathbb{Q}^{n \times n}$ can be brought into Smith normal form by unimodular row- and column-transformations, i.e., there exist unimodular matrices $U, V \in \mathbb{Z}^{n \times n}$, such that $S = VAU$ is in Smith normal form.

Proof. Without loss of generality we can again restrict ourselves to integral matrices. We can bring A into the form

$$V_1 A U_1 = \tilde{A} = \begin{bmatrix} \sigma_1 & 0 \\ 0 & \tilde{A}_{2:n,2:n} \end{bmatrix},$$

by repeatedly applying the following operations:

1. Using elementary column operations, we can eliminate all nonzero entries above the diagonal in the first column $\left[a_{1,2} \mid a_{1,3} \mid \dots \mid a_{1,n} \right]$ in a similar way as we did in step 3 in the proof of Theorem 2.5 using the Euclidean algorithm.
2. Analogously, using elementary row operations, we can eliminate all nonzero entries below the diagonal in the first row $\left[a_{2,1} \mid a_{3,1} \mid \dots \mid a_{n,1} \right]^T$.

This needs to be done repeatedly as column operations may introduce nonzero entries in the first row whereas row operations introduce nonzero entries in the first column. Nevertheless, after each step, the diagonal entry is equal to the greatest common divisor of the first row or column, respectively. Thus, it gets smaller in every single step until it is equal to the greatest common divisor $\sigma_1 = \text{gcd}(A)$ of all matrix entries $a_{i,j}$, $i, j = 1, \dots, n$.

Note, that $\text{gcd}(A)$ is a divisor of $\text{gcd}(\tilde{A}_{2:n,2:n})$ due to

$$\mathbb{Z}^{n \times n} \ni V_1 \frac{A}{\text{gcd}(A)} U_1 = \frac{\tilde{A}}{\text{gcd}(A)}.$$

This procedure can repeatedly be applied to the remaining blocks $\tilde{A}_{i:n,i:n}$, $i = 2, \dots, n$, until we obtain a diagonal matrix which is in SNF. \square

Remark 2.10. The Smith normal form S of a matrix A is again unique as the product $\sigma_1 \cdots \sigma_i$ is equal to the gcd of all $i \times i$ minors of A for all i [41, p. 50].

Remark 2.11. *The given constructive proofs to compute the Hermite and Smith normal form are impractical for large matrices for stability and complexity reasons. An overview of various algorithms for the calculation of these normal forms can be found in [18]. Implementations for the computation of these normalforms are for example part of the PARI software package [32].*

Crystalline structures

In this chapter we introduce some of the basic principles of lattices and crystals. Most of the basic results presented in this section can be found in [19, 41]. An (ideal) crystal is an infinite repetition of some structure element. The structure element can for example be a single atom or some arbitrary complex molecule consisting of very many atoms. For our purposes it is simply a subset of points which are defined later on. At first, we analyze its infinite repetition which is specified by the Bravais lattice defined below. We especially study these basic structures with respect to their non-uniqueness. These results are eventually used in the automation process of the LFA.

3.1. Lattices

Definition 3.1. *Let $a_1, a_2, \dots, a_n \in \mathbb{R}^n$ be linearly independent vectors. An n -dimensional (Bravais) lattice \mathbb{L} is the set of points*

$$\mathbb{L} = \left\{ x = \sum_{\ell=1}^n \alpha_\ell a_\ell \in \mathbb{R}^n : \alpha_1, \alpha_2, \dots, \alpha_n \in \mathbb{Z} \right\}.$$

The vectors a_1, a_2, \dots, a_n are known as the primitive vectors of \mathbb{L} . Using matrix notation, i.e., $\mathcal{A} := \begin{bmatrix} a_1 & a_2 & \cdots & a_n \end{bmatrix}$, we can abbreviate the notation

$$\mathbb{L}(\mathcal{A}) := \mathcal{A}\mathbb{Z}^n = \mathbb{L}$$

and call \mathcal{A} the lattice basis.

Remark 3.2. *One easily sees that $(\mathbb{L}, +)$ forms a group, i.e., $0 \in \mathbb{L}$ and for $x, y \in \mathbb{L}$ we have $x + y \in \mathbb{L}$ as well as $-x \in \mathbb{L}$.*

An example of a 2-dimensional Bravais lattice is given in Figure 3.1. As it can be seen, the set of primitive vectors spanning a lattice is not unique. In fact, for any n -dimensional lattice \mathbb{L} , $n > 1$, there are infinitely many different sets of primitive vectors.

Lemma 3.3. *Let $\mathbb{L}(\mathcal{A})$ and $\mathbb{L}(\mathcal{C})$ be two Bravais lattices. We have $\mathbb{L}(\mathcal{A}) \supset \mathbb{L}(\mathcal{C})$ if and only if $M := \mathcal{A}^{-1}\mathcal{C} \in \mathbb{Z}^{n \times n}$. We call $\mathbb{L}(\mathcal{C})$ a sublattice of $\mathbb{L}(\mathcal{A})$.*

Proof. First, let $\mathbb{L}(\mathcal{A}) \supset \mathbb{L}(\mathcal{C})$. For every unit vector e_j there exist $m_j \in \mathbb{Z}^n$, such that

$$\mathcal{C}e_j = \mathcal{A}m_j \iff \mathcal{A}^{-1}\mathcal{C}e_j = m_j.$$

Hence $M = \left[m_1 \mid m_2 \mid \dots \mid m_n \right] = \mathcal{A}^{-1}\mathcal{C} \in \mathbb{Z}^{n \times n}$.

On the other hand, let $M = \mathcal{A}^{-1}\mathcal{C} \in \mathbb{Z}^{n \times n}$ and $x \in \mathbb{L}(\mathcal{C})$, i.e., there exists $y \in \mathbb{Z}^n$ such that $x = \mathcal{C}y$. We then have $\mathcal{A}(\mathcal{A}^{-1}\mathcal{C}y) = x \in \mathbb{L}(\mathcal{A})$ due to $\mathcal{A}^{-1}\mathcal{C}y \in \mathbb{Z}^n$ and thus, $\mathbb{L}(\mathcal{A}) \supset \mathbb{L}(\mathcal{C})$. \square

Theorem 3.4. *Let $\mathbb{L}(\mathcal{A})$ and $\mathbb{L}(\mathcal{C})$ be two lattices. We have the following equivalence.*

- (i) $\mathbb{L}(\mathcal{A}) = \mathbb{L}(\mathcal{C})$.
- (ii) $\mathcal{A}^{-1}\mathcal{C} \in \mathbb{Z}^{n \times n}$ and $\mathcal{C}^{-1}\mathcal{A} \in \mathbb{Z}^{n \times n}$.
- (iii) There exists a unimodular matrix U , such that $\mathcal{C} = \mathcal{A}U$.
- (iv) \mathcal{A} and \mathcal{C} have the same Hermite normal form.

Proof. The equivalences (i) \Leftrightarrow (ii) and (iii) \Leftrightarrow (iv) are given by Lemma 3.3 and Theorem 2.5, respectively. The statement (iii) \Rightarrow (ii) is clear due to Lemma 2.3, i.e., $U = \mathcal{A}^{-1}\mathcal{C} \in \mathbb{Z}^{n \times n}$ and $U^{-1} = \mathcal{C}^{-1}\mathcal{A} \in \mathbb{Z}^{n \times n}$.

Regarding the statement (ii) \Rightarrow (iii) we make the observation $\det(\mathcal{A}^{-1}\mathcal{C}) = \frac{\det(\mathcal{C})}{\det(\mathcal{A})} \in \mathbb{Z}$ and its inverse $\det(\mathcal{C}^{-1}\mathcal{A}) = \frac{\det(\mathcal{A})}{\det(\mathcal{C})} \in \mathbb{Z}$. Thus, both determinants must simultaneously be +1 or -1 and hence $\mathcal{C} = \mathcal{A}U$ with $U := \mathcal{A}^{-1}\mathcal{C}$ unimodular. \square

Remark 3.5. *Theorem 3.4 especially states that $\mathbb{L}(U) = \mathbb{Z}^n$ for every unimodular matrix $U \in \mathbb{Z}^{n \times n}$.*

The following theorem plays a key-role in the automation process of the local Fourier analysis as we eventually want to find a matching description of the underlying structure of two operators and rewrite their representation accordingly.

Theorem 3.6. *Let $\mathbb{L}(\mathcal{A})$ and $\mathbb{L}(\mathcal{B})$ be two n -dimensional lattices. If there is an integer r , such that*

$$M = r\mathcal{A}^{-1}\mathcal{B} \in \mathbb{Z}^{n \times n}, \quad (3.1)$$

then there is a lattice $\mathbb{L}(\mathcal{C})$ with $\mathbb{L}(\mathcal{C}) \subset \mathbb{L}(\mathcal{A})$ and $\mathbb{L}(\mathcal{C}) \subset \mathbb{L}(\mathcal{B})$ with $|\det(\mathcal{C})|$ as small as possible. A lattice basis of $\mathbb{L}(\mathcal{C})$ is then given by

$$\mathcal{C} = \mathcal{B}T^{-1}N_{\mathcal{B}},$$

where $N_{\mathcal{B}}$ is a diagonal matrix with

$$N_{\mathcal{B}} := \text{diag} \left(\frac{r}{\gcd(r, \sigma_1)}, \dots, \frac{r}{\gcd(r, \sigma_n)} \right)$$

and $S = V^{-1}MT^{-1} = \text{diag}(\sigma_1, \dots, \sigma_n)$ is the Smith normal form of M . We call $\mathbb{L}(\mathcal{C})$ the least common multiple of $\mathbb{L}(\mathcal{A})$ and $\mathbb{L}(\mathcal{B})$ and write

$$\mathbb{L}(\mathcal{C}) = \text{lcm}(\mathbb{L}(\mathcal{A}), \mathbb{L}(\mathcal{B})).$$

Remark 3.7. *An integer r such that equation (3.1) holds can always be found if \mathcal{A} and \mathcal{B} are rational matrices. In the case of $\mathcal{A}, \mathcal{B} \in \mathbb{Z}^{n \times n}$, $r = \det(\mathcal{A})$ is a valid choice due to the formula*

$$\mathcal{A}^{-1} = \frac{1}{\det(\mathcal{A})} \text{cof}(\mathcal{A})^T.$$

The case $M = r\mathcal{A}^{-1}\mathcal{B} \notin \mathbb{Z}^{n \times n}$ for all $r \in \mathbb{Z}$ implies that there is no lattice basis \mathcal{C} with $\mathbb{L}(\mathcal{C}) \subset \mathbb{L}(\mathcal{A})$ and $\mathbb{L}(\mathcal{C}) \subset \mathbb{L}(\mathcal{B})$.

Proof. Due to Lemma 3.3, we need to find integral matrices $N_{\mathcal{A}}, N_{\mathcal{B}}$, such that

$$\mathbb{L}(\mathcal{C}) = \mathbb{L}(\mathcal{A}N_{\mathcal{A}}) = \mathbb{L}(\mathcal{B}N_{\mathcal{B}})$$

with $|\det(N_{\mathcal{A}})|$ and $|\det(N_{\mathcal{B}})|$ as small as possible. Making use of Theorem 3.4, i.e.,

$$\mathbb{L}(\mathcal{B}) = \mathbb{L}(\mathcal{B}V_1), \quad \mathbb{L}(\mathcal{C}) = \mathbb{L}(\mathcal{C}U_1),$$

for any unimodular matrices U_1, V_1 , we can assume the equality

$$\mathcal{A}N_{\mathcal{A}} = \mathcal{B}UN_{\mathcal{B}}$$

for any unimodular U and $N_{\mathcal{B}}$ in Hermite normal form (cf. Theorem 2.5). Plugging in the Smith decomposition VST of $M = r\mathcal{A}^{-1}\mathcal{B}$ and defining $U := T^{-1}$, we find

$$\begin{aligned} N_{\mathcal{A}} &= \mathcal{A}^{-1}\mathcal{B}T^{-1}N_{\mathcal{B}} \\ &= \frac{1}{r}VSN_{\mathcal{B}}. \end{aligned}$$

Both matrices

$$N_{\mathcal{B}} = \begin{bmatrix} (N_{\mathcal{B}})_{1,1} & \cdots & (N_{\mathcal{B}})_{1,n} \\ & \ddots & \vdots \\ & & (N_{\mathcal{B}})_{n,n} \end{bmatrix} \quad \text{and} \quad \frac{1}{r}SN_{\mathcal{B}} = \begin{bmatrix} \frac{\sigma_1}{r}(N_{\mathcal{B}})_{1,1} & \cdots & (N_{\mathcal{B}})_{1,n} \frac{\sigma_1}{r} \\ & \ddots & \vdots \\ & & (N_{\mathcal{B}})_{n,n} \frac{\sigma_n}{r} \end{bmatrix}$$

have to be integral with

$$|\det(N_{\mathcal{B}})| = \left| \prod_{i=1}^n (N_{\mathcal{B}})_{i,i} \right| \quad \text{and} \quad \left| \det\left(\frac{1}{r}SN_{\mathcal{B}}\right) \right| = \left| \prod_{i=1}^n (N_{\mathcal{B}})_{i,i} \frac{\sigma_i}{r} \right|$$

as small as possible. It can easily be verified that

$$(N_{\mathcal{B}})_{i,i} := \frac{r}{\gcd(r, \sigma_i)}$$

is the optimal choice for the diagonal entries. With this choice, the off-diagonal entries $(N_{\mathcal{B}})_{i,j}$ have to be integral multiples of $(N_{\mathcal{B}})_{i,i}$. Due to the fact that $N_{\mathcal{B}}$ is in Hermite normal form, the off-diagonal entries are zero. \square

3.2. Primitive cells

Definition 3.8. A primitive cell $\Xi = \Xi(\mathcal{A}) \subset \mathbb{R}^n$ of a Bravais lattice $\mathbb{L}(\mathcal{A})$ is a (connected) volume of space that, if translated by all vectors of \mathbb{L} , fills up \mathbb{R}^n completely without any overlap, i.e.,

$$\dot{\cup}_{x \in \mathbb{L}} \{x + \xi : \xi \in \Xi\} = \mathbb{R}^n.$$

Sometimes Ξ is called a tiling of \mathbb{R}^n . A common choice for primitive cells is given by

$$\mathcal{P}(\mathcal{A}) := \mathcal{A}[0, 1)^n = \left\{ y \in \mathbb{R}^n : y = \sum_{\ell=1}^n \alpha_{\ell} a_{\ell}, 0 \leq \alpha_{\ell} < 1 \right\},$$

i.e., parallelotopes spanned by the primitive vectors of $\mathbb{L}(\mathcal{A})$.

Another common choice is the Wigner-Seitz cell Ξ_x , which is the set of all points whose distance from a central lattice point $x \in \mathbb{L}$ is smaller than the distance from any other lattice point, i.e.,

$$\Xi_x := \{y \in \mathbb{R}^n : \|x - y\|_2 < \|\tilde{x} - y\|_2, \tilde{x} \in \mathbb{L} \setminus \{x\}\}.^1$$

The Wigner-Seitz cell is more widely used in crystallography as in addition to its independence of the primitive vectors, it inherits the full symmetry of the

¹This set actually only becomes a primitive cell if half the boundary is added.

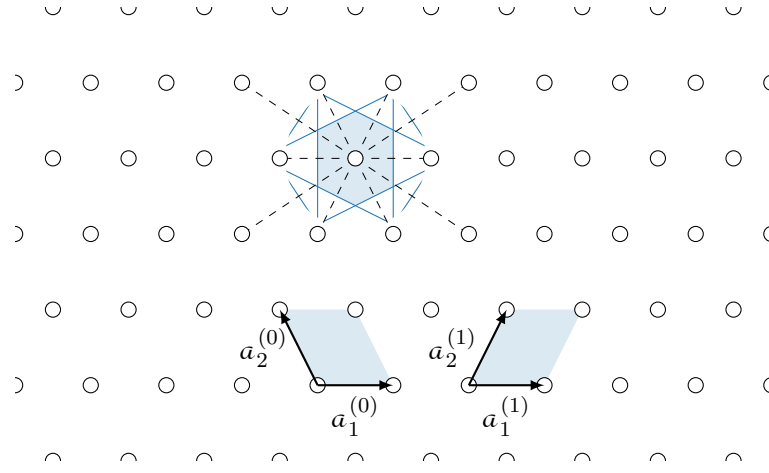


Figure 3.1.: A Bravais lattice, two different sets of primitive vectors $\mathcal{A}^{(0)}$ and $\mathcal{A}^{(1)}$ as well as three examples of primitive cells. The Wigner-Seitz cell Ξ_x reveals symmetries of the lattice which cannot directly be deduced from the parallelotopes $\mathcal{P}(\mathcal{A}^{(0)})$ and $\mathcal{P}(\mathcal{A}^{(1)})$.

Bravais lattice [19]. An example is given in Figure 3.1, where the Wigner-Seitz cell shows an invariance under reflection along the horizontal and vertical axis while the depicted parallelotopes do not reveal this property of the Bravais lattice.

Remark 3.9. *Regarding primitive cells we would like to note the following.*

- A Voronoi decomposition of a lattice consists exclusively of congruent Wigner-Seitz cells.
- Every primitive cell Ξ inherits exactly one lattice point, i.e., $|\mathbb{L} \cap \Xi| = 1$.

Theorem 3.10. *All primitive cells Ξ of a lattice $\mathbb{L}(\mathcal{A})$ have the same size. Thus, its volume is given by $\text{vol}(\Xi) = \text{vol}(\mathcal{P}(\mathcal{A})) = |\det(\mathcal{A})|$.*

Proof. We denote the characteristic function by $\mathbb{1}_\Xi$ with $\mathbb{1}_\Xi(x) = 1$ if $x \in \Xi$ and 0 else. Since Ξ is a primitive cell, we have for every $x \in \mathbb{R}^n$ exactly one $y \in \mathbb{L}$, such that $\mathbb{1}_\Xi(x + y) = 1$ and $\mathbb{1}_\Xi(x + \tilde{y}) = 0$ for $\tilde{y} \in \mathbb{L} \setminus \{y\}$. Thus, we have

$$\begin{aligned} \text{vol}(\Xi) &= \int_{\mathbb{R}^n} \mathbb{1}_\Xi(x) \, dx = \int_{\mathcal{P}(\mathcal{A})} \sum_{y \in \mathbb{L}} \mathbb{1}_\Xi(x + y) \, dx \\ &= \int_{\mathcal{P}(\mathcal{A})} dx = \text{vol}(\mathcal{P}(\mathcal{A})). \end{aligned} \quad \square$$

3.3. Crystals

In this section we extend the above theory to crystals which is not just an infinite repetition of one single point, but instead an infinite repetition of an arbitrary structure. Without loss of generality we restrict the structure elements to primitive cells of the lattice.

Definition 3.11. *Let $\mathbb{L}(\mathcal{A})$ be a lattice and $\mathfrak{s} \in \Xi(\mathcal{A})^m$, $m \in \mathbb{N}$ be the structure element. A crystal is defined by the set of tuples*

$$\mathbb{L}^{\mathfrak{s}}(\mathcal{A}) := \{(x + \mathfrak{s}_1, x + \mathfrak{s}_2, \dots, x + \mathfrak{s}_m) : x \in \mathbb{L}(\mathcal{A}), \mathfrak{s} = (\mathfrak{s}_1, \dots, \mathfrak{s}_m)\}.$$

We abbreviate the notation of the elements of $\mathbb{L}^{\mathfrak{s}}(\mathcal{A})$ with $x + \mathfrak{s} = (x + \mathfrak{s}_1, x + \mathfrak{s}_2, \dots, x + \mathfrak{s}_m)$.

Remark 3.12.

- *Every lattice is a crystal with the structure element being a single point, i.e., $\mathbb{L}(\mathcal{A}) = \mathbb{L}^{(0)}(\mathcal{A})$.*
- *We denote the structure elements as tuples instead of a set of points, since we want to study value distributions on crystals and particular operators which manipulate them. For this purpose, the order of a structure element is of importance.*

3.4. Quotient spaces

Given a sublattice $\mathbb{L}(\mathcal{C}) \subset \mathbb{L}(\mathcal{A})$, we obviously have that $(\mathbb{L}(\mathcal{C}), +)$ is a subgroup of $\mathbb{L}(\mathcal{A})$. Thus, we can consider the *quotient group* or *factor group*

$$\mathbb{L}(\mathcal{A}) / \mathbb{L}(\mathcal{C}).$$

One can interpret this as a finite sample of $\mathbb{L}(\mathcal{A})$ corresponding to a primitive cell of $\mathbb{L}(\mathcal{C})$ where opposing boundaries are identified. As we can fill up the space of this quotient space completely by an integral number of primitive cells $\mathcal{P}(\mathcal{A})$ without any overlap, it makes also sense to consider

$$\mathbb{L}^{\mathfrak{s}}(\mathcal{A}) / \mathbb{L}(\mathcal{C}).$$

For quotient spaces we have two different applications in mind. The primary purpose is, that it allows us to turn an infinite dimensional setting, a crystal or lattice, to a finite one. This is discussed in more detail in Chapter 4. Additionally, in the automation process of LFA, we rewrite crystals and operators on crystals with respect to a coarser (least common) sublattice. The notion of quotient spaces helps to implicitly define an appropriate structure element as we will see in this section.

Definition 3.13. Let $\mathbb{L}^s(\mathcal{A})$ be a crystal and $\mathbb{L}(\mathcal{C}) \subset \mathbb{L}(\mathcal{A})$ be a sublattice. We define the crystal torus $T_{\mathcal{A},\mathcal{C}}^s$ by

$$T_{\mathcal{A},\mathcal{C}}^s := \mathbb{L}^s(\mathcal{A}) / \mathbb{L}(\mathcal{C}).$$

For every $x + \mathfrak{s} \in \mathbb{L}^s(\mathcal{A})$, their equivalence class $[x + \mathfrak{s}]$ is in $T_{\mathcal{A},\mathcal{C}}^s$. Furthermore, the elements of $T_{\mathcal{A},\mathcal{C}}^s$ are defined by the equivalence

$$[x + \mathfrak{s}] = [y + \mathfrak{s}] \iff \text{there exists } z \in \mathbb{L}(\mathcal{C}), \text{ such that } x = y + z.$$

Remark 3.14. We may call $T_{\mathcal{A},\mathcal{C}}^{(0)}$ a lattice torus and just denote it by $T_{\mathcal{A},\mathcal{C}}$.

Remark 3.15. The number of elements in $T_{\mathcal{A},\mathcal{C}}^s$ are equal to $|\det(\mathcal{A}^{-1}\mathcal{C})|$ due to

$$|\mathbb{L}(\mathcal{A}) / \mathbb{L}(\mathcal{C})| = \frac{\text{vol}(\mathcal{P}(\mathcal{C}))}{\text{vol}(\mathcal{P}(\mathcal{A}))} = \frac{|\det(\mathcal{C})|}{|\det(\mathcal{A})|} = |\det(\mathcal{A}^{-1}\mathcal{C})|.$$

For theoretical and practical reasons, e.g., in Theorem 4.3 and Algorithm A.3, it is necessary to be able to list all elements of a torus $T_{\mathcal{A},\mathcal{A}M}^s = \{[x] \in T_{\mathcal{A},\mathcal{A}M}^s : x \in \mathcal{P}(\mathcal{A}M) \cap \mathbb{L}^s(\mathcal{A})\}$, $M \in \mathbb{Z}^{n \times n}$, uniquely.

Example 3.1. To illustrate this point, consider an arbitrary lattice $\mathbb{L}(\mathcal{A})$ with $\mathcal{A} \in \mathbb{R}^{2 \times 2}$, and the lattice torus $T_{\mathcal{A},\mathcal{A}M}$ with

$$M = \begin{bmatrix} m_1 & m_2 \end{bmatrix} = \begin{bmatrix} 2 & 3 \\ 2 & -2 \end{bmatrix}, \quad m_1, m_2 \in \mathbb{Z}^2,$$

as depicted in Figure 3.2. Even though we know that the quotient space consists of $|T_{\mathcal{A},\mathcal{A}M}| = |\det(M)| = 10$ different elements, there is no apparent canonical list of these elements. We briefly interrupt this example in order to show how such a canonical ordering of lattice points on a torus can be formulated using the Hermite or Smith normal form of M .

Theorem 3.16. Let $T_{\mathcal{A},\mathcal{C}}$ be arbitrary, i.e., $\mathcal{C} = \mathcal{A}M$ for some $M \in \mathbb{Z}^{n \times n}$.

- Let $H \in \mathbb{Z}^{n \times n}$ be the HNF of M with entries H_{ij} (cf. Definition 2.4). Defining the index set $I = I_1 \times I_2 \times \dots \times I_n$ by $I_\ell := \{0, 1, \dots, H_{\ell\ell} - 1\}$, we then obtain

$$T_{\mathcal{A},\mathcal{C}}^s = \{[x_j + \mathfrak{s}] : x_j = \mathcal{A}j, j \in I\}$$

with $[x_j + \mathfrak{s}] \neq [x_{j'} + \mathfrak{s}] \iff j \neq j' \in I$.

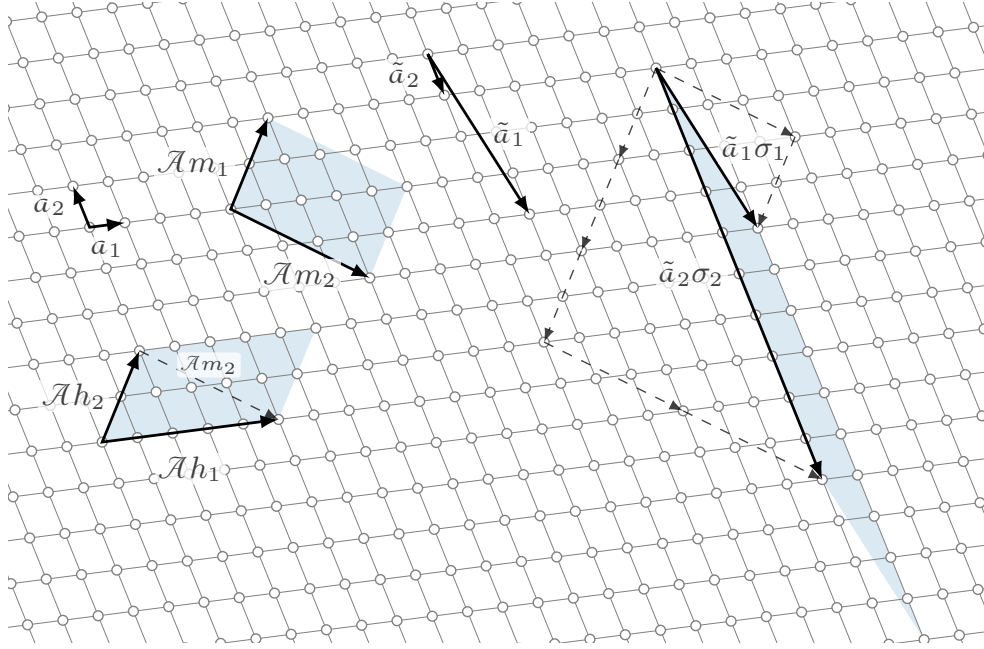


Figure 3.2.: The Hermite normal form H and the Smith normal form S of M yield lattice bases which allows us to define a canonical lexicographic ordering of the lattice points of a crystal torus $T_{\mathcal{A}, \mathcal{A}M} = T_{\mathcal{A}, \mathcal{A}H} = T_{\tilde{\mathcal{A}}, \tilde{\mathcal{A}}S}$.

- Let $S = U^{-1}MV \in \mathbb{Z}^{n \times n}$ denote the Smith decomposition of M with diagonal entries σ_i (cf. Definition 2.8) and unimodular matrices U, V . Defining the index set $\tilde{I} = \tilde{I}_1 \times \tilde{I}_2 \times \dots \times \tilde{I}_n$ by $\tilde{I}_\ell := \{0, 1, \dots, \sigma_\ell - 1\}$, we then obtain

$$T_{\mathcal{A}, \mathcal{C}}^{\mathfrak{s}} = \{[x_j + \mathfrak{s}] : x_j = \tilde{\mathcal{A}}j, j \in \tilde{I}\}$$

with $[x_j + \mathfrak{s}] \neq [x_{j'} + \mathfrak{s}] \Leftrightarrow j \neq j' \in \tilde{I}$, where $\tilde{\mathcal{A}} := \mathcal{A}U$ denotes the altered lattice basis.

Proof. Both statements are a direct consequence of the triangular or diagonal shape of the normal forms and Theorem 3.4, i.e., lattices are not changed by unimodular column transformations. On the one hand we have

$$T_{\mathcal{A}, \mathcal{C}}^{\mathfrak{s}} = T_{\mathcal{A}, \mathcal{A}M}^{\mathfrak{s}} = T_{\mathcal{A}, \mathcal{A}H}^{\mathfrak{s}}.$$

The second statement follows from $\tilde{\mathcal{A}}S = \mathcal{C}V$ and hence

$$T_{\mathcal{A}, \mathcal{C}}^{\mathfrak{s}} = T_{\mathcal{A}U, \mathcal{C}V}^{\mathfrak{s}} = T_{\tilde{\mathcal{A}}, \tilde{\mathcal{A}}S}^{\mathfrak{s}}. \quad \square$$

Example 3.1. We continue with Example 3.1 by applying Theorem 3.16 which yields:

- The Hermite normal form H of M is given by

$$H = \begin{bmatrix} h_1 & h_2 \\ 0 & 2 \end{bmatrix} = \begin{bmatrix} 5 & 2 \\ 0 & 2 \end{bmatrix}, \quad h_1, h_2 \in \mathbb{Z}^2.$$

Thus, a unique list of all representatives of $T_{\mathcal{A}, \mathcal{A}M}$ is given by

$$T_{\mathcal{A}, \mathcal{A}M} = T_{\mathcal{A}, \mathcal{A}H} = \{[x] = [j_1 a_1 + j_2 a_2] : j_1 \in \{0, 1, 2, 3, 4\}, j_2 \in \{0, 1\}\}.$$

- The Smith decomposition of M is given by

$$S = \begin{bmatrix} s_1 & 0 \\ 0 & s_2 \end{bmatrix} = \begin{bmatrix} 1 & 0 \\ 0 & 10 \end{bmatrix} = \begin{bmatrix} 1 & 0 \\ -4 & -1 \end{bmatrix} M \begin{bmatrix} -1 & -3 \\ 1 & 2 \end{bmatrix}.$$

Thus, another unique list of all representatives of $T_{\mathcal{A}, \mathcal{A}M}$ is given by

$$T_{\mathcal{A}, \mathcal{A}M} = T_{\tilde{\mathcal{A}}, \tilde{\mathcal{A}}S} = \{[x] = [j_1 \tilde{a}_1 + j_2 \tilde{a}_2] : j_1 \in \{0\}, j_2 \in \{0, 1, \dots, 9\}\},$$

$$\text{where } \tilde{\mathcal{A}} = \begin{bmatrix} \tilde{a}_1 & \tilde{a}_2 \end{bmatrix} = \mathcal{A} \begin{bmatrix} 1 & 0 \\ -4 & -1 \end{bmatrix}.$$

All tori representations $T_{\mathcal{A}, \mathcal{A}M}$, $T_{\mathcal{A}, \mathcal{A}H}$ and $T_{\tilde{\mathcal{A}}, \tilde{\mathcal{A}}S}$ are depicted in Figure 3.2.

In the remainder we drop the bracket notation for reasons of readability.

Besides the fact that the primitive vectors of a lattice are not unique, a crystal can further be rewritten with respect to another coarser (sub-)lattice. This statement is captured in detail in the following theorem.

Theorem 3.17 (Rewriting a crystal with respect to a sublattice).

Let $\mathbb{L}^s(\mathcal{A})$ be a crystal and $\mathbb{L}(\mathcal{C}) \subset \mathbb{L}(\mathcal{A})$ a sublattice. Denoting $T_{\mathcal{A}, \mathcal{C}} = \{\mathfrak{t}_1, \dots, \mathfrak{t}_p\}$,² the set

$$\Xi(\mathcal{C}) := \{x + \delta \in \mathbb{R}^n : \delta \in \mathcal{P}(\mathcal{A}), x \in \{\mathfrak{t}_1, \dots, \mathfrak{t}_p\}\}$$

defines a primitive cell of $\mathbb{L}(\mathcal{C})$, and the tuple

$$\mathbf{u} = (\mathfrak{t}_1 + \mathfrak{s}_1, \dots, \mathfrak{t}_1 + \mathfrak{s}_m, \mathfrak{t}_2 + \mathfrak{s}_1, \dots, \mathfrak{t}_p + \mathfrak{s}_m) \in \Xi(\mathcal{C})^{p \cdot m}$$

defines a structure element of $\mathbb{L}^u(\mathcal{C})$ such that $\mathbb{L}^u(\mathcal{C}) \cong \mathbb{L}^s(\mathcal{A})$, meant as a one-to- p correspondence.

²Recall that a unique list of representatives $T_{\mathcal{A}, \mathcal{C}} = \{\mathfrak{t}_1, \dots, \mathfrak{t}_p\}$ can be found via Theorem 3.16.

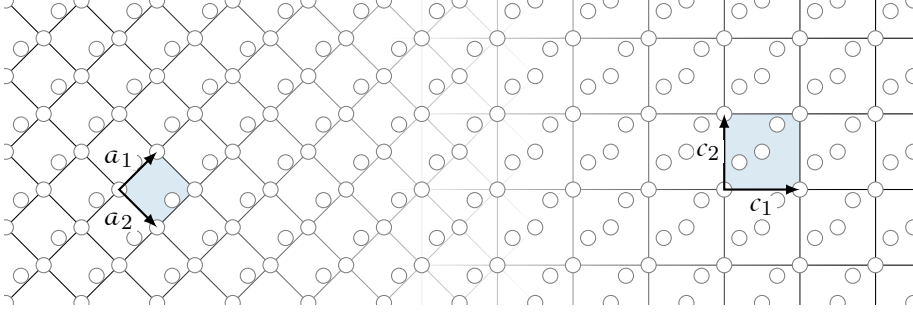


Figure 3.3.: Two different representations of an infinite repetition of some structure. Left: A crystal represented by $\mathbb{L}^s(\mathcal{A})$ with a structure element of size 2. Right: The same crystal represented by $\mathbb{L}^{T^s_{\mathcal{A},c}}(\mathcal{C})$ with a structure element of size 4.

Proof. Without loss of generality we may assume $\mathfrak{t}_j \in \mathcal{P}(\mathcal{C})$, $j = 1, \dots, p$. Then, each element in $\mathbb{L}^s(\mathcal{A})$ can be written as

$$z = (\mathcal{A}x + \mathfrak{s}_1, \dots, \mathcal{A}x + \mathfrak{s}_m)$$

and there is a unique y , such that $\mathcal{A}x = Cy = C[y] + C(y - [y])$ with $C[y] \in \mathbb{L}(\mathcal{C})$ and $C(y - [y]) = \mathfrak{t}_j \in \mathcal{P}(\mathcal{C}) \cap \mathbb{L}(\mathcal{A})$. Thus, we find z as a unique part of the element

$$C[y] + \mathfrak{u} = (\dots, C[y] + \mathfrak{t}_j + \mathfrak{s}, \dots) = (\dots, z, \dots).$$

This argument works in the other direction in the same way. \square

In order to make the following presentation as comprehensible as possible we opt to write $\mathbb{L}^{T^s_{\mathcal{A},c}}(\mathcal{C})$ instead of $\mathbb{L}^u(\mathcal{C})$ as defined in Theorem 3.17.

This theorem is illustrated in Figure 3.3, where a repetitive structure X is represented in two different ways. On the left it is represented by $\mathbb{L}^s(\mathcal{A}) \cong X$ with a structure element of size 2. On the right it is represented by $\mathbb{L}^{T^s_{\mathcal{A},c}}(\mathcal{C}) \cong X$, where the underlying lattice is a sublattice of lesser density $\mathbb{L}(\mathcal{C}) \subset \mathbb{L}(\mathcal{A})$ and a structure element consisting of all 4 points found in one primitive cell of $\mathbb{L}(\mathcal{C})$. A classification of X with a denser lattice than $\mathbb{L}(\mathcal{A})$ and/or structure element of smaller size than 2 does not exist.

Remark 3.18. Due to Theorem 3.17 we also have

$$T^s_{\mathcal{A},\mathcal{Z}} = \mathbb{L}^s(\mathcal{A}) / \mathbb{L}(\mathcal{Z}) \cong \mathbb{L}^{T^s_{\mathcal{A},c}}(\mathcal{C}) / \mathbb{L}(\mathcal{Z}) = T^s_{c,\mathcal{Z}}$$

as long as $\mathbb{L}(\mathcal{Z}) \subset \mathbb{L}(\mathcal{C}) \subset \mathbb{L}(\mathcal{A})$.

3.5. The dual lattice

For the analysis of operators on lattices/crystals as introduced in Chapter 4 the concept of the dual lattice comes in handy.

Definition 3.19. Let $\mathbb{L}(\mathcal{A})$ be a lattice. Its dual lattice $\mathbb{L}(\mathcal{A})^*$ is the set

$$\mathbb{L}(\mathcal{A})^* := \{k \in \mathbb{R}^n : \langle k, x \rangle_2 \in \mathbb{Z} \text{ for all } x \in \mathbb{L}\}.$$

The elements of $\mathbb{L}(\mathcal{A})^*$ may often be referred to as wave vectors.

Lemma 3.20. The dual lattice $\mathbb{L}(\mathcal{A})^* = \mathbb{L}(\mathcal{B})$ is given by $\mathcal{B} := (\mathcal{A}^{-1})^T$. The primitive vectors $b_1, b_2, \dots, b_n \in \mathbb{R}^n$ of $\mathbb{L}(\mathcal{B})$, i.e., the columns of \mathcal{B} , fulfill the condition $\langle b_i, a_j \rangle_2 = \delta_{ij}$, $i, j = 1, 2, \dots, n$.

Proof. Let $x \in \mathbb{L}(\mathcal{A})$ and $k \in \mathbb{L}(\mathcal{B})$ be arbitrary. There exists $\lambda, \kappa \in \mathbb{Z}^n$, such that $x = \mathcal{A}\lambda$ and $k = \mathcal{B}\kappa$. The inner product of k and x is

$$\langle k, x \rangle_2 = \langle \mathcal{B}\kappa, \mathcal{A}\lambda \rangle_2 = \langle \kappa, \mathcal{B}^T \mathcal{A}\lambda \rangle_2 = \langle \kappa, (\mathcal{A}^{-T})^T \mathcal{A}\lambda \rangle_2 = \langle \kappa, \lambda \rangle_2 \in \mathbb{Z}.$$

Thus, we have $\mathbb{L}(\mathcal{B}) \subset \mathbb{L}(\mathcal{A})^*$.

For the other direction let $k \in \mathbb{L}(\mathcal{A})^*$. There exists a unique $\kappa \in \mathbb{R}^n$, such that $\mathcal{B}\kappa = k$. Then

$$\mathbb{Z} \supset \langle k, \mathcal{A}e_i \rangle_2 = (\mathcal{B}\kappa)^T \mathcal{A}e_i = \kappa^T \mathcal{A}^{-1} \mathcal{A}e_i = \kappa_i,$$

where e_i denotes the i th unit vector. Hence $\kappa \in \mathbb{Z}^n$, i.e., $\mathbb{L}(\mathcal{A})^* \subset \mathbb{L}(\mathcal{B})$. \square

Remark 3.21. Regarding the dual lattice, we like to point out the following:

- Many different names are commonly used for the Bravais lattice \mathbb{L} and the dual lattice \mathbb{L}^* depending on the context. The former is also referred to as the direct lattice, primal lattice or position space. In a physics context it is more common to use the reciprocal lattice (also known as the phase space) instead of the dual lattice which is simply a scaled version of the dual lattice defined by $\langle b_i, a_j \rangle_2 = 2\pi\delta_{ij}$. The Wigner-Seitz cell of the reciprocal lattice is known as the first Brillouin zone.
- The dual of the dual lattice is again the direct lattice as $(\mathcal{A}^{-T})^{-T} = \mathcal{A}$.
- The volume of a primitive cell of the dual lattice is equal to the reciprocal volume the direct lattice, i.e., $\text{vol}(\mathcal{P}(\mathcal{A}^{-T})) = \text{vol}(\mathcal{P}(\mathcal{A}))^{-1}$.
- The dual of a lattice torus is given by

$$T_{\mathcal{A}, \mathcal{Z}}^* = \left(\mathbb{L}(\mathcal{A}) / \mathbb{L}(\mathcal{Z}) \right)^* = \mathbb{L}(\mathcal{Z})^* / \mathbb{L}(\mathcal{A})^*.$$

An illustration of a lattice torus $T_{\mathcal{A}, \mathcal{Z}}$ along with its dual $T_{\mathcal{A}, \mathcal{Z}}^*$ is given in Figure 3.4.

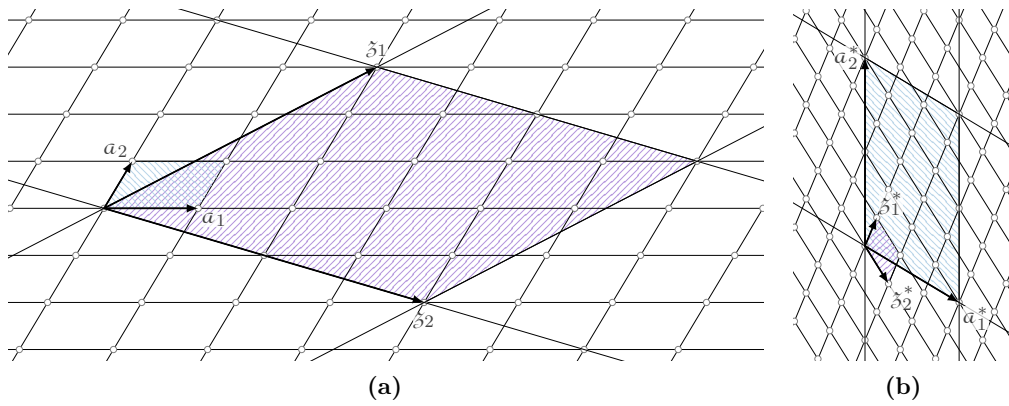


Figure 3.4.: A lattice torus $T_{\mathcal{A}, \mathcal{Z}}$ (a) and its dual torus $T_{\mathcal{A}^*, \mathcal{Z}^*}$ (b). In here, the lattices bases are denoted by $\mathcal{A} = [a_1 \mid a_2]$, $\mathcal{Z} = [\check{z}_1 \mid \check{z}_2]$ and $\mathcal{A}^{-T} = [a_1^* \mid a_2^*]$, $\mathcal{Z}^{-T} = [\check{z}_1^* \mid \check{z}_2^*]$.

Operators on lattices and crystals

LFA is usually understood as an idealized analysis of operators on repetitive structures by neglecting boundary conditions and considering an infinite domain. To some extent this perspective justifies the analysis of methods which can be described using a (constant) stencil for all unknowns which do not lie at or near the boundary, as it is the case for lexicographic Gauss-Seidel type smoother (cf. Section 5.2). However, this point of view has some drawbacks. We only work with operators as part of numerical simulations, i.e., we face only a finite numbers of unknowns/lattice points anyway. Furthermore, an exact mathematical theory in an artificial infinite setting is unnecessarily complicated and, from this point of view, we do not have a one-to-one connection to an actually implemented method.

Thus, in this thesis we restrict ourselves to a finite setting by considering quotient groups of crystals

$$T_{\mathcal{A},\mathcal{Z}}^s = \mathbb{L}^s(\mathcal{A}) / \mathbb{L}(\mathcal{Z})$$

with $\mathbb{L}(\mathcal{Z}) \subset \mathbb{L}(\mathcal{A})$ being an arbitrary sparse sublattice of $\mathbb{L}(\mathcal{A})$. The main purpose is to simplify the theory. Additionally, we always have a one-to-one link to a finite problem with periodic boundary conditions. Occasionally, in case we do not want to specify \mathcal{Z} explicitly, we may use the term $T_{\mathcal{A}}$ to describe arbitrary large but finite tori $T_{\mathcal{A},\mathcal{Z}}$, $\mathbb{L}(\mathcal{Z}) \subset \mathbb{L}(\mathcal{A})$.

4.1. Function spaces

Let us now elaborate on the function space of such quotient groups in order to describe value distributions and operators which manipulate them.

Definition 4.1. Let $T_{\mathcal{A},\mathcal{Z}}^{\mathfrak{s}} = \mathbb{L}^{\mathfrak{s}}(\mathcal{A}) / \mathbb{L}(\mathcal{Z})$, $\mathfrak{s} \in \Xi(\mathcal{A})^m$. We equip the function space

$$\mathcal{L}(T_{\mathcal{A},\mathcal{Z}}^{\mathfrak{s}}) := \mathcal{L}(T_{\mathcal{A},\mathcal{Z}}, \mathbb{C}^m) := \{f = (f_1, \dots, f_m) : T_{\mathcal{A},\mathcal{Z}} \rightarrow \mathbb{C}^m\}$$

with the scalar product

$$\langle f, g \rangle := \frac{1}{|T_{\mathcal{A},\mathcal{Z}}|} \sum_{x \in T_{\mathcal{A},\mathcal{Z}}} \langle f(x), g(x) \rangle_2,$$

where the summands $\langle f(x), g(x) \rangle_2 := \sum_{\ell=1}^m f_{\ell}(x) \overline{g_{\ell}(x)}$ denote the Euclidean scalar product on \mathbb{C}^m .

Remark 4.2. In the above definition each function f_j corresponds to the values on the shifted sublattice $(T_{\mathcal{A},\mathcal{Z}} + \mathfrak{s}_j)$ even though the argument of the function does not reflect the additional shift by \mathfrak{s}_j . Another possible definition would be

$$\hat{\mathcal{L}}(T_{\mathcal{A},\mathcal{Z}}^{\mathfrak{s}}) := \{\hat{f} = (\hat{f}_1, \dots, \hat{f}_m) : \hat{f}_j : (T_{\mathcal{A},\mathcal{Z}} + \mathfrak{s}_j) \rightarrow \mathbb{C}\}$$

which would clarify this issue, but then again this approach would get inconvenient later on.

Theorem 4.3. The functions

$$e^{2\pi i \langle k, \cdot \rangle_2} : T_{\mathcal{A},\mathcal{Z}} \rightarrow \mathbb{C}, \quad k \in T_{\mathcal{A},\mathcal{Z}}^*$$

(i) are well-defined and

(ii) form an orthonormal basis of $\mathcal{L}(T_{\mathcal{A},\mathcal{Z}}) = \{f : T_{\mathcal{A},\mathcal{Z}} \rightarrow \mathbb{C}\}$ w.r.t. $\langle \cdot, \cdot \rangle$.

Proof. Without loss of generality we assume that $S = \mathcal{A}^{-1}\mathcal{Z} \in \mathbb{Z}^{n \times n}$ is in Smith normal form with diagonal entries $\sigma_1, \sigma_2, \dots, \sigma_n$ (cf. Theorem 3.16).

Regarding (i), let $x, y \in \mathbb{L}(\mathcal{A})$ with $x - y \in \mathbb{L}(\mathcal{Z})$, i.e., $[x] = [y] \in T_{\mathcal{A},\mathcal{Z}}$. Then there exists a $z \in \mathbb{Z}^n$, such that $x - y = \mathcal{Z}z = \mathcal{A}Sz$. Furthermore, let $[k] \in T_{\mathcal{A},\mathcal{Z}}^* = T_{\mathcal{Z}^{-T}, \mathcal{A}^{-T}}$, i.e., $k = \mathcal{Z}^{-T}\kappa = \mathcal{A}^{-T}S^{-T}\kappa$ for some $\kappa \in \mathbb{Z}^n$. Then,

$$e^{2\pi i \langle k, x-y \rangle_2} = e^{2\pi i \langle \mathcal{A}^{-T}S^{-T}\kappa, \mathcal{A}Sz \rangle_2} = e^{2\pi i \langle \kappa, z \rangle_2} = 1.$$

Hence, $e^{2\pi i \langle k, x \rangle_2} = e^{2\pi i \langle k, y \rangle_2}$ if $[x] = [y]$.

Regarding (ii), we first observe that the number of wave functions is equal to the number of lattice points due to

$$|T_{\mathcal{A},\mathcal{Z}}| = \frac{|\det(\mathcal{Z})|}{|\det(\mathcal{A})|} = |\det(S)| = \frac{|\det(\mathcal{A}^{-T})|}{|\det(\mathcal{Z}^{-T})|} = |T_{\mathcal{A},\mathcal{Z}}^*|.$$

Now let $k', k'' \in T_{\mathcal{A}, \mathcal{Z}}^*$ be arbitrary. By defining $k = k' - k''$ the scalar product can be rewritten as follows

$$\langle e^{2\pi i \langle k', \cdot \rangle_2}, e^{2\pi i \langle k'', \cdot \rangle_2} \rangle = \frac{1}{|T_{\mathcal{A}, \mathcal{Z}}|} \sum_{x \in T_{\mathcal{A}, \mathcal{Z}}} e^{2\pi i \langle k, x \rangle_2}.$$

For $k = 0$ we obviously get

$$\frac{1}{|T_{\mathcal{A}, \mathcal{Z}}|} \sum_{x \in T_{\mathcal{A}, \mathcal{Z}}} e^{2\pi i \langle k, x \rangle_2} = \frac{1}{|T_{\mathcal{A}, \mathcal{Z}}|} \sum_{x \in T_{\mathcal{A}, \mathcal{Z}}} 1 = 1.$$

Thus, we assume $k \neq 0$ and show that this sum equals zero. Using $\mathcal{D} := \mathcal{Z}^{-T}$ and the fact that S is in SNF, we have

$$\begin{aligned} T_{\mathcal{A}, \mathcal{Z}} &= T_{\mathcal{A}, \mathcal{A}S} = \{x = \sum_{\ell=1}^n j_\ell a_\ell : (j_1, j_2, \dots, j_n) \in I\}, \\ T_{\mathcal{A}, \mathcal{Z}}^* &= T_{\mathcal{Z}^{-T}, \mathcal{A}^{-T}} = T_{\mathcal{D}, \mathcal{D}S} = \{k = \sum_{\ell=1}^n k_\ell d_\ell : (k_1, k_2, \dots, k_n) \in I\}, \end{aligned}$$

where the index set $I = I_1 \times I_2 \times \dots \times I_n$ is defined by $I_\ell := \{0, 1, \dots, \sigma_\ell - 1\}$ for all ℓ (cf. Theorem 3.16). Furthermore, the columns of $\mathcal{D} = \mathcal{B}S^{-1}$ are simply given by $d_\ell = \sigma_\ell^{-1} b_\ell$. Now let κ denote the smallest index of a nonzero coefficient of k , then the wavevector k can be expressed as

$$k = \sum_{\ell=\kappa}^n k_\ell d_\ell = \sum_{\ell=\kappa}^n k_\ell \sigma_\ell^{-1} b_\ell = k_\kappa \sigma_\kappa^{-1} b_\kappa + \sum_{\ell=\kappa+1}^n k_\ell \sigma_\ell^{-1} b_\ell.$$

Using this representation of k in the initial scalar product, we get

$$\begin{aligned} & \frac{1}{|T_{\mathcal{A}, \mathcal{Z}}|} \sum_{x \in T_{\mathcal{A}, \mathcal{Z}}} e^{2\pi i \langle k, x \rangle_2} \\ &= \frac{1}{|T_{\mathcal{A}, \mathcal{Z}}|} \sum_{\ell=1}^n \sum_{j_\ell=0}^{\sigma_\ell-1} e^{2\pi i \langle k, \sum_{\xi=1}^n j_\xi a_\xi \rangle_2} \\ &= \frac{1}{|T_{\mathcal{A}, \mathcal{Z}}|} \sum_{\ell=1}^n \sum_{j_\ell=0}^{\sigma_\ell-1} e^{2\pi i \langle k_\kappa \sigma_\kappa^{-1} b_\kappa + \sum_{\zeta=\kappa+1}^n k_\zeta \sigma_\zeta^{-1} b_\zeta, \sum_{\xi=1}^n j_\xi a_\xi \rangle_2} \\ &= \frac{1}{|T_{\mathcal{A}, \mathcal{Z}}|} \sum_{\ell=1}^n \sum_{j_\ell=0}^{\sigma_\ell-1} e^{2\pi i \langle \sum_{\zeta=\kappa+1}^n k_\zeta \sigma_\zeta^{-1} b_\zeta, j_\zeta a_\zeta \rangle_2} \cdot e^{2\pi i \langle k_\kappa \sigma_\kappa^{-1} b_\kappa, j_\kappa a_\kappa \rangle_2} \\ &= \frac{1}{|T_{\mathcal{A}, \mathcal{Z}}|} \sum_{\substack{\ell=1, \dots, n \\ \ell \neq \kappa}} \sum_{j_\ell=0}^{\sigma_\ell-1} e^{2\pi i \langle \sum_{\zeta=\kappa+1}^n k_\zeta \sigma_\zeta^{-1} b_\zeta, j_\zeta a_\zeta \rangle_2} \cdot \left[\sum_{j_\kappa=0}^{\sigma_\kappa-1} e^{2\pi i \langle k_\kappa \sigma_\kappa^{-1} b_\kappa, j_\kappa a_\kappa \rangle_2} \right]. \end{aligned}$$

Finally, using the geometric sum formula¹ as well as the fact that $k_\ell \in \{1, \dots, \sigma_\ell - 1\} \subset \mathbb{Z}$, the innermost sum can be rewritten to

$$\sum_{j_\kappa=0}^{\sigma_\kappa-1} e^{2\pi i \langle k_\kappa \sigma_\kappa^{-1} b_\kappa, j_\kappa a_\kappa \rangle_2} = \sum_{j_\kappa=0}^{\sigma_\kappa-1} \left[e^{(\frac{2\pi i k_\kappa}{\sigma_\kappa})} \right]^{j_\kappa} = 0. \quad \square$$

Theorem 4.4. *An orthonormal basis for the function space $\mathcal{L}(T_{\mathcal{A}, \mathcal{Z}}^{\mathfrak{s}})$ is given by the wave functions*

$$\begin{aligned} e_{1,k} &:= (e^{2\pi i \langle k, \cdot \rangle_2}, 0, 0, \dots, 0), \\ e_{2,k} &:= (0, e^{2\pi i \langle k, \cdot \rangle_2}, 0, \dots, 0), \\ &\vdots \\ e_{m,k} &:= (0, 0, \dots, 0, e^{2\pi i \langle k, \cdot \rangle_2}), \end{aligned}$$

with $k \in T_{\mathcal{A}, \mathcal{Z}}^*$ and $\mathfrak{s} = (\mathfrak{s}_1, \dots, \mathfrak{s}_m)$.

Proof. The basis functions $e_{j,k}$, $k \in T_{\mathcal{A}, \mathcal{Z}}^*$ form an orthonormal basis of the lattice torus $\mathcal{L}(T_{\mathcal{A}, \mathcal{Z}} + \mathfrak{s}_j)$ due to Theorem 4.3. Thus, it is clear that these functions $e_{j,k}$, $j = 1, \dots, m$, $k \in T_{\mathcal{A}, \mathcal{Z}}^*$ form an orthonormal basis of $\mathcal{L}(T_{\mathcal{A}, \mathcal{Z}}^{\mathfrak{s}})$. \square

The orthonormal basis of Theorem 4.4 can be split into subsets with respect to the wavevector k .

Definition 4.5. *We denote the m -dimensional space of harmonics of the function space $\mathcal{L}(T_{\mathcal{A}, \mathcal{Z}}^{\mathfrak{s}})$ by*

$$H_k = \text{span}\{e_{j,k} : j = 1, \dots, m\},$$

where $e_{j,k}$ denotes the wavefunction as specified in Theorem 4.4. Thus we find $\bigcup_{k \in T_{\mathcal{A}, \mathcal{Z}}^*} H_k = \mathcal{L}(T_{\mathcal{A}, \mathcal{Z}}^{\mathfrak{s}})$.

The basis we use is particularly simple in terms of its theoretical utility and, as we will see later-on, its practical application. Each space of harmonics H_k is spanned by the basis which consists of $m = |\mathfrak{s}|$ wavefunctions with frequency k , where each single one only takes values on a certain torus $T_{\mathcal{A}, \mathcal{Z}} + \mathfrak{s}_j$, $j = 1, \dots, m$.

Now recall that for each crystal $T_{\mathcal{A}, \mathcal{Z}}^{\mathfrak{s}}$ and a sublattice $\mathbb{L}(\mathcal{C}) \subset \mathbb{L}(\mathcal{A})$ there is a congruent crystal representation $T_{\mathcal{C}, \mathcal{Z}}^{\mathfrak{u}} \cong T_{\mathcal{A}, \mathcal{Z}}^{\mathfrak{s}}$, $\mathfrak{u} \cong T_{\mathcal{A}, \mathcal{C}}^{\mathfrak{s}}$ according to Theorem 3.17. This theorem further implies a congruence of the function spaces

$$\mathcal{L}(T_{\mathcal{A}, \mathcal{Z}}^{\mathfrak{s}}) \cong \mathcal{L}(T_{\mathcal{C}, \mathcal{Z}}^{\mathfrak{u}})$$

given by the following natural isomorphism.

¹ $\sum_{k=0}^{n-1} r^k = \frac{1-r^n}{1-r}$ for $r \neq 1$.

Definition 4.6. Let $T_{\mathcal{A},\mathcal{Z}}^{\mathfrak{s}} \cong T_{\mathcal{C},\mathcal{Z}}^{\mathfrak{u}}$ be two representations of one crystal with $\mathbb{L}(\mathcal{C}) \subset \mathbb{L}(\mathcal{A})$ and $\mathfrak{u} = (\mathfrak{t}_1 + \mathfrak{s}_1, \dots, \mathfrak{t}_1 + \mathfrak{s}_m, \mathfrak{t}_2 + \mathfrak{s}_1, \dots, \mathfrak{t}_p + \mathfrak{s}_m) \cong T_{\mathcal{A},\mathcal{C}}^{\mathfrak{s}}$. The natural isomorphism $\eta : \mathcal{L}(T_{\mathcal{A},\mathcal{Z}}^{\mathfrak{s}}) \rightarrow \mathcal{L}(T_{\mathcal{C},\mathcal{Z}}^{\mathfrak{u}})$ between these two corresponding function spaces is given by

$$\mathcal{L}(T_{\mathcal{A},\mathcal{Z}}^{\mathfrak{s}}) \ni f(\cdot) \mapsto (\eta f)(\cdot) = (f(\cdot + \mathfrak{t}_1), \dots, f(\cdot + \mathfrak{t}_p)) \in \mathcal{L}(T_{\mathcal{C},\mathcal{Z}}^{\mathfrak{u}})$$

as (f) and (ηf) describe the same value distribution on the crystal.

Remark 4.7. This natural isomorphism implies that the coarsest possible crystal interpretation is simply the complex coordinate space

$$\mathbb{C}^{mp} = \mathcal{L}(T_{\mathcal{Z},\mathcal{Z}}^{T_{\mathcal{A},\mathcal{Z}}^{\mathfrak{s}}}) \cong \mathcal{L}(T_{\mathcal{A},\mathcal{Z}}^{\mathfrak{s}})$$

with $p := |T_{\mathcal{A},\mathcal{Z}}|$. Note, that the scalar product on $\mathcal{L}(T_{\mathcal{A},\mathcal{Z}}^{\mathfrak{s}})$ is equal to the Euclidean scalar product on \mathbb{C}^{mp} up to the factor p .

According to Definition 4.5 an orthonormal basis of the spaces of harmonics $H_k^{\mathcal{C}}$ of $\mathcal{L}(T_{\mathcal{C},\mathcal{Z}}^{\mathfrak{u}})$ is given by $e_{j,k}^{\mathcal{C}}$. Applying the natural isomorphism of Definition 4.6 to the orthonormal basis $e_{j,k}^{\mathcal{A}}$ of the spaces of harmonics $H_k^{\mathcal{A}}$ of $\mathcal{L}(T_{\mathcal{A},\mathcal{Z}}^{\mathfrak{s}})$ yields another basis of $H_k^{\mathcal{C}}$ as it lifts the functions from $\mathcal{L}(T_{\mathcal{A},\mathcal{Z}}^{\mathfrak{s}})$ to $\mathcal{L}(T_{\mathcal{C},\mathcal{Z}}^{\mathfrak{u}})$. The following theorem shows that this basis is orthogonal and answers the questions how these two bases are related.

Theorem 4.8. Let $T_{\mathcal{A},\mathcal{Z}}^{\mathfrak{s}} \cong T_{\mathcal{C},\mathcal{Z}}^{\mathfrak{u}}$ be two representations of one crystal with $\mathbb{L}(\mathcal{C}) \subset \mathbb{L}(\mathcal{A})$, $\mathfrak{s} = (\mathfrak{s}_1, \dots, \mathfrak{s}_m)$, $\mathfrak{t} = (\mathfrak{t}_1, \dots, \mathfrak{t}_p) \cong T_{\mathcal{A},\mathcal{C}}$ and $(\mathfrak{u}_1, \dots, \mathfrak{u}_{mp}) = (\mathfrak{t}_1 + \mathfrak{s}, \dots, \mathfrak{t}_p + \mathfrak{s})$. Let us further denote the corresponding spaces of harmonics with $H_k^{\mathcal{A}} = \text{span}\{e_{j,k}^{\mathcal{A}} : j = 1, \dots, m\}$ and $H_k^{\mathcal{C}} = \text{span}\{e_{j,k}^{\mathcal{C}} : j = 1, \dots, mp\}$. Then, for each $k \in T_{\mathcal{C},\mathcal{Z}}^*$ we find

$$H_k^{\mathcal{C}} = \text{span}\{\eta e_{j,k+k_i}^{\mathcal{A}} : k_i \in T_{\mathcal{A},\mathcal{C}}^*, j = 1, \dots, m\}.$$

This set of basis functions $\eta e_{j,k+k_i}^{\mathcal{A}}$ is indeed orthogonal. Thus, another (ordered) orthonormal basis of $H_k^{\mathcal{C}}$ is given by the columns of the block matrix $E = \frac{1}{p}(E_{i,j})_{i,j}$ with

$$E_{i,j} = \text{diag}(e^{2\pi i \langle k+k_j, \cdot + \mathfrak{t}_i + \mathfrak{s}_1 \rangle_2}, e^{2\pi i \langle k+k_j, \cdot + \mathfrak{t}_i + \mathfrak{s}_2 \rangle_2}, \dots, e^{2\pi i \langle k+k_j, \cdot + \mathfrak{t}_i + \mathfrak{s}_m \rangle_2}).$$

where $(k_1, \dots, k_p) \cong T_{\mathcal{A},\mathcal{C}}^*$.

Proof. Note, that the columns of E correspond to $\eta e_{j,k+k_i}^{\mathcal{A}}$ up to the scaling p . Furthermore, by using $e^{2\pi i \langle k_i, x \rangle_2} = 1$ for all $x \in T_{\mathcal{C},\mathcal{Z}}$ and $k_i \in T_{\mathcal{A},\mathcal{C}}^*$ this statement can be proven analogously to Theorem 4.3. \square

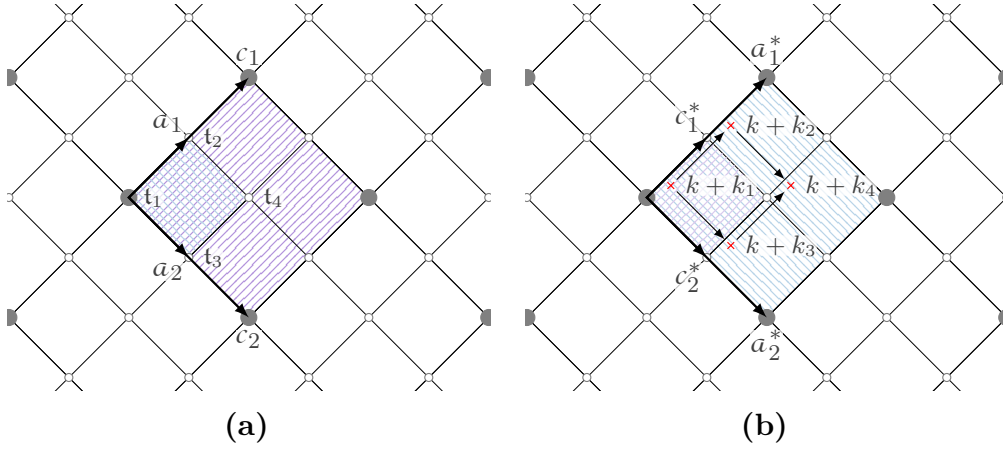


Figure 4.1.: In (a) two representations $T_{\mathcal{A}}^{(0)} \cong T_{\mathcal{C}}^{\mathbf{t}}$, $\mathbf{t} = (\mathbf{t}_1, \mathbf{t}_2, \mathbf{t}_3, \mathbf{t}_4) \cong T_{\mathcal{A}, \mathcal{C}}$, $\mathcal{C} = 2\mathcal{A}$, of the same crystal are depicted. In (b) the corresponding dual space is depicted. The transition from $\mathcal{L}(T_{\mathcal{A}, \mathcal{Z}}^{(0)})$ to $\mathcal{L}(T_{\mathcal{C}, \mathcal{Z}}^{\mathbf{t}})$ in position space is a superimposition in frequency space such that the spaces of harmonics $H_{k+k_i}^{\mathcal{A}}$ of $\mathcal{L}(T_{\mathcal{A}, \mathcal{Z}}^{(0)})$ collapse to the space of harmonics $H_k^{\mathcal{C}}$ of $\mathcal{L}(T_{\mathcal{C}, \mathcal{Z}}^{\mathbf{t}})$.

This theorem basically tells us that the transition from $\mathcal{L}(T_{\mathcal{A}, \mathcal{Z}}^{\mathfrak{s}})$ to $\mathcal{L}(T_{\mathcal{C}, \mathcal{Z}}^{\mathbf{u}})$ in position space is a superimposition in frequency space such that the spaces of harmonics $H_{k+k_i}^{\mathcal{A}}$ collapse to $H_k^{\mathcal{C}}$. This connection is illustrated in Figure 4.1 for $\mathcal{C} = 2\mathcal{A}$ and $\mathfrak{s} = (0)$. As already stated, each (block-)column of the ordered basis E of Theorem 4.8 is simply the result of the application of the natural isomorphism η to the wavefunctions $e_{j, k+k_i}^{\mathcal{A}} : T_{\mathcal{A}, \mathcal{Z}} \rightarrow \mathbb{C}^{|\mathfrak{s}|}$ and thus, this basis is still connected to the primal frequency $k + k_i \in T_{\mathcal{A}, \mathcal{Z}}^*$, $k \in T_{\mathcal{C}, \mathcal{Z}}$.

This lifted basis $\eta e_{j, k}^{\mathcal{A}}$ is commonly used in conventional LFA (cf. [47]). It is especially useful in what is known as a *smoothing analysis*, which is explained in detail in Section 5.5.

Independent of the particular choice of basis for the spaces of harmonics, we further need the Fourier transform of value distributions on crystal tori for theoretical purposes which is defined as follows.

Definition 4.9. The Fourier transformation $\mathcal{F} : \mathcal{L}(T_{\mathcal{A}, \mathcal{Z}}) \rightarrow \mathcal{L}(T_{\mathcal{A}, \mathcal{Z}}^*)$ is defined by

$$\hat{f}(\cdot) := (\mathcal{F}f)(\cdot) = \frac{1}{\sqrt{|T_{\mathcal{A}, \mathcal{Z}}|}} \sum_{x \in T_{\mathcal{A}, \mathcal{Z}}} f(x) e^{-2\pi i \langle \cdot, x \rangle_2}.$$

It is a bijection and the inverse Fourier transform is given by

$$f(\cdot) = (\mathcal{F}^{-1}\hat{f})(\cdot) = \frac{1}{\sqrt{|T_{\mathcal{A}, \mathcal{Z}}|}} \sum_{k \in T_{\mathcal{A}, \mathcal{Z}}^*} \hat{f}(k) e^{2\pi i \langle k, \cdot \rangle_2}.$$

Proof. We have

$$\begin{aligned}
 (\mathcal{F}(\mathcal{F}^{-1}\hat{f}))(k) &= \left[\mathcal{F} \left(\frac{1}{\sqrt{|T_{\mathcal{A},\mathcal{Z}}|}} \sum_{\tilde{k} \in T_{\mathcal{A},\mathcal{Z}}^*} \hat{f}(\tilde{k}) e^{2\pi i \langle \tilde{k}, \cdot \rangle_2} \right) \right] (k) \\
 &= \frac{1}{|T_{\mathcal{A},\mathcal{Z}}|} \sum_{x \in T_{\mathcal{A},\mathcal{Z}}} \left[\sum_{\tilde{k} \in T_{\mathcal{A},\mathcal{Z}}^*} \hat{f}(\tilde{k}) e^{2\pi i \langle \tilde{k}, x \rangle_2} \right] e^{-2\pi i \langle k, x \rangle_2} \\
 &= \frac{1}{|T_{\mathcal{A},\mathcal{Z}}|} \sum_{\tilde{k} \in T_{\mathcal{A},\mathcal{Z}}^*} \hat{f}(\tilde{k}) \left[\sum_{x \in T_{\mathcal{A},\mathcal{Z}}} e^{2\pi i \langle \tilde{k} - k, x \rangle_2} \right] \\
 &= \sum_{\tilde{k} \in T_{\mathcal{A},\mathcal{Z}}^*} \hat{f}(\tilde{k}) \delta_{k\tilde{k}} = \hat{f}(k)
 \end{aligned}$$

for every $k \in T_{\mathcal{A},\mathcal{Z}}^*$ due to Theorem 4.3. Obviously $(\mathcal{F}^{-1}\mathcal{F}f)(x) = f(x)$ has to be true, since we can just exchange the roles of the direct $T_{\mathcal{A},\mathcal{Z}}^*$ and the dual lattice $(T_{\mathcal{A},\mathcal{Z}}^*)^* = T_{\mathcal{A},\mathcal{Z}}$. \square

Definition 4.10. *The Fourier transformation $\mathcal{F} : \mathcal{L}(T_{\mathcal{A},\mathcal{Z}}^s) \rightarrow \mathcal{L}((T_{\mathcal{A},\mathcal{Z}}^s)^*)$ for value distributions on crystal tori is defined componentwise*

$$\mathcal{F}f := (\mathcal{F}f_1, \dots, \mathcal{F}f_m), \quad f = (f_1, \dots, f_m) \in \mathcal{L}(T_{\mathcal{A},\mathcal{Z}}^s).$$

4.2. Operators

In this section we take a look at specific *operators* L which alter value distributions $f \in \mathcal{L}(T_{\mathcal{A},\mathcal{Z}}^s)$ on crystal tori.

Definition 4.11. *A lattice-operator is a linear function*

$$L : \mathcal{L}(T_{\mathcal{A},\mathcal{Z}}) \rightarrow \mathcal{L}(T_{\mathcal{A},\mathcal{Z}}),$$

where

$$\mathcal{L}(T_{\mathcal{A},\mathcal{Z}}) = \{f : T_{\mathcal{A},\mathcal{Z}} \rightarrow \mathbb{C}\}$$

is the set of all value distributions on a lattice.

Definition 4.12. *A crystal-operator is a linear function*

$$\begin{aligned}
 L = (L_1, L_2, \dots, L_n) : \mathcal{L}(T_{\mathcal{A},\mathcal{Z}}^s) &\rightarrow \mathcal{L}(T_{\mathcal{A},\mathcal{Z}}^t), \\
 f \mapsto Lf &= (L_1(f_1, \dots, f_m), \dots, L_n(f_1, \dots, f_m)).
 \end{aligned}$$

We call the linear functions $L_j : \mathcal{L}(T_{\mathcal{A},\mathcal{Z}}^s) \rightarrow \mathcal{L}(T_{\mathcal{A},\mathcal{Z}}^{t_j})$ subcrystal-operators which alter value distributions $f_j \in \mathcal{L}(T_{\mathcal{A},\mathcal{Z}}^{t_j}) = \mathcal{L}(T_{\mathcal{A},\mathcal{Z}})$ associated to the shifted lattice tori $T_{\mathcal{A},\mathcal{Z}} + \mathfrak{t}_j$.

Remark 4.13. • Every lattice-operator $L : \mathcal{L}(T_{\mathcal{A}, \mathcal{Z}}) \rightarrow \mathcal{L}(T_{\mathcal{A}, \mathcal{Z}})$ can always be seen as a subcrystal-operator L_j via $L_j(f_1, f_2, \dots, f_m) := Lf_j$. On the other hand a subcrystal-operator may depend on all subcrystal functions (f_1, f_2, \dots, f_m) , thus it can in general not be seen as a lattice operator.

- Whenever we apply a lattice-operator $L : \mathcal{L}(T_{\mathcal{A}, \mathcal{Z}}) \rightarrow \mathcal{L}(T_{\mathcal{A}, \mathcal{Z}})$ to a crystal-function $f = (f_1, \dots, f_m) \in \mathcal{L}(T_{\mathcal{A}, \mathcal{Z}}^s)$, it is meant componentwise, i.e., we have $Lf := \tilde{L}f$ where $\tilde{L} : \mathcal{L}(T_{\mathcal{A}, \mathcal{Z}}^s) \rightarrow \mathcal{L}(T_{\mathcal{A}, \mathcal{Z}}^s)$ given by $\tilde{L}f := (Lf_1, Lf_2, \dots, Lf_m)$.

In the context of local Fourier analysis we are interested in operators which can be represented in (block) stencil notation. That is, translationally invariant operators that can be written as multiplication operators. These two properties are in fact equivalent as it is a well-known result from functional analysis (cf. [44, Theorem 3.16]). In this section we give a proof for this theorem fitting our setting and notation. In order to proof this statement we further show another important result, namely that the spaces of harmonics H_k (cf. Definition 4.5) are invariant subspaces of translationally crystal operators. This immediately provides information about the spectrum of these types of operators.

For each $a \in \mathbb{L}(\mathcal{A})$ a *translation operator* is defined by

$$\mathbb{T}_a : \mathcal{L}(T_{\mathcal{A}}) \rightarrow \mathcal{L}(T_{\mathcal{A}}), \mathbb{T}_a f(\cdot) = f(\cdot + a).$$

We can express an arbitrary translation operator by concatenating translations of primitive vectors. Due to $a = \sum_{\ell} j_{\ell} \alpha_{\ell}$, we have $\mathbb{T}_a = \mathbb{T}_{\alpha_1}^{j_1} \dots \mathbb{T}_{\alpha_n}^{j_n}$. These primitive translations lead to the definition of translationally invariant operators.

Definition 4.14. Let $L : \mathcal{L}(T_{\mathcal{A}}^s) \rightarrow \mathcal{L}(T_{\mathcal{A}}^t)$ be a crystal operator. It is called (\mathcal{A} -)translationally invariant if it commutes with every translation by a primitive vector, i.e.,

$$L\mathbb{T}_a - \mathbb{T}_a L = 0 \text{ for all primitive vectors } a \text{ of } \mathbb{L}(\mathcal{A}).$$

Lemma 4.15. The eigenfunctions of an \mathcal{A} -translationally invariant lattice-operator $L : \mathcal{L}(T_{\mathcal{A}, \mathcal{Z}}) \rightarrow \mathcal{L}(T_{\mathcal{A}, \mathcal{Z}})$ are $e^{2\pi i \langle k, \cdot \rangle_2}$, $k \in T_{\mathcal{A}, \mathcal{Z}}^*$.

Proof. Due to Theorem 4.3 we know that the wavefunctions form an orthonormal basis of $\mathcal{L}(T_{\mathcal{A}, \mathcal{Z}})$, i.e.,

$$\mathcal{L}(T_{\mathcal{A}, \mathcal{Z}}) = \text{span} \left\{ e^{2\pi i \langle k, \cdot \rangle_2} : k = \sum_{\ell=1}^n k_{\ell} \beta_{\ell}, (k_1, \dots, k_n) \in I \right\},$$

for some set $I = I_1 \times \cdots \times I_n \subset [0, 1]^n$. Let $k = \sum_{\ell=1}^n k_\ell \beta_\ell$ for some $(k_1, \dots, k_n) \in I$ be arbitrary. We can rewrite the application of L on a wavefunction by

$$Le^{2\pi i \langle k, \cdot \rangle_2} = \sum_{k' \in I} \alpha_{k'} e^{2\pi i \langle k', \cdot \rangle_2} \quad (4.1)$$

for some $\alpha_{k'} \in \mathbb{C}$. On the one hand we have

$$\mathbb{T}_{\alpha_j} Le^{2\pi i \langle k, \cdot \rangle_2} = \sum_{k' \in I} \alpha_{k'} \mathbb{T}_{\alpha_j} e^{2\pi i \langle k', \cdot \rangle_2} = \sum_{k' \in I} \alpha_{k'} e^{2\pi i k'_j} e^{2\pi i \langle k', \cdot \rangle_2}.$$

On the other hand we find

$$\mathbb{T}_{\alpha_j} Le^{2\pi i \langle k, \cdot \rangle_2} = L \mathbb{T}_{\alpha_j} e^{2\pi i \langle k, \cdot \rangle_2} = Le^{2\pi i k_j} e^{2\pi i \langle k, \cdot \rangle_2} = e^{2\pi i k_j} (Le^{2\pi i \langle k, \cdot \rangle_2}),$$

and, by inserting equation (4.1) we get

$$e^{2\pi i k_j} (Le^{2\pi i \langle k, \cdot \rangle_2}) = e^{2\pi i k_j} \sum_{k' \in I} \alpha_{k'} e^{2\pi i \langle k', \cdot \rangle_2} = \sum_{k' \in I} \alpha_{k'} e^{2\pi i k_j} e^{2\pi i \langle k', \cdot \rangle_2}.$$

Thus, for every k' we have

$$\alpha_{k'} e^{2\pi i k_j} = \alpha_{k'} e^{2\pi i k'_j} \iff \alpha_{k'} (e^{2\pi i k_j} - e^{2\pi i k'_j}) = 0.$$

Hence, we must have $\alpha_{k'} = 0$ whenever $k_j \neq k'_j$ (due to $k_j, k'_j \in \mathcal{P}(\mathcal{B})$, $\mathcal{B} = \mathcal{A}^{-T}$). Since j was arbitrary, we find

$$Le^{2\pi i \langle k, \cdot \rangle_2} = \alpha_k e^{2\pi i \langle k, \cdot \rangle_2}. \quad \square$$

This statement can be extended to translationally invariant crystal operators.

Theorem 4.16. *Let $L : \mathcal{L}(T_{\mathcal{A}, \mathcal{Z}}^{\mathfrak{s}}) \rightarrow \mathcal{L}(T_{\mathcal{A}, \mathcal{Z}}^{\mathfrak{s}})$ be an \mathcal{A} -translationally invariant crystal-operator. Then, for each subcrystal operator $L_j : \mathcal{L}(T_{\mathcal{A}, \mathcal{Z}}^{\mathfrak{s}}) \rightarrow \mathcal{L}(T_{\mathcal{A}, \mathcal{Z}}^{\mathfrak{s}_j})$, $j \in \{1, \dots, m\}$, we have*

$$L_j(e_{\ell, k}) \in \text{span}\{e^{2\pi i \langle k, \cdot \rangle_2}\}$$

for every $\ell \in \{1, \dots, m\}$, $k \in T_{\mathcal{A}, \mathcal{Z}}^{\mathfrak{s}}$. Thus $H_k = \text{span}\{e_{j, k} : j = 1, \dots, m\}$ is L -invariant, i.e.,

$$L(H_k) \subset H_k.$$

Proof. We restrict ourselves to a single component of L , i.e., a subcrystal operator $L_j : \mathcal{L}(T_{\mathcal{A}, \mathcal{Z}}^{\mathfrak{s}}) \rightarrow \mathcal{L}(T_{\mathcal{A}, \mathcal{Z}}^{\mathfrak{s}_j})$ associated to $T_{\mathcal{A}, \mathcal{Z}} + \mathfrak{s}_j$. We have

$$L_j e_{\ell, k} = L_j(0, \dots, 0, e^{2\pi i \langle k, \cdot \rangle_2}, 0, \dots, 0) = \sum_{k'} \alpha_{k'}^{j, \ell} e^{2\pi i \langle k', \cdot \rangle_2}$$

for some $\alpha_{k'}^{j, \ell} \in \mathbb{C}$. Now, in a very similar manner to the proof of Lemma 4.15, we eventually obtain $L_j e_{\ell, k} = \alpha_k^{j, \ell} e^{2\pi i \langle k, \cdot \rangle_2}$ for every ℓ . Hence, $L(H_k) \subset H_k$. \square

Due to this theorem we are able to make a connection to multiplication operators, which are formally defined as follows.

Definition 4.17. A multiplication operator $L : \mathcal{L}(T_{\mathcal{A}, \mathcal{Z}}^{\mathfrak{s}}) \rightarrow \mathcal{L}(T_{\mathcal{A}, \mathcal{Z}}^{\mathfrak{t}})$, $|\mathfrak{s}| = m$, $|\mathfrak{t}| = n$, is defined by multiplication matrices $m_L^{(y)} \in \mathbb{C}^{n \times m}$, $y \in T_{\mathcal{A}, \mathcal{Z}}$, such that

$$(Lf)(x) = \sum_{y \in T_{\mathcal{A}, \mathcal{Z}}} m_L^{(y)} f(x + y)$$

for each $f = (f_1, \dots, f_m)^T \in \mathcal{L}(T_{\mathcal{A}, \mathcal{Z}}^{\mathfrak{s}})$ and $x \in T_{\mathcal{A}, \mathcal{Z}}$.

Theorem 4.18. Every \mathcal{A} -translationally invariant crystal-operator

$$L : \mathcal{L}(T_{\mathcal{A}, \mathcal{Z}}^{\mathfrak{s}}) \rightarrow \mathcal{L}(T_{\mathcal{A}, \mathcal{Z}}^{\mathfrak{t}})$$

is a multiplication operator and vice versa.

Proof. It is easy to see that a multiplication operator L with multipliers $m_L^{(y)} \in \mathbb{C}^{n \times m}$ is translationally invariant. We have

$$(\mathbb{T}_a Lf)(x) = (Lf)(x + a) = \sum_{y \in \mathbb{L}} m_L^{(y)} f(x + a + y)$$

as well as

$$(L\mathbb{T}_a f)(x) = \sum_{y \in \mathbb{L}} m_L^{(y)} (\mathbb{T}_a f)(x + y) = \sum_{y \in \mathbb{L}} m_L^{(y)} f(x + a + y).$$

In order to see that a translationally invariant operator is a multiplication operator we make use of the Fourier transform

$$f(\cdot) = \frac{1}{\sqrt{|T_{\mathcal{A}, \mathcal{Z}}|}} \sum_{k \in T_{\mathcal{A}, \mathcal{Z}}^*} \hat{f}(k) e^{2\pi i \langle k, \cdot \rangle_2} \in \mathcal{L}(T_{\mathcal{A}, \mathcal{Z}}^{\mathfrak{s}})$$

with

$$\hat{f}(\cdot) = \frac{1}{\sqrt{|T_{\mathcal{A}, \mathcal{Z}}|}} \sum_{x \in T_{\mathcal{A}, \mathcal{Z}}} f(x) e^{-2\pi i \langle \cdot, x \rangle_2} \in \mathcal{L}((T_{\mathcal{A}, \mathcal{Z}}^{\mathfrak{s}})^*) = \mathcal{L}((T_{\mathcal{A}, \mathcal{Z}})^*, \mathbb{C}^m)$$

to obtain

$$\begin{aligned} (\mathcal{F}\mathbb{T}_a f)(\hat{k}) &= \mathcal{F} \left(\frac{1}{\sqrt{|T_{\mathcal{A}, \mathcal{Z}}|}} \sum_{k \in T_{\mathcal{A}, \mathcal{Z}}^*} \hat{f}(k) e^{2\pi i \langle k, \cdot + a \rangle_2} \right) (\hat{k}) \\ &= \frac{1}{|T_{\mathcal{A}, \mathcal{Z}}|} \sum_{x \in T_{\mathcal{A}, \mathcal{Z}}} \left(\sum_{k \in T_{\mathcal{A}, \mathcal{Z}}^*} \hat{f}(k) e^{2\pi i \langle k, x + a \rangle_2} e^{-2\pi i \langle \hat{k}, x \rangle_2} \right) \\ &= e^{2\pi i \langle \hat{k}, a \rangle_2} \frac{1}{|T_{\mathcal{A}, \mathcal{Z}}|} \sum_{k \in T_{\mathcal{A}, \mathcal{Z}}^*} \left(\hat{f}(k) \sum_{x \in T_{\mathcal{A}, \mathcal{Z}}} e^{2\pi i \langle k - \hat{k}, x + a \rangle_2} \right) \\ &= e^{2\pi i \langle \hat{k}, a \rangle_2} \sum_{k \in T_{\mathcal{A}, \mathcal{Z}}^*} (\hat{f}(k) \delta_{\hat{k}k}) \\ &= e^{2\pi i \langle \hat{k}, a \rangle_2} (\mathcal{F}f)(\hat{k}) = e^{2\pi i \langle \hat{k}, a \rangle_2} \hat{f}(\hat{k}). \end{aligned} \tag{4.2}$$

Furthermore there exist numbers $\alpha_k^{j,\zeta} \in \mathbb{C}$ due to Theorem 4.16 such that

$$L_j e_{\zeta,k} = \alpha_k^{j,\zeta} e^{2\pi i \langle k, \cdot \rangle_2} \quad (4.3)$$

for each j , and

$$\begin{aligned} f(x) &= \frac{1}{\sqrt{|T_{\mathcal{A},\mathcal{Z}}|}} \sum_{k \in T_{\mathcal{A},\mathcal{Z}}^*} \hat{f}(k) e^{2\pi i \langle k, x \rangle_2} \\ &= \frac{1}{\sqrt{|T_{\mathcal{A},\mathcal{Z}}|}} \sum_{k \in T_{\mathcal{A},\mathcal{Z}}^*} (\hat{f}_1(k), \dots, \hat{f}_m(k)) e^{2\pi i \langle k, x \rangle_2} \\ &= \frac{1}{\sqrt{|T_{\mathcal{A},\mathcal{Z}}|}} \sum_{k \in T_{\mathcal{A},\mathcal{Z}}^*} \sum_{\zeta=1}^m e_{\zeta,k}(x) \hat{f}_{\zeta}(k). \end{aligned} \quad (4.4)$$

Using equations (4.2) to (4.4) we find

$$\begin{aligned} (L_j f)(x) &= \frac{1}{\sqrt{|T_{\mathcal{A},\mathcal{Z}}|}} \sum_{k \in T_{\mathcal{A},\mathcal{Z}}^*} \sum_{\zeta=1}^m L_j e_{\zeta,k}(x) \hat{f}_{\zeta}(k) \\ &= \frac{1}{\sqrt{|T_{\mathcal{A},\mathcal{Z}}|}} \sum_{k \in T_{\mathcal{A},\mathcal{Z}}^*} \sum_{\zeta=1}^m \alpha_k^{j,\zeta} e^{2\pi i \langle k, x \rangle_2} \hat{f}_{\zeta}(k) \\ &= \frac{1}{\sqrt{|T_{\mathcal{A},\mathcal{Z}}|}} \sum_{k \in T_{\mathcal{A},\mathcal{Z}}^*} \sum_{\zeta=1}^m \alpha_k^{j,\zeta} (\mathcal{F} \mathbb{T}_x f_{\zeta})(k) \\ &= \frac{1}{\sqrt{|T_{\mathcal{A},\mathcal{Z}}|}} \sum_{k \in T_{\mathcal{A},\mathcal{Z}}^*} \sum_{\zeta=1}^m \alpha_k^{j,\zeta} (\mathcal{F} f_{\zeta}(\cdot + x))(k) \\ &= \frac{1}{\sqrt{|T_{\mathcal{A},\mathcal{Z}}|}} \sum_{k \in T_{\mathcal{A},\mathcal{Z}}^*} \sum_{\zeta=1}^m \alpha_k^{j,\zeta} \sum_{y \in T_{\mathcal{A},\mathcal{Z}}} f_{\zeta}(y + x) e^{-2\pi i \langle k, y \rangle_2} \\ &= \sum_{y \in T_{\mathcal{A},\mathcal{Z}}} \sum_{\zeta=1}^m f_{\zeta}(y + x) \left(\frac{1}{\sqrt{|T_{\mathcal{A},\mathcal{Z}}|}} \sum_{k \in T_{\mathcal{A},\mathcal{Z}}^*} \alpha_k^{j,\zeta} e^{-2\pi i \langle k, y \rangle_2} \right). \end{aligned}$$

Now, using colon notation², we have

$$(L_j f)(x) = \sum_{y \in T_{\mathcal{A},\mathcal{Z}}} (m_L^{(y)})_{j,:} f(x + y)$$

with

$$(m_L^{(y)})_{j,:} = \frac{1}{\sqrt{|T_{\mathcal{A},\mathcal{Z}}|}} \sum_{k \in T_{\mathcal{A},\mathcal{Z}}^*} e^{-2\pi i \langle k, y \rangle_2} (\alpha_k^{j,1}, \dots, \alpha_k^{j,m})$$

and we are able to rewrite the application of L by

$$(L f)(x) = (L_1 f, \dots, L_n f)$$

² $A_{i,:}$ refers to row i , $A_{:,j}$ refers to column j of a matrix A .

$$\begin{aligned}
 &= \sum_{y \in T_{\mathcal{A}, \mathcal{Z}}} ((m_L^{(y)})_{1, \cdot} f(x+y), \dots, (m_L^{(y)})_{n, \cdot} f(x+y)) \\
 &= \sum_{y \in T_{\mathcal{A}, \mathcal{Z}}} \begin{bmatrix} (m_L^{(y)})_{1,1} & \dots & (m_L^{(y)})_{1,m} \\ \vdots & \ddots & \vdots \\ (m_L^{(y)})_{n,1} & \dots & (m_L^{(y)})_{n,m} \end{bmatrix} \begin{bmatrix} f_1(x+y) \\ \vdots \\ f_m(x+y) \end{bmatrix} \\
 &= \sum_{y \in T_{\mathcal{A}, \mathcal{Z}}} m_L^{(y)} f(x+y). \quad \square
 \end{aligned}$$

Due to the fact that the subspaces H_k are L -invariant, we can easily represent any \mathcal{A} -translationally invariant operator via its *symbols*.

Definition 4.19. Let $L : \mathcal{L}(T_{\mathcal{A}, \mathcal{Z}}^{\mathfrak{s}}) \rightarrow \mathcal{L}(T_{\mathcal{A}, \mathcal{Z}}^{\mathfrak{t}})$ be a multiplication operator with

$$(Lf)(x) = \sum_{y \in T_{\mathcal{A}, \mathcal{Z}}} m_L^{(y)} f(x+y), \quad m_L^{(y)} \in \mathbb{C}^{|\mathfrak{t}| \times |\mathfrak{s}|}.$$

We define the symbol of L by

$$L_k := \sum_{y \in T_{\mathcal{A}, \mathcal{Z}}} m_L^{(y)} m_k^{(y)} \quad \text{with } m_k^{(y)} := e^{2\pi i \langle k, y \rangle}.$$

In case $\mathfrak{s} = \mathfrak{t}$ the spectrum of L can then be extracted from its symbols L_k .

Corollary 4.20. Let $L : \mathcal{L}(T_{\mathcal{A}, \mathcal{Z}}^{\mathfrak{s}}) \rightarrow \mathcal{L}(T_{\mathcal{A}, \mathcal{Z}}^{\mathfrak{s}})$ be a multiplication operator with

$$(Lf)(x) = \sum_{y \in T_{\mathcal{A}, \mathcal{Z}}} m_L^{(y)} f(x+y), \quad m_L^{(y)} \in \mathbb{C}^{|\mathfrak{s}| \times |\mathfrak{s}|}.$$

Then $\text{spec}(L) = \cup_{k \in T_{\mathcal{A}, \mathcal{Z}}^*} \text{spec}(L_k)$.

Proof. Follows immediately due to the orthonormality of the basis $e_{\ell, k}$ (cf. Theorem 4.4) and the L -invariance of the subspaces H_k (cf. Theorem 4.16). \square

Remark 4.21. As already stated in the beginning of this chapter, the main purpose of \mathcal{Z} , i.e., the set of primitive vectors that define an arbitrary sublattice $\mathbb{L}(\mathcal{Z})$ of $\mathbb{L}(\mathcal{A})$, is to simplify the theory developed in Section 4.2 by turning an infinite dimensional setting (a crystal $\mathbb{L}^{\mathfrak{s}}(\mathcal{A})$) to an (arbitrarily large) finite one (a crystal tori $T_{\mathcal{A}, \mathcal{Z}}^{\mathfrak{s}}$). Then, in Corollary 4.20 \mathcal{Z} explicitly specifies the resolution of the frequency space as seen in Figure 3.4, i.e.,

$$T_{\mathcal{A}, \mathcal{Z}}^* = \mathbb{L}(\mathcal{Z}^{-T}) \cap \mathcal{P}(\mathcal{A}^{-T}),$$

where the spectrum of the multiplication operator is sampled. Due to the reciprocal nature of the dual space, the larger $|\det(\mathcal{Z})|$ is, the finer the resolution becomes. This corresponds to a one-to-one link to a finite domain with periodic boundary conditions.

We illustrate these results with an example.

Example 4.1. Consider the discrete Laplacian (cf. Example 1.1) on $T_{\mathcal{A},\mathcal{Z}}^{\mathfrak{s}}$ with

$$\mathcal{Z} = \left[\begin{array}{c|c} 1 & 0 \\ \hline 0 & 1 \end{array} \right], \quad \mathcal{A} = h\mathcal{Z} = \left[\begin{array}{c|c} a_1 & a_2 \\ \hline & \end{array} \right], \quad h \in \frac{1}{N} \text{ and } \mathfrak{s} = (0),$$

given by $\mathbf{L}[\mathcal{A},\mathfrak{s}] : \mathcal{L}(T_{\mathcal{A},\mathcal{Z}}^{\mathfrak{s}}) \rightarrow \mathcal{L}(T_{\mathcal{A},\mathcal{Z}}^{\mathfrak{s}})$ with nonzero multipliers:

$$\begin{aligned} m_{\mathbf{L}[\mathcal{A},\mathfrak{s}]}^{(a_1)} &= -\frac{1}{h^2} \\ m_{\mathbf{L}[\mathcal{A},\mathfrak{s}]}^{(-a_2)} &= -\frac{1}{h^2} & m_{\mathbf{L}[\mathcal{A},\mathfrak{s}]}^{(0)} &= \frac{4}{h^2} & m_{\mathbf{L}[\mathcal{A},\mathfrak{s}]}^{(a_2)} &= -\frac{1}{h^2} \\ m_{\mathbf{L}[\mathcal{A},\mathfrak{s}]}^{(-a_1)} &= -\frac{1}{h^2} \end{aligned}$$

A plot of this stencil is given in Figure 4.2a. We can compute its symbol according to Definition 4.19:

$$\begin{aligned} (\mathbf{L}[\mathcal{A},\mathfrak{s}])_k &= \frac{1}{h^2} (4 - e^{2\pi i k_1} - e^{-2\pi i k_1} - e^{2\pi i k_2} - e^{-2\pi i k_2}) \\ &= \frac{2}{h^2} (2 - \cos(2\pi k_1) - \cos(2\pi k_2)). \end{aligned}$$

The complete spectrum $\text{spec}(\mathbf{L}[\mathcal{A},\mathfrak{s}])$ is given by the set of all scalar symbols $(\mathbf{L}[\mathcal{A},\mathfrak{s}])_k$ with

$$k \in (T_{\mathcal{A},\mathcal{Z}}^{\mathfrak{s}})^* = \mathcal{P}(\mathcal{B}^{(1)}) \cap \mathbb{Z}^2 = \mathcal{B}^{(1)}[0,1]^2 \cap \mathbb{Z}^2, \quad \mathcal{B}^{(1)} = \mathcal{A}^{-T} = \left[\begin{array}{c|c} h & 0 \\ \hline 0 & h \end{array} \right],$$

cf. Corollary 4.20. Thus, the spectrum can be plotted with respect to the wavevector $k \in T_{\mathcal{A},\mathcal{Z}}^*$ as shown in Figure 4.2b. In here, we used a spacing of $h = 1/64$ resulting in 64^2 symbols or eigenvalues.

Remark 4.22. The symbol L_k of a multiplication operator $L : \mathcal{L}(T_{\mathcal{C},\mathcal{Z}}^{\mathfrak{u}}) \rightarrow \mathcal{L}(T_{\mathcal{C},\mathcal{Z}}^{\mathfrak{u}})$, $\mathfrak{s} = (\mathfrak{u}_1, \dots, \mathfrak{u}_r)$, is the transformation matrix of the linear transformation $L|_{H_k} : H_k \rightarrow H_k$ with respect to the ordered basis $[e_{1,k} \ e_{2,k} \ \dots \ e_{r,k}]$ of H_k , cf. Theorem 4.4. The computation of this symbol is particularly easy as it is simply the sum over all multipliers $m_L^{(y)}$ times a specific phase in dependence of the position y .

Recall Theorem 4.8, i.e., let $T_{\mathcal{A},\mathcal{Z}}^{\mathfrak{s}} \cong T_{\mathcal{C},\mathcal{Z}}^{\mathfrak{u}}$ be two representations of one crystal with $\mathbb{L}(\mathcal{C}) \subset \mathbb{L}(\mathcal{A})$, $\mathfrak{s} = (\mathfrak{s}_1, \dots, \mathfrak{s}_m)$, $\mathfrak{t} = (\mathfrak{t}_1, \dots, \mathfrak{t}_p) \cong T_{\mathcal{A},\mathcal{C}}$ and $(\mathfrak{u}_1, \dots, \mathfrak{u}_{mp}) = (\mathfrak{t}_1 + \mathfrak{s}, \dots, \mathfrak{t}_p + \mathfrak{s})$. Then, another ordered orthonormal basis E of H_k is given by Theorem 4.8. The symbol of $L|_{H_k}$ with respect to this new basis is then given by $\hat{L}_k = E^{-1}L_kE$. This change of basis plays an important role in the so-called smoothing analysis which we are going to use in Section 5.5. Note, that in case the underlying operator L is \mathcal{A} -translationally invariant, the matrix \hat{L}_k is block diagonal.

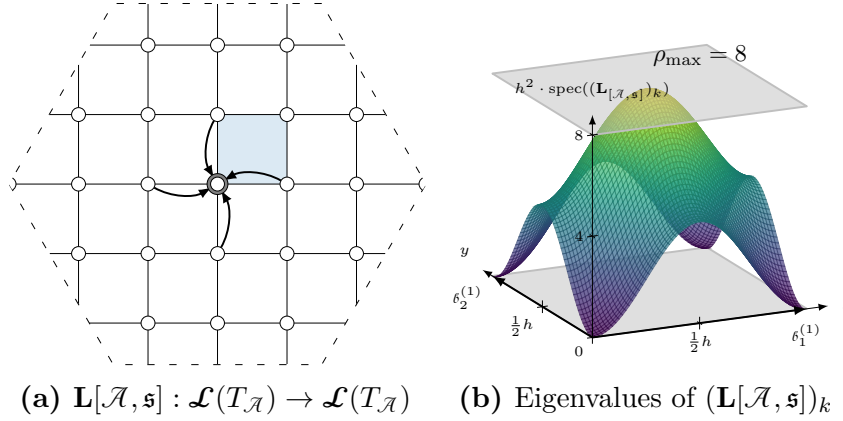


Figure 4.2.: (a) A schematic representation of the discrete Laplacian $\mathbf{L}[\mathcal{A}, \mathfrak{s}]$. (b) A plot of its spectrum with respect to $k \in (T_{\mathcal{A}, \mathcal{Z}})^*$.

4.3. Automated Local Fourier Analysis (aLFA)

Up to now we introduced notation and derived some general statements about individual multiplication or translationally invariant operators. Using this, we are able to fully analyze a single multiplication operator. However, we are often interested in analyzing a composition of several operators using LFA. Such a composition of operators typically corresponds to an *error propagator* of an iterative method as we will see in Chapter 5. In this section we deal with compositions of multiplication operators in two steps.

First, we give rules of computation on the level of multiplication operators and on the level of their symbols under the condition that the corresponding domains and codomains are compatible.

Second, we derive statements to automatically make codomains and domains compatible in order to allow for a user friendly description of all occurring operators. That is, it should be possible to describe operators in terms of their individual translational invariance and ordering of the structure element without having to worry about compatibility issues with other operators on the input level of the analysis. These statements make up a large part of the automation process of this framework. The algorithms corresponding to these statements are listed in Appendix A.

Compositions of multiplication operators

Calculus of multiplication operators plays a key-role in local Fourier analysis. In this section we list all elementary operations, such as addition and multiplication. As long as the corresponding domains and codomains of multiplication

operators are identical we can use the following rules of computation on the level of multiplication operators.

Lemma 4.23. *Let two multiplication operators be given by*

$$\begin{aligned} L : \mathcal{L}(T_{\mathcal{A}, \mathcal{Z}}^{\mathfrak{s}}) &\rightarrow \mathcal{L}(T_{\mathcal{A}, \mathcal{Z}}^{\mathfrak{t}}), & (Lf)(x) &= \sum_{y \in T_{\mathcal{A}, \mathcal{Z}}} m_L^{(y)} f(x+y), & m_L^{(y)} &\in \mathbb{C}^{|\mathfrak{t}| \times |\mathfrak{s}|}, \\ G : \mathcal{L}(T_{\mathcal{A}, \mathcal{Z}}^{\mathfrak{u}}) &\rightarrow \mathcal{L}(T_{\mathcal{A}, \mathcal{Z}}^{\mathfrak{v}}), & (Gf)(x) &= \sum_{y \in T_{\mathcal{A}, \mathcal{Z}}} m_G^{(y)} f(x+y), & m_G^{(y)} &\in \mathbb{C}^{|\mathfrak{v}| \times |\mathfrak{u}|}. \end{aligned}$$

Then the following operators are multiplication operators as well:

- (i) If $\mathfrak{s} = \mathfrak{u}$ and $\mathfrak{t} = \mathfrak{v}$, then $L + G : \mathcal{L}(T_{\mathcal{A}, \mathcal{Z}}^{\mathfrak{s}}) \rightarrow \mathcal{L}(T_{\mathcal{A}, \mathcal{Z}}^{\mathfrak{t}})$ with $m_{L+G}^{(y)} = m_L^{(y)} + m_G^{(y)}$.
- (ii) If $\mathfrak{v} = \mathfrak{s}$, then $L \cdot G : \mathcal{L}(T_{\mathcal{A}, \mathcal{Z}}^{\mathfrak{u}}) \rightarrow \mathcal{L}(T_{\mathcal{A}, \mathcal{Z}}^{\mathfrak{t}})$ with $m_{L \cdot G}^{(z)} = \sum_{y+w=z} m_L^{(y)} \cdot m_G^{(w)}$.
- (iii) The adjoint is given by $L^* : \mathcal{L}(T_{\mathcal{A}, \mathcal{Z}}^{\mathfrak{t}}) \rightarrow \mathcal{L}(T_{\mathcal{A}, \mathcal{Z}}^{\mathfrak{s}})$ with $m_{L^*}^{(y)} = (m_L^{(-y)})^*$.

Proof. Straight-forward calculation yields:

- (i)
$$\begin{aligned} (Lf)(x) + (Gf)(x) &= \sum_y m_L^{(y)} f(x+y) + \sum_y m_G^{(y)} f(x+y) \\ &= \sum_y (m_L^{(y)} + m_G^{(y)}) f(x+y). \end{aligned}$$
- (ii)
$$\begin{aligned} [L(Gf)](x) &= \sum_y m_L^{(y)} \sum_w m_G^{(w)} f(x+y+w) \\ &= \sum_z \left[\sum_{y+w=z} m_L^{(y)} m_G^{(w)} \right] f(x+z). \end{aligned}$$
- (iii) L^* is the unique operator such that $\langle Lf, g \rangle = \langle f, L^*g \rangle$ for all value distributions $f \in \mathcal{L}(T_{\mathcal{A}, \mathcal{Z}}^{\mathfrak{s}})$, $g \in \mathcal{L}(T_{\mathcal{A}, \mathcal{Z}}^{\mathfrak{t}})$. Thus,

$$\begin{aligned} |T_{\mathcal{A}, \mathcal{Z}}| \cdot \langle Lf, g \rangle &= \sum_{x \in T_{\mathcal{A}, \mathcal{Z}}} \sum_{y \in T_{\mathcal{A}, \mathcal{Z}}} \langle m_L^{(y)} f(x+y), g(x) \rangle_2 \\ &= \sum_{x \in T_{\mathcal{A}, \mathcal{Z}}} \sum_{y \in T_{\mathcal{A}, \mathcal{Z}}} \langle f(x+y), (m_L^{(y)})^* g(x+y-y) \rangle_2 \\ &= \sum_{z \in T_{\mathcal{A}, \mathcal{Z}}} \langle f(z), \sum_{w \in T_{\mathcal{A}, \mathcal{Z}}} (m_L^{(-w)})^* g(z+w) \rangle_2 \\ &= \sum_{z \in T_{\mathcal{A}, \mathcal{Z}}} \langle f(z), \sum_{w \in T_{\mathcal{A}, \mathcal{Z}}} m_{L^*}^{(w)} g(z+w) \rangle_2 \\ &= |T_{\mathcal{A}, \mathcal{Z}}| \cdot \langle f, L^*g \rangle. \end{aligned}$$

□

We further show computation rules on the level of symbols (cf. Definition 4.19). While computing the sum, a product and taking the transpose can easily be done on both levels, taking the (pseudo-)inverse is simple only on the level of symbols. The (pseudo-)inverse of a multiplication operator may have an arbitrarily large number³ of multipliers $m_{L^{-1}}^{(y)} \neq 0$ and thus there is no simple rule to compute it.

Theorem 4.24. *Let two multiplication operators be given by*

$$\begin{aligned} L : \mathcal{L}(T_{\mathcal{A}, \mathcal{Z}}^{\mathfrak{s}}) &\rightarrow \mathcal{L}(T_{\mathcal{A}, \mathcal{Z}}^{\mathfrak{t}}), & (Lf)(x) &= \sum_{y \in T_{\mathcal{A}, \mathcal{Z}}} m_L^{(y)} f(x+y), & m_L^{(y)} &\in \mathbb{C}^{|\mathfrak{t}| \times |\mathfrak{s}|}, \\ G : \mathcal{L}(T_{\mathcal{A}, \mathcal{Z}}^{\mathfrak{u}}) &\rightarrow \mathcal{L}(T_{\mathcal{A}, \mathcal{Z}}^{\mathfrak{v}}), & (Gf)(x) &= \sum_{y \in T_{\mathcal{A}, \mathcal{Z}}} m_G^{(y)} f(x+y), & m_G^{(y)} &\in \mathbb{C}^{|\mathfrak{v}| \times |\mathfrak{u}|} \end{aligned}$$

with corresponding symbols L_k and G_k . Then we have the following statements.

- (i) Assuming that $\mathfrak{s} = \mathfrak{u}$ and $\mathfrak{t} = \mathfrak{v}$, the symbols of $L + G$ are given by $L_k + G_k$.
- (ii) Assuming that $\mathfrak{v} = \mathfrak{s}$, the symbols of $L \cdot G$ are given by $L_k \cdot G_k$.
- (iii) The symbols of L^* are given by L_k^* .
- (iv) If $L|_{H_k}$ is nonsingular, then the symbol $((L|_{H_k})^{-1})_k$ is given by $(L_k)^{-1}$.

Proof. Let $e_k(x)$ denote an arbitrary value distribution in H_k . That is, given $\alpha_1, \dots, \alpha_m \in \mathbb{C}$ we have

$$e_k(x) = \sum_{\ell} \alpha_{\ell} e_{\ell, k} = (\alpha_1 e^{2\pi i \langle k, x + \mathfrak{s}_1 \rangle}, \dots, \alpha_m e^{2\pi i \langle k, x + \mathfrak{s}_m \rangle})^T \in \text{span}(H_k).$$

Using Lemma 4.23 we obtain by direct calculation:

- (i) $(L^* e_k)(x) = \sum_y (m_L^{(-y)})^* e_k(x+y) = \left(\sum_{-y} m_L^{(y)} m_k^{(y)} \right)^* e_k(x) = L_k^* e_k(x)$.
- (ii) $(L G e_k)(x) = \left(\sum_y m_L^{(y)} m_k^{(y)} \right) \left(\sum_w m_G^{(w)} m_k^{(w)} \right) e_k(x) = L_k G_k e_k(x)$.
- (iii) $((L + G) e_k)(x) = \sum_y m_L^{(y)} e_k(x+y) + \sum_y m_G^{(y)} e_k(x+y) = (L_k + G_k) e_k(x)$.
- (iv) Follows immediately from $e_k(x) = L_k (L^{-1})_k e_k(x) = (L^{-1})_k L_k e_k(x)$. \square

³Bounded by the number of lattice points on the (arbitrarily large) torus.

Crystal representations, natural isomorphisms and similarity transformations

In general, we are given several multiplication operators, each defined with respect to their own (minimal) translational invariance. In order to analyze such a composition we thus need to find a common denominator, i.e., a lattice basis corresponding to the collective translational invariance, and rewrite the operators accordingly. Such a (smallest) common denominator is given by Theorem 3.6.

Given a multiplication operator defined on some crystal, a change of the representation of a crystal turns out to be a similarity transformation. In the following we work out such transformations using the natural isomorphism η of function spaces introduced in Definition 4.6.

Theorem 4.25 (Rewriting an operator with respect to a sublattice). *Consider crystals $\mathbb{L}^{\mathfrak{d}}(\mathcal{A})$, $\mathbb{L}^{\mathfrak{c}}(\mathcal{A})$, a sublattice $\mathbb{L}(\mathcal{C}) \subset \mathbb{L}(\mathcal{A})$ and a multiplication operator*

$$L : \mathcal{L}(T_{\mathcal{A}}^{\mathfrak{d}}) \rightarrow \mathcal{L}(T_{\mathcal{A}}^{\mathfrak{c}}), \quad (Lf)(x) := \sum_{y \in T_{\mathcal{A}}} m_L^{(y)} f(x + y), \quad m_L^{(y)} \in \mathbb{C}^{|\mathfrak{c}| \times |\mathfrak{d}|}.$$

Then, using $T_{\mathcal{A}, \mathcal{C}} = \{\mathfrak{t}_1, \dots, \mathfrak{t}_p\}$, the multiplication operator

$$(Gg)(x) = \sum_{y \in T_{\mathcal{C}}} m_G^{(y)} g(x + y), \quad m_G^{(y)} \in \mathbb{C}^{p|\mathfrak{c}| \times p|\mathfrak{d}|}$$

with block matrices $(m_G^{(y)})_{i,k} := m_L^{(y - \mathfrak{t}_i + \mathfrak{t}_k)} \in \mathbb{C}^{|\mathfrak{c}| \times |\mathfrak{d}|}$ fulfills the commutative diagram:

$$\begin{array}{ccc} \mathcal{L}(T_{\mathcal{A}}^{\mathfrak{d}}) & \xrightarrow{L} & \mathcal{L}(T_{\mathcal{A}}^{\mathfrak{c}}) \\ \downarrow \eta^{\mathfrak{d}} & & \downarrow \eta^{\mathfrak{c}} \\ \mathcal{L}(T_{\mathcal{C}}^{\hat{\mathfrak{d}}}) & \xrightarrow{G} & \mathcal{L}(T_{\mathcal{C}}^{\hat{\mathfrak{c}}}). \end{array}$$

Here, the mappings for $\mathfrak{s} \in \{\mathfrak{d}, \mathfrak{c}\}$,

$$\eta^{\mathfrak{s}} : \mathcal{L}(T_{\mathcal{A}}^{\mathfrak{s}}) \rightarrow \mathcal{L}(T_{\mathcal{C}}^{\hat{\mathfrak{s}}}), \quad f(\cdot) \mapsto (f(\cdot + \mathfrak{t}_1), \dots, f(\cdot + \mathfrak{t}_p)),$$

denote the natural isomorphisms between the congruent crystal representations.

Proof. A straightforward calculation for each block-row i yields

$$\begin{aligned} [(\eta^{\mathfrak{c}} Lf)(x)]_i &= (Lf)(x + \mathfrak{t}_i) = \sum_{k=1}^p \sum_{y \in T_{\mathcal{C}}} m_L^{(y + \mathfrak{t}_k)} f(x + y + \mathfrak{t}_i + \mathfrak{t}_k) \\ &= \sum_{k=1}^p \sum_{y \in T_{\mathcal{C}}} m_L^{(y - \mathfrak{t}_i + \mathfrak{t}_k)} f(x + y + \mathfrak{t}_k) \\ &= \sum_{y \in T_{\mathcal{C}}} \sum_{k=1}^p (m_G^{(y)})_{i,k} f(x + y + \mathfrak{t}_k) \\ &= [G(f(x + \mathfrak{t}_1), \dots, f(x + \mathfrak{t}_p))]_i = [(G\eta^{\mathfrak{d}} f)(x)]_i. \end{aligned} \quad \square$$

We illustrate this theorem with an example.

Example 4.2. We now express the discrete Laplacian $\mathbf{L}[\mathcal{A}, \mathfrak{s}] : \mathcal{L}(T_{\mathcal{A}, \mathcal{Z}}^{\mathfrak{s}}) \rightarrow \mathcal{L}(T_{\mathcal{A}, \mathcal{Z}}^{\mathfrak{s}})$, already introduced and analyzed in Example 4.1, with respect to the sublattice

$$\mathbb{L}(\mathcal{C}) \subset \mathbb{L}(\mathcal{A}), \quad \mathcal{C} = \left[\begin{array}{c|c} \mathbf{a}_1 + \mathbf{a}_2 & \mathbf{a}_1 - \mathbf{a}_2 \end{array} \right] = \left[\begin{array}{c|c} c_1 & c_2 \end{array} \right].$$

The structure element $\widehat{\mathfrak{s}} := (0, \mathbf{a}_1) \cong T_{\mathcal{A}, \mathcal{C}}^{\mathfrak{s}}$, which fulfills $T_{\mathcal{A}, \mathcal{Z}}^{\mathfrak{s}} \cong T_{\mathcal{C}, \mathcal{Z}}^{\widehat{\mathfrak{s}}}$, consists of two points depicted as gray and white circles in Figure 4.3a. We have

$$\mathbf{L}[\mathcal{C}, \widehat{\mathfrak{s}}] = \eta \mathbf{L}[\mathcal{A}, \mathfrak{s}] \eta^{-1} : \mathcal{L}(T_{\mathcal{C}, \mathcal{Z}}^{\widehat{\mathfrak{s}}}) \rightarrow \mathcal{L}(T_{\mathcal{C}, \mathcal{Z}}^{\widehat{\mathfrak{s}}}), \quad \eta : \mathcal{L}(T_{\mathcal{A}, \mathcal{Z}}^{\mathfrak{s}}) \rightarrow \mathcal{L}(T_{\mathcal{C}, \mathcal{Z}}^{\widehat{\mathfrak{s}}}),$$

with nonzero multipliers:

$$\begin{aligned} m_{\mathbf{L}[\mathcal{C}, \widehat{\mathfrak{s}}]}^{(-c_2)} &= \frac{1}{h^2} \begin{bmatrix} 0 & -1 \\ 0 & 0 \end{bmatrix} & m_{\mathbf{L}[\mathcal{C}, \widehat{\mathfrak{s}}]}^{(c_1)} &= \frac{1}{h^2} \begin{bmatrix} 0 & 0 \\ -1 & 0 \end{bmatrix} \\ m_{\mathbf{L}[\mathcal{C}, \widehat{\mathfrak{s}}]}^{(-c_1-c_2)} &= \frac{1}{h^2} \begin{bmatrix} 0 & -1 \\ 0 & 0 \end{bmatrix} & m_{\mathbf{L}[\mathcal{C}, \widehat{\mathfrak{s}}]}^{(0)} &= \frac{1}{h^2} \begin{bmatrix} 4 & -1 \\ -1 & 4 \end{bmatrix} & m_{\mathbf{L}[\mathcal{C}, \widehat{\mathfrak{s}}]}^{(c_1+c_2)} &= \frac{1}{h^2} \begin{bmatrix} 0 & 0 \\ -1 & 0 \end{bmatrix} \\ m_{\mathbf{L}[\mathcal{C}, \widehat{\mathfrak{s}}]}^{(-c_1)} &= \frac{1}{h^2} \begin{bmatrix} 0 & -1 \\ 0 & 0 \end{bmatrix} & m_{\mathbf{L}[\mathcal{C}, \widehat{\mathfrak{s}}]}^{(c_2)} &= \frac{1}{h^2} \begin{bmatrix} 0 & 0 \\ -1 & 0 \end{bmatrix} \end{aligned}$$

The application of this operator reads as

$$\begin{aligned} \mathbf{L}[\mathcal{C}, \widehat{\mathfrak{s}}] \Psi(x) &= \frac{1}{h^2} \left[\begin{array}{c} \begin{bmatrix} 4 & -1 \\ -1 & 4 \end{bmatrix} \Psi(x) \\ + \begin{bmatrix} 0 & -1 \\ 0 & 0 \end{bmatrix} [\Psi(x - c_1) + \Psi(x - c_2) + \Psi(x - c_1 - c_2)] \\ + \begin{bmatrix} 0 & 0 \\ -1 & 0 \end{bmatrix} [\Psi(x + c_1) + \Psi(x + c_2) + \Psi(x + c_1 + c_2)] \end{array} \right]. \end{aligned}$$

for each function $\Psi(x) = \begin{bmatrix} u(x) \\ u(x + \mathbf{a}_1) \end{bmatrix} \in \mathcal{L}(T_{\mathcal{C}, \mathcal{Z}}^{\widehat{\mathfrak{s}}})$. A schematic plot of this representation is given in Figure 4.3a. According to Definition 4.19, its symbol is given by

$$(\mathbf{L}[\mathcal{C}, \widehat{\mathfrak{s}}])_k = \frac{1}{h^2} \begin{bmatrix} 4 & \overline{\gamma}_k \\ \gamma_k & 4 \end{bmatrix}, \quad \gamma_k = -1 - e^{4\pi i k_1} - e^{4\pi i k_2} - e^{4\pi i (k_1 + k_2)},$$

with

$$k \in \mathcal{P}(\mathcal{B}^{(2)}) \cap \mathbb{Z}^2, \quad \mathcal{B}^{(2)} = \mathcal{C}^{-T} = \begin{bmatrix} 1/2 & 1/2 \\ 1/2 & -1/2 \end{bmatrix} h.$$

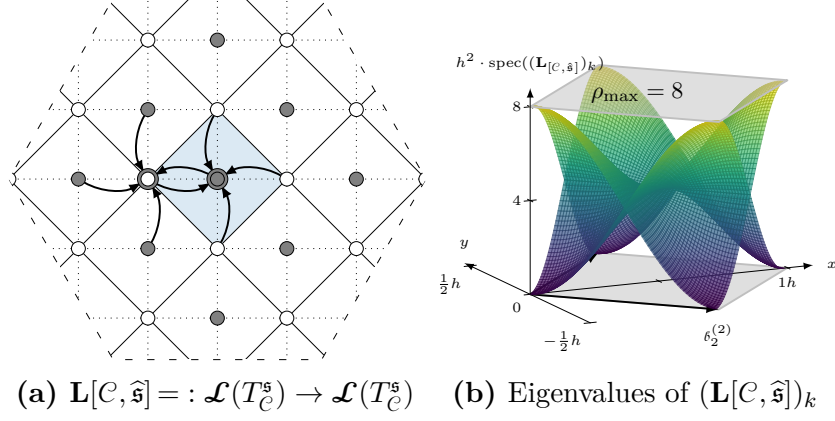


Figure 4.3.: (a) A schematic representation of the discrete Laplacian with respect to another representation of the underlying crystal. (b) A plot of its spectrum plotted along $\mathcal{P}(\mathcal{B}^{(2)})$, $\mathcal{B}^{(2)} = \mathcal{C}^{-T}$.

In contrast to Example 4.1, this symbol now has two eigenvalues instead of one, resulting in two surfaces plotted along the primitive cell $\mathcal{P}(\mathcal{B}^{(2)})$ in Figure 4.3b, which is half the size of $\mathcal{P}(\mathcal{B}^{(1)})$. This plot illustrates once more that coarsening in position space corresponds to a superimposition in frequency space as already worked out in Theorem 4.8. One can obtain the plot of $(\mathbf{L}[\mathcal{A}, \widehat{\mathfrak{s}}])_k$, given in Figure 4.2b, from the plot of $(\mathbf{L}[C, \widehat{\mathfrak{s}}])_k$, given in Figure 4.3b, by disassembling the two surfaces into several pieces and shifting them along integral multiples of $b_1^{(2)}$ and $b_2^{(2)}$.

Example 4.3. The system matrix

$$A = \frac{1}{h^2} \begin{bmatrix} B & -I & & -I \\ -I & B & \ddots & \\ & \ddots & \ddots & -I \\ -I & & -I & B \end{bmatrix}$$

of Example 1.1 is obtained by a transformation of the discrete Laplacian $\mathbf{L}[\mathcal{A}, \widehat{\mathfrak{s}}]$ to the coarsest possible crystal interpretation $\mathbf{L}[\mathcal{Z}, T_{\mathcal{A}, \mathcal{Z}}^{\mathfrak{s}}]$, i.e., the underlying lattice torus consists of a single lattice point whereas the structure element contains all unknowns. This operator $\mathbf{L}[\mathcal{Z}, T_{\mathcal{A}, \mathcal{Z}}^{\mathfrak{s}}]$ fulfills the following commutative diagram

$$\begin{array}{ccc} \mathcal{L}(T_{\mathcal{A}, \mathcal{Z}}) & \xrightarrow{\mathbf{L}[\mathcal{A}, \widehat{\mathfrak{s}}]} & \mathcal{L}(T_{\mathcal{A}, \mathcal{Z}}) \\ \downarrow \eta & & \downarrow \eta \\ \mathcal{L}(T_{\mathcal{Z}, \mathcal{Z}}^{T_{\mathcal{A}, \mathcal{Z}}}) & \xrightarrow{\mathbf{L}[\mathcal{Z}, T_{\mathcal{A}, \mathcal{Z}}^{\mathfrak{s}}]} & \mathcal{L}(T_{\mathcal{Z}, \mathcal{Z}}^{T_{\mathcal{A}, \mathcal{Z}}}). \end{array}$$

Due to the fact that the lattice torus $T_{\mathcal{Z}, \mathcal{Z}}$ only consists of a single point, i.e., $[x] = [y]$ for each $[x], [y] \in T_{\mathcal{Z}, \mathcal{Z}}$, the matrix A is equal (up to a permutation)

to the sum of all multipliers

$$A = \sum_{y \in \mathbb{L}(\mathcal{Z})} m_{\mathbb{L}[\mathcal{Z}, T_{\mathcal{A}, \mathcal{Z}}^{\mathfrak{s}}]}^{(y)}.$$

This observation shows that this framework can also be used to quickly produce the necessary matrices in order to prototype a multigrid method – even though we use it mainly for the extraction of its spectrum in order to improve multigrid methods and obtain their convergence rates.

We again like to emphasize that \mathcal{Z} implies the resolution of the frequency space as already mentioned in Remark 4.21. The complete spectrum of the system matrix A is equal to the eigenvalues of $(\mathbf{L}_{[\mathcal{A}, \mathfrak{s}]})_k$ when k is sampled along $\mathbb{L}(\mathcal{Z}^{-T})$, i.e.,

$$\text{spec}(A) = \{\text{spec}((\mathbf{L}_{[\mathcal{A}, \mathfrak{s}]})_k) : k \in \mathcal{P}(\mathcal{A}^{-T}) \cap \mathbb{L}(\mathcal{Z}^{-T})\}.$$

Using Theorem 4.25 we now know how to rewrite multiple multiplication operators with respect to some common crystal structure with a coarser translational invariance. Due to the fact that we do not make any assumption on the initial representation of the crystal structures, the resulting structure elements of Theorem 3.16 might differ in their orderings and might contain shifts with respect to the common shift invariance. To automatically remove these differences and determine the corresponding transformations of the associated multiplication operators we first define the notion of congruent structure elements.

Definition 4.26. Two crystal tori $T_{\mathcal{A}}^{\mathfrak{s}} \cong T_{\mathcal{A}}^{\mathfrak{t}}$, $\mathcal{A} \in \mathbb{R}^n$ are congruent with respect to $\mathbb{L}(\mathcal{A})$ if the structure elements are of the same size, i.e., $|\mathfrak{s}| = |\mathfrak{t}| = m$, and there is a permutation $\pi : \{1, \dots, m\} \rightarrow \{1, \dots, m\}$ as well as shifts $y_j \in \mathbb{L}(\mathcal{A})$, such that

$$\mathfrak{s}_j = y_j + \mathfrak{t}_{\pi(j)}$$

For the sake of automation, we need a unique representation of a structure element. We introduce the following *normal form* and the required transformations to transfer any operator to this form.

Definition 4.27. Let $L : \mathcal{L}(T_{\mathcal{A}}^{\mathfrak{d}}) \rightarrow \mathcal{L}(T_{\mathcal{A}}^{\mathfrak{c}})$ be a multiplication operator. We say L is in normal form if

- the coordinates of the structure elements are found in the primitive cell, i.e., $\mathfrak{d}_i, \mathfrak{c}_j \in \mathcal{P}(\mathcal{A}) = \mathcal{A}[0, 1)^n$ for each i, j ,
- the structure elements \mathfrak{d} and \mathfrak{c} are sorted lexicographically.⁴

⁴In case $\mathfrak{d}_i = \mathfrak{d}_j$ or $\mathfrak{c}_i = \mathfrak{c}_j$ for any $i \neq j$ a consistent ordering of i, j has to be defined a priori.

We now derive the implications of Definition 4.26 for multiplication operators when the structure element is element wise shifted or permuted. We do so in two steps, Theorem 4.28 and Theorem 4.29. First, we show that a shift of an entry of the structure element in the codomain or domain results in a modification of the corresponding row or column of the non-zero multipliers, respectively.

Theorem 4.28 (Shifted structure elements). *Consider the two multiplication operators $L : \mathcal{L}(T_{\mathcal{A}}^s) \rightarrow \mathcal{L}(T_{\mathcal{A}}^t)$ and $G : \mathcal{L}(T_{\mathcal{A}}^t) \rightarrow \mathcal{L}(T_{\mathcal{A}}^u)$ defined by*

$$(Lf)(x) = \sum_{y \in T_{\mathcal{A}}} m_L^{(y)} f(x + y), \quad m_L^{(y)} \in \mathbb{C}^{|\mathfrak{t}| \times |\mathfrak{s}|},$$

$$(Gg)(x) = \sum_{y \in T_{\mathcal{A}}} m_G^{(y)} g(x + y), \quad m_G^{(y)} \in \mathbb{C}^{|\mathfrak{u}| \times |\mathfrak{t}|}.$$

Let further $\hat{\mathfrak{t}}$ be a structure element which is obtained from \mathfrak{t} when shifted element-wise along $\mathbb{L}(\mathcal{A})$, i.e.,

$$\mathfrak{t} = (\mathfrak{t}_1, \dots, \mathfrak{t}_m) = (\hat{\mathfrak{t}}_1 + y_1, \dots, \hat{\mathfrak{t}}_m + y_m) = \hat{\mathfrak{t}} + (y_1, \dots, y_m),$$

where $y_1, \dots, y_m \in \mathbb{L}(\mathcal{A})$ and $m = |\mathfrak{t}|$. Then, the operators \hat{L} and \hat{G} given by

$$(\hat{L}f)(x) = \sum_{y \in T_{\mathcal{A}}} m_{\hat{L}}^{(y)} f(x + y), \quad m_{\hat{L}}^{(y)} \in \mathbb{C}^{|\hat{\mathfrak{t}}| \times |\mathfrak{s}|}, \quad (m_{\hat{L}}^{(y)})_{i,j} := (m_L^{(y+y_i)})_{i,j},$$

$$(\hat{G}f)(x) = \sum_{y \in T_{\mathcal{A}}} m_{\hat{G}}^{(y)} f(x + y), \quad m_{\hat{G}}^{(y)} \in \mathbb{C}^{|\mathfrak{u}| \times |\hat{\mathfrak{t}}|}, \quad (m_{\hat{G}}^{(y)})_{i,j} := (m_G^{(y-y_j)})_{i,j}$$

fulfill the commutative diagram:

$$\begin{array}{ccccc} \mathcal{L}(T_{\mathcal{A}}^s) & \xrightarrow{L} & \mathcal{L}(T_{\mathcal{A}}^t) & \xrightarrow{G} & \mathcal{L}(T_{\mathcal{A}}^u) \\ & \searrow \hat{L} & \downarrow \mathbb{T} & \nearrow \hat{G} & \\ & & \mathcal{L}(T_{\mathcal{A}}^{\hat{\mathfrak{t}}}) & & \end{array}$$

Proof. The natural isomorphism between the two corresponding function spaces is given by

$\mathbb{T} : \mathcal{L}(T_{\mathcal{A}}^t) \rightarrow \mathcal{L}(T_{\mathcal{A}}^{\hat{\mathfrak{t}}})$, $f = (f_1, \dots, f_m) \mapsto (f_1(\cdot - y_1), \dots, f_m(\cdot - y_m)) = \mathbb{T}f$ as f and $(\mathbb{T}f)$ describe the same value distribution on the crystal.⁵ Again, a straightforward calculation yields

$$\begin{aligned} [(\mathbb{T}Lf)(x)]_i &= [(Lf)(x - y_i)]_i = \sum_{y \in T_{\mathcal{A}}} \sum_{j=1}^{|\mathfrak{s}|} (m_L^{(y)})_{i,j} f_j(x - y_i + y) \\ &= \sum_{y \in T_{\mathcal{A}}} \sum_{j=1}^{|\mathfrak{s}|} (m_L^{(y+y_i)})_{i,j} f_j(x + y) = [\sum_{y \in T_{\mathcal{A}}} m_{\hat{L}}^{(y)} f(x + y)]_i. \end{aligned}$$

Analogously we find $[(G\mathbb{T}^{-1}g)(x)]_i = [\sum_{y \in T_{\mathcal{A}}} (m_G^{(y)}) g(x + y)]_i$. \square

⁵The left-hand side of $[(\mathbb{T}f)(x)]_i = f_i(x - y_i)$ corresponds to the value at position $x + \hat{\mathfrak{t}}_i = (x - y_i) + \mathfrak{t}_i$ which coincides with the position of the value of the right-hand side.

Finally, we show that permutations of the entries of the structure element result in a transformation of the non-zero multipliers by corresponding permutation matrices.

Theorem 4.29 (Permuted structure elements). *Consider the two multiplication operators $L : \mathcal{L}(T_{\mathcal{A}}^s) \rightarrow \mathcal{L}(T_{\mathcal{A}}^t)$ and $G : \mathcal{L}(T_{\mathcal{A}}^t) \rightarrow \mathcal{L}(T_{\mathcal{A}}^u)$ defined by*

$$(Lf)(x) = \sum_{y \in T_{\mathcal{A}}} m_L^{(y)} f(x+y), \quad m_L^{(y)} \in \mathbb{C}^{|\mathfrak{t}| \times |\mathfrak{s}|},$$

$$(Gg)(x) = \sum_{y \in T_{\mathcal{A}}} m_G^{(y)} g(x+y), \quad m_G^{(y)} \in \mathbb{C}^{|\mathfrak{u}| \times |\mathfrak{t}|}.$$

Let further $\hat{\mathfrak{t}}$ be a structure element which is a permuted version of \mathfrak{t} , i.e.,

$$\hat{\mathfrak{t}} = (\hat{\mathfrak{t}}_1, \dots, \hat{\mathfrak{t}}_m) = (\mathfrak{t}_{\pi(1)}, \dots, \mathfrak{t}_{\pi(m)}) = m_{\pi} \mathfrak{t}$$

where $m = |\mathfrak{t}|$, $\pi : \{1, \dots, m\} \rightarrow \{1, \dots, m\}$ is a permutation and $m_{\pi} \in \{0, 1\}^{m \times m}$ the corresponding permutation matrix. Then, the operators \hat{L} and \hat{G} given by

$$(\hat{L}f)(x) = \sum_{y \in T_{\mathcal{A}}} m_{\hat{L}}^{(y)} f(x+y), \quad m_{\hat{L}}^{(y)} \in \mathbb{C}^{|\hat{\mathfrak{t}}| \times |\mathfrak{s}|} \quad \text{with} \quad m_{\hat{L}}^{(y)} := m_{\pi} m_L^{(y)},$$

$$(\hat{G}f)(x) = \sum_{y \in T_{\mathcal{A}}} m_{\hat{G}}^{(y)} f(x+y), \quad m_{\hat{G}}^{(y)} \in \mathbb{C}^{|\mathfrak{u}| \times |\hat{\mathfrak{t}}|} \quad \text{with} \quad m_{\hat{G}}^{(y)} := m_G^{(y)} m_{\pi}^{-1}$$

fulfill the commutative diagram:

$$\begin{array}{ccccc} \mathcal{L}(T_{\mathcal{A}}^s) & \xrightarrow{L} & \mathcal{L}(T_{\mathcal{A}}^t) & \xrightarrow{G} & \mathcal{L}(T_{\mathcal{A}}^u) \\ & \searrow \hat{L} & \downarrow p & \nearrow \hat{G} & \\ & & \mathcal{L}(T_{\mathcal{A}}^{\hat{\mathfrak{t}}}) & & \end{array}$$

Proof. Due to the fact that the natural isomorphism $p : \mathcal{L}(T_{\mathcal{A}}^t) \rightarrow \mathcal{L}(T_{\mathcal{A}}^{\hat{\mathfrak{t}}})$ is a multiplication operator defined by $(pf)(x) = m_{\pi} f(x)$ for all $x \in \mathbb{L}(\mathcal{A})$, the statement is true due to the rules of computation in Lemma 4.23. \square

Implementation algorithms

Theorem 3.16 and Theorems 3.6, 3.17, 4.25, 4.28 and 4.29 allow for the automatic adjustment of crystal representations within the LFA. The corresponding detailed algorithms which make use of these results are given in Appendix A.

Throughout Sections 5.2 and 5.3 we illustrate how to use these algorithms in order to analyze iterative methods. This should serve to some extent as a tutorial. In here, we only use function calls of Algorithms A.1, A.4 and A.7 explicitly. We briefly present their function header:

- Algorithm A.4 corresponds to Theorem 4.25. It is used to rewrite a multiplication operator $L : \mathcal{L}(T_{\mathcal{A}}^{\hat{0}}) \rightarrow \mathcal{L}(T_{\mathcal{A}}^{\hat{c}})$ with respect to a sublattice $\mathbb{L}(\mathcal{C}) \subset \mathbb{L}(\mathcal{A})$ such that $L \cong G : \mathcal{L}(T_{\mathcal{C}}^{\hat{0}}) \rightarrow \mathcal{L}(T_{\mathcal{C}}^{\hat{c}})$ via

$$G \leftarrow \text{LatticeCoarsening}(L, \mathcal{C})$$

as already illustrated in Example 4.2.

- Algorithm A.7 corresponds to Theorems 4.28 and 4.29 and is used to modify the structure element of the domain and codomain of a single multiplication operator $L : \mathcal{L}(T_{\mathcal{A}}^{\hat{0}}) \rightarrow \mathcal{L}(T_{\mathcal{A}}^{\hat{c}})$ via

$$\hat{L} \leftarrow \text{ChangeStructureElement}(L, \hat{\mathfrak{d}}, \hat{\mathfrak{c}}),$$

such that $L \cong \hat{L} : \mathcal{L}(T_{\mathcal{A}}^{\hat{0}}) \rightarrow \mathcal{L}(T_{\mathcal{A}}^{\hat{c}})$.

- Algorithm A.1 is used to automatically compute the complete spectrum

$$X := \{\text{spec}(f(L^{(1)}, \dots, L^{(K)})_k) : k \in \mathcal{P}(\mathcal{A}^{-T}) \cap \mathbb{L}(\mathcal{Z}^{-T})\}$$

of a composition $f(L^{(1)}, \dots, L^{(K)}) : \mathcal{L}(T_{\mathcal{A}, \mathcal{Z}}^{\mathfrak{s}}) \rightarrow \mathcal{L}(T_{\mathcal{A}, \mathcal{Z}}^{\mathfrak{s}})$ of several multiplication operators $L^{(j)} : T_{\mathcal{A}^{(j)}, \mathcal{Z}}^{\mathfrak{s}^{(j)}} \rightarrow T_{\mathcal{A}^{(j)}, \mathcal{Z}}^{\mathfrak{t}^{(j)}}$ via

$$X \leftarrow \text{ComputeSpectrum}(f, (L^{(1)}, \dots, L^{(K)}), \mathcal{Z}).$$

In here, the (smallest) common denominator of all lattices $\mathbb{L}(\mathcal{A}) = \text{lcm}(\mathbb{L}(\mathcal{A}^{(i)}), \mathbb{L}(\mathcal{A}^{(j)}))$, $i, j = 1, \dots, K$, is automatically computed and all operators are rewritten with respect to this translational invariance. After that, all structure elements are normalized such that the domains and codomains of the operators are compatible among each other. Finally, the operator composition $f((L^{(1)})_k, \dots, (L^{(K)})_k)$ and its eigenvalues are computed on the level of the symbols for each $k \in T_{\mathcal{A}, \mathcal{Z}}^* = \mathcal{P}(\mathcal{A}^{-T}) \cap \mathbb{L}(\mathcal{Z}^{-T})$. Thus, \mathcal{Z} should be a basis of a sublattice of $\mathbb{L}(\mathcal{A})$ as it specifies the resolution of the frequency domain $\mathcal{P}(\mathcal{A}^{-T})$. In case we are not interested in a specific resolution of the frequency space this input \mathcal{Z} should be omitted. Then, a standard equidistant discretization of, for example, 20^n points is used which corresponds to $\mathcal{Z} := 20\mathcal{A}$. The algorithmic procedure is summarized in Figure 4.4.

The remaining Algorithms A.2, A.3, A.5 and A.6 are implicitly used within Algorithms A.1, A.4 and A.7. This collection of algorithms are the basis of the framework *aLFA: automated local Fourier analysis*.

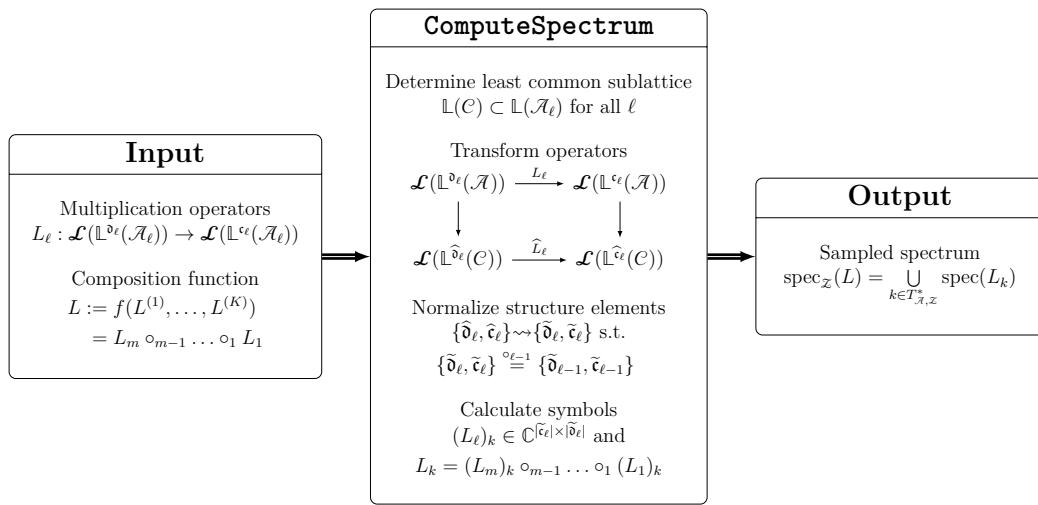


Figure 4.4.: The algorithmic procedure of the automated local Fourier analysis to compute the spectrum of a composition of several multiplication operators.

Linear iterative methods

In this chapter we introduce, based on [40], a class of iterative methods in order to solve linear systems of equations

$$Ax = b, \quad (5.1)$$

where $A \in \mathbb{C}^{n \times n}$ and $b \in \mathbb{C}^n$ correspond to the system matrix and the right hand side, respectively.

An iterative method is a process which starts with an initial guess $x^{(0)} \in \mathbb{C}^n$ and produces a series of iterates $x^{(0)}, x^{(1)}, \dots$ which (hopefully) converges to a solution of equation (5.1).

We restrict ourselves to the following kind of linear iterative methods.

Definition 5.1. *A (consistent and stationary) linear iterative method is defined by the iteration rule*

$$x^{(k+1)} = (I - S^{-1}A)x^{(k)} + S^{-1}b$$

for some matrix $S \in \mathbb{C}^{n \times n}$.

Remark 5.2. *Regarding this definition we like to note the following.*

- *This method is called consistent due to the fact that a solution x of $Ax = b$ is a fixpoint of this method, i.e., $(I - S^{-1}A)x + S^{-1}b = x - S^{-1}b + S^{-1}b = x$.*
- *It is called stationary as the iteration rule is independent of the iteration count k .*
- *The matrix S is typically some approximation of A with the property that the systems $Sy = z$ are inexpensive to solve.*

- We may also consider singular matrices S . Then, the iteration rule is replaced by

$$(I - S^\dagger A)x^{(k)} + S^\dagger b,$$

where S^\dagger denotes the Moore-Penrose pseudoinverse [33].

Definition 5.3. Let x denote the solution of $Ax = b$ and $x^{(k)}$ the iterate of an iterative method. We denote the k th iteration error and residual by

$$e^{(k)} := x - x^{(k)} \quad \text{and} \quad r^{(k)} := Ae^{(k)} = b - Ax^{(k)},$$

respectively.

Lemma 5.4. Given an iterative method we have

$$e^{(k+1)} = (I - S^{-1}A)e^{(k)}.$$

Thus, the operator $(I - S^{-1}A)$ is referred to as the error propagator.

Proof. On the left hand side we have

$$\begin{aligned} e^{(k+1)} &= x - x^{k+1} = x - ((I - S^{-1}A)x^{(k)} + S^{-1}b) \\ &= x - S^{-1}b - (I - S^{-1}A)x^{(k)}, \end{aligned}$$

and on the other side we have

$$(I - S^{-1}A)e^{(k)} = (I - S^{-1}A)(x - x^{(k)}) = x - S^{-1}b - (I - S^{-1}A)x^{(k)}. \quad \square$$

Remark 5.5. When we use the phrasing the (iterative) method $(I - S^{-1}A)$ we mean the corresponding consistent linear iterative method

$$x^{(k+1)} = (I - S^{-1}A)x^{(k)} + S^{-1}b.$$

Lemma 5.6. Starting with the initial guess $x^{(0)} = 0$, the iterates $x^{(k)}$ of a linear iterative method $(I - S^{-1}A)$ are given by

$$x^{(k)} = (I - [I - S^{-1}A]^k)A^{-1}b$$

Proof (by induction). The statement is obviously true for $k = 0$. Thus, we assume that the statement is true for some $k \in \mathbb{N}$ and find

$$\begin{aligned} x^{(k+1)} &= (I - S^{-1}A)x^{(k)} + S^{-1}b \\ &= (I - S^{-1}A)(I - [I - S^{-1}A]^k)A^{-1}b + S^{-1}b \\ &= ([I - S^{-1}A] - [I - S^{-1}A]^{k+1})A^{-1}b + S^{-1}b \\ &= (I - [I - S^{-1}A]^{k+1})A^{-1}b. \end{aligned} \quad \square$$

5.1. Convergence theory

With respect to the convergence of linear iterative methods we like to review several important results.

Theorem 5.7. *A linear iterative method $(I - S^{-1}A)$ converges for any initial guess to a solution x iff*

$$\lim_{k \rightarrow \infty} (I - S^{-1}A)^k = 0.$$

Proof. We have

$$\lim_{k \rightarrow \infty} e^{(k)} = 0 \Leftrightarrow \lim_{k \rightarrow \infty} (I - S^{-1}A)^k e^{(0)} = 0 \Leftrightarrow \lim_{k \rightarrow \infty} (I - S^{-1}A)^k = 0. \quad \square$$

Theorem 5.8. *We have the equivalence*

$$\rho(G) < 1 \iff \lim_{k \rightarrow \infty} G^k = 0$$

and

$$\rho(G) > 1 \iff \lim_{k \rightarrow \infty} \|G^k\| = \infty,$$

where $\rho(G) := \max\{|\lambda| : \lambda \text{ eigenvalue of } G\}$ denotes the spectral radius of G . Thus, a linear iterative method converges for any initial starting guess iff $\rho(I - S^{-1}A) < 1$.

Proof. Let us denote with $J = XGX^{-1}$ the Jordan canonical form of G with

$$J = \begin{bmatrix} J_1 & & & \\ & J_2 & & \\ & & \ddots & \\ & & & J_\ell \end{bmatrix}, \quad J_i = \begin{bmatrix} \lambda_i & 1 & & \\ & \lambda_i & 1 & \\ & & \ddots & \ddots \\ & & & \lambda_i & 1 \\ & & & & \lambda_i \end{bmatrix},$$

where λ_i denote the eigenvalues of G . Now, let us consider a single Jordan block $J_i = (\lambda_i \cdot \text{id} + E)$ of size p , where E denotes the nilpotent part of the matrix. Then, for $k \geq p$, we have $E^k = 0$ and thus

$$J^k = (\lambda_i \cdot \text{id} + E)^k = \sum_{j=0}^{p-1} \binom{k}{j} \lambda_i^{k-j} E^j.$$

As increasing the exponent of E^j simply shifts its ones to the right, all the entries in J^k are (located in the upper triangular part and) given by $\alpha_k := \binom{k}{j} \lambda_i^{k-j}$ and we have

$$\alpha_{k+1} = \alpha_k \cdot \left(\lambda_i \cdot \frac{k+1}{k-j-1} \right) = \alpha_k \cdot \left(\lambda_i \cdot \left(1 + \frac{2+j}{k-j-1} \right) \right).$$

This recurrence relation tells us that all the entries converge to zero iff $|\lambda_i| < 1$ due to $j < p$ and thus

$$\lim_{k \rightarrow \infty} J_i^k = 0 \iff |\lambda_i| < 1$$

as well as

$$\lim_{k \rightarrow \infty} \|J_i\|^k = \infty \iff |\lambda_i| > 1.$$

Hence,

$$\lim_{k \rightarrow \infty} G^k = \lim_{k \rightarrow \infty} X^{-1} J^k X = 0 \iff \rho(G) < 1$$

and

$$\lim_{k \rightarrow \infty} \|G^k\| = \lim_{k \rightarrow \infty} \|X^{-1} J^k X\| = \infty \iff \rho(G) > 1. \quad \square$$

Despite the question whether an iterative method $G := I - S^{-1}A$ converges or not, a statement about the *convergence speed* is at least of similar importance, i.e., we are interested in a number $\nu \in \mathbb{R}$, such that

$$\|e^{(k+1)}\| < \nu \|e^{(k)}\|$$

is true for every error $e^{(k)}$ which implies

$$\|e^{(k)}\| < \nu^k \|e^{(0)}\|.$$

Such an upper bound is obviously given by $\nu := \|G\|$, but this bound is in general too pessimistic. We would like to point out a connection to the eigenvalues of G . In general we just have $\|G\| \geq \rho(G)$ for any matrix norm [40]. Equality holds for hermitian matrices, i.e.,

$$G = G^* \implies \|G\| = \rho(G),$$

due to the fact that the singular values of hermitian matrices are equal to its absolute eigenvalues [46]. Except for this class of matrices we at least find that $\rho(G)$ is an average measure due to the following formula.

Theorem 5.9 (Gelfand's formula). *We have*

$$\rho(G) = \lim_{k \rightarrow \infty} \|G^k\|^{\frac{1}{k}}.$$

Proof. This formula is a direct consequence of Theorem 5.8 applied to $\frac{G}{\rho(G)+\varepsilon}$ and $\frac{G}{\rho(G)-\varepsilon}$, $\varepsilon > 0$, in order to obtain $\|G^k\|^{\frac{1}{k}} < \rho(G) + \varepsilon$ and $\|G^k\|^{\frac{1}{k}} > \rho(G) - \varepsilon$ respectively for large k . \square

Thus, for large k we find

$$\|e^{(k+1)}\| \approx \rho(G) \|e^{(k)}\|$$

as long as the initial error $e^{(0)}$ contains a component in direction of the eigenfunction corresponding to the largest absolute eigenvalue. Thus, $\rho(G)$ is often referred to as the *general convergence factor*.

5.2. Splitting methods

The operator S of an iterative method $(I - S^{-1}A)$ often results from a splitting of the system matrix A . We introduce certain splitting methods and bring it into the context of Chapter 4 in order to extract the eigenvalues of the error propagator using the algorithms in Appendix A.

In the following we consider the translationally invariant operator

$$L : \mathcal{L}(T_{\mathcal{A}, \mathcal{Z}}^{\mathfrak{s}}) \rightarrow \mathcal{L}(T_{\mathcal{A}, \mathcal{Z}}^{\mathfrak{s}}), \quad (Lf)(x) := \sum_{y \in T_{\mathcal{A}, \mathcal{Z}}} m_L^{(y)} f(x + y), \quad |\mathfrak{s}| = m.$$

Then, the system matrix A obtained from the commutative diagram

$$\begin{array}{ccc} \mathcal{L}(T_{\mathcal{A}, \mathcal{Z}}^{\mathfrak{s}}) & \xrightarrow{L} & \mathcal{L}(T_{\mathcal{A}, \mathcal{Z}}^{\mathfrak{s}}) \\ \downarrow \eta & & \downarrow \eta \\ \mathcal{L}(T_{\mathcal{Z}, \mathcal{Z}}^{T_{\mathcal{A}, \mathcal{Z}}^{\mathfrak{s}}}) & \xrightarrow{A} & \mathcal{L}(T_{\mathcal{Z}, \mathcal{Z}}^{T_{\mathcal{A}, \mathcal{Z}}^{\mathfrak{s}}}). \end{array}$$

is a block matrix consisting of the blocks $m_L^{(y)} \in \mathbb{C}^{m \times m}$.

Non-overlapping block methods

Now consider a splitting of the system matrix A into a block-diagonal part A_D , $(A_D)_{i,i} = m_L^{(0)}$, and the lower and upper remainder A_L and A_U , i.e., schematically we have

$$\begin{array}{|c|} \hline A \\ \hline \end{array} = \begin{array}{|c|} \hline A_D \\ \hline \end{array} + \begin{array}{|c|} \hline A_L \\ \hline \end{array} + \begin{array}{|c|} \hline A_U \\ \hline \end{array}.$$

The most common splitting methods are

1. relaxed (block-) *Jacobi*,

$$S_{J, \omega} := \frac{1}{\omega} A_D,$$

2. and relaxed (block-) *Gauss-Seidel*,

$$S_{GS, \omega} = \frac{1}{\omega} A_D + A_L,$$

where $\omega = 1$ corresponds to the unrelaxed scheme, $\omega < 1$ to under- and $\omega > 1$ to over-relaxation. The Jacobi scheme is obviously translationally invariant itself with

$$(L_{J,\omega}f)(x) = (\eta^{-1}S_{J,\omega}\eta f)(x) = \frac{1}{\omega}m_L^{(0)}f(x).$$

In contrast, the Gauss-Seidel method is not translationally invariant. But, provided that the unknowns are lexicographically ordered and that A only interacts with neighbors of small distance, i.e.,

$$m_L^{(y)} = 0 \quad \Leftrightarrow \quad \|y\|_2 < d$$

for some $d > 0$, an application of Gauss-Seidel can be expressed as a multiplication operator for all unknowns with distance greater than d from the boundary.

Thus, in order to analyze a (block)-Gauss-Seidel scheme, we use the multiplication operator

$$(L_{GS,\omega}f)(x) = \sum_{y < x} m_L^{(y)}f(x+y) + \frac{1}{\omega}m_L^{(0)}f(x),$$

where $y < x$ corresponds to the ordering of the unknowns.

Remark 5.10. *The application of a block Jacobi or Gauss-Seidel sweep with a blocksize smaller than the size of the structure element of the given crystal operator results in an additional splitting of the central multiplier $m_L^{(0)}$. An example is given in Section 6.3 in the analysis of the Kaczmarz method applied to the tight-binding Hamiltonian. (This basically corresponds to a scalar Gauss-Seidel method applied to a crystal operator with a structure element of size 2.)*

Example 5.1. *We again consider the discrete Laplacian of Example 1.1,*

$$A = \eta L \eta^{-1} : \mathcal{L}(T_{\mathcal{Z},\mathcal{Z}}^{T_{\mathcal{A}}}) \rightarrow \mathcal{L}(T_{\mathcal{Z},\mathcal{Z}}^{T_{\mathcal{A}}})$$

with

$$\mathcal{Z} = \left[\begin{array}{c|c} 1 & 0 \\ \hline 0 & 1 \end{array} \right], \quad \mathcal{A} = h\mathcal{Z} = \left[\begin{array}{c|c} a_1 & a_2 \\ \hline & \end{array} \right], \quad h = \frac{1}{20}.$$

By applying the relaxed Jacobi iteration, $\omega = \frac{4}{5}$, to $Ax = b$ with some highly oscillating initial error $e^{(0)}$, we see in Figure 5.1 that this method quickly damps the highly oscillatory part. In contrast, a (remaining) smooth error is only reduced very slowly.

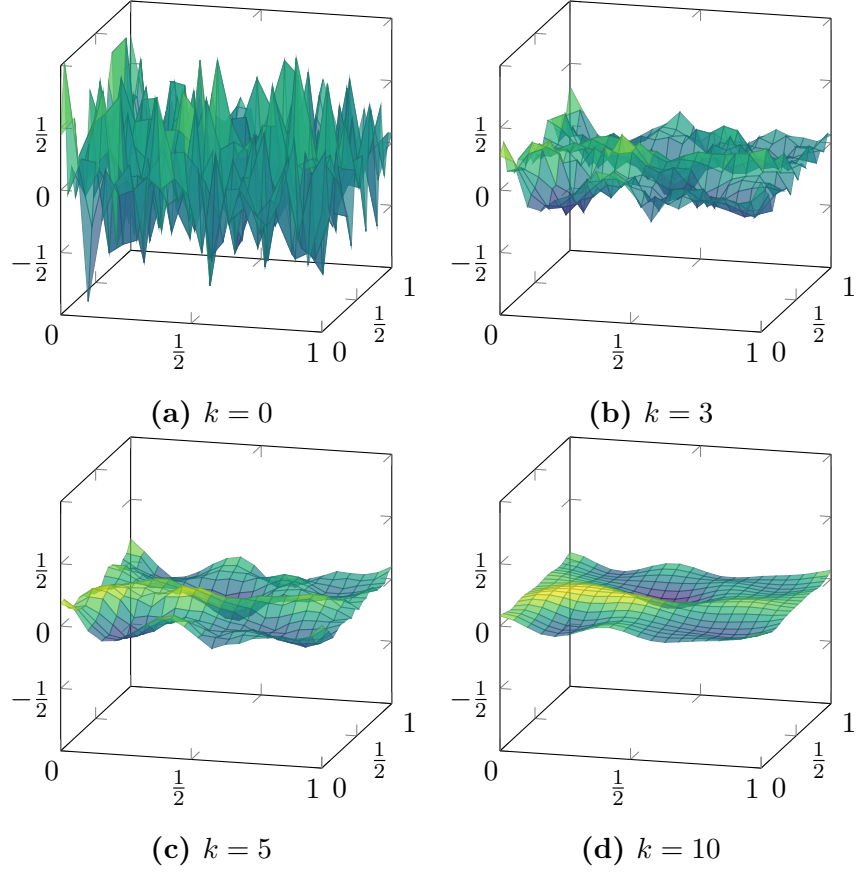


Figure 5.1.: The k th iteration error of (relaxed) Jacobi, $\omega = \frac{4}{5}$, applied to the Laplace equation after $k = 0, 3, 5$ and 10 iterations.

In order to explain this behavior, we take a look at the spectral radius of the error propagator. The symbol of the error propagator is given by

$$\begin{aligned}
 G_k &= (I - L_{J,\omega}^{-1}L)_k = \left(1 - \frac{h^2}{5}(L)_k\right) \\
 &= \left(1 - \frac{h^2}{5} \frac{2}{h^2} (2 - \cos(2\pi k_1) - \cos(2\pi k_2))\right) \\
 &= \frac{1}{5} (1 + 2 \cos(2\pi k_1) + 2 \cos(2\pi k_2)).
 \end{aligned}$$

A plot of the spectral radii $\rho(G_k)$ is shown in Figure 5.2. This plot shows the factor by which an error in the direction of $e^{2\pi i \langle k, \cdot \rangle_2}$ is decreased by one Jacobi iteration. It can be seen that smooth functions, i.e., wave functions corresponding to wavevectors k near the corners of $\mathcal{P}(\mathcal{B})$, $\mathcal{B} = \mathcal{A}^{-T}$, are way less damped than oscillatory wave functions.

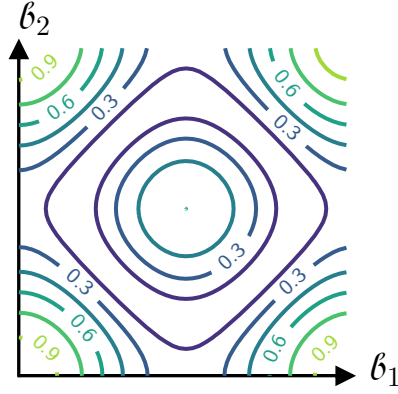


Figure 5.2.: Spectral radii of the relaxed Jacobi method $G_k = (I - L_{J, \frac{4}{5}}^{-1} L)_k$ plotted along $\mathcal{P}(\mathcal{B})$, $\mathcal{B} = \mathcal{A}^{-T}$.

Colored and overlapping block-methods

Consider a subset $\mathfrak{s}^{(1)}$ of the structure element \mathfrak{s} , i.e.,

$$\mathfrak{s}^{(1)} = (\mathfrak{s}_{i_1^{(1)}}, \dots, \mathfrak{s}_{i_{k_1}^{(1)}}), \quad \{i_1^{(1)}, \dots, i_{k_1}^{(1)}\} \subset \{1, \dots, m\},$$

such that

$$\bigcup_{\ell=1}^{k_1} \{\mathfrak{s}_{i_\ell^{(1)}}\} \subset \bigcup_{\ell=1}^m \{\mathfrak{s}_\ell\}.$$

A simultaneous update of all unknowns $T_{\mathcal{A}, \mathcal{Z}}^{\mathfrak{s}^{(1)}}$ corresponds to the method

$$(I - (L_{J, \omega}^{(1)})^\dagger L) \quad \text{with} \quad (L_{J, \omega}^{(1)} f)(x) = \left(\frac{1}{\omega} m_{P^{(1)}} m_L^{(0)} m_{P^{(1)}}\right) f(x),$$

where $m_{P^{(1)}}$ denotes a projection onto the subset $\mathfrak{s}^{(1)}$, i.e., it is a diagonal matrix defined by

$$(m_{P^{(1)}})_{\ell, j} = \begin{cases} 1 & \text{if } \ell = j \in \{i_1^{(1)}, \dots, i_{k_1}^{(1)}\} \\ 0 & \text{else.} \end{cases}$$

In matrix format this method relates to the error propagator

$$[I - (S_{J, \omega}^{(1)})^\dagger A] : \mathcal{L}(T_{\mathcal{Z}, \mathcal{Z}}^{T_{\mathcal{A}, \mathcal{Z}}^{\mathfrak{s}^{(1)}}}) \rightarrow \mathcal{L}(T_{\mathcal{Z}, \mathcal{Z}}^{T_{\mathcal{A}, \mathcal{Z}}^{\mathfrak{s}^{(1)}}})$$

with

$$S_{J, \omega}^{(1)} = \eta L_{J, \omega}^{(1)} \eta^{-1} := \frac{1}{\omega} A_{D^{(1)}}$$

where the splitting is schematically given by

$$A = A_{D^{(1)}} + A_{L^{(1)}} + A_{U^{(1)}}.$$

Using multiple such subsets $\mathfrak{s}^{(1)}, \dots, \mathfrak{s}^{(s)}$ with

$$\bigcup_{j=1}^s \bigcup_{\ell=1}^{k_j} \{\mathfrak{s}_{i_\ell}^{(j)}\} = \bigcup_{\ell=1}^m \{\mathfrak{s}_\ell\},$$

the iterative method corresponding to the error propagator

$$\prod_{j=1}^s (I - (L_{J,\omega}^{(j)})^\dagger L) \quad \text{or} \quad \prod_{j=1}^s (I - (S_{J,\omega}^{(j)})^\dagger A)$$

defines a colored block-method. In here, each $\mathfrak{s}^{(i)}$ corresponds to a single color. An *overlap* exists if the domain decomposition is not disjoint.

Remark 5.11. *Usually these subsets $\mathfrak{s}^{(i)}$ are chosen in a way, such that all non-central multipliers $m_{P^{(1)}} m_L^{(y)} m_{P^{(1)}}$, $y \neq 0$, are 0. In this case the subsystem decomposes into several small decoupled systems and the matrix inversion of $S_{J,\omega}^{(1)} = A_{D^{(1)}}$ is cheap and can easily be parallelized.*

Example 5.2. *The red-black Gauss-Seidel method results from a splitting of unknowns in two sets $X = X_{red} \cup X_{black}$ such that any two unknowns $x_i, x_j \in X_\ell$, $\ell = red, black$, are not adjacent to each other as illustrated in Figure 5.3a. We already introduced this crystal $X \cong T_{\mathcal{C}, \mathcal{Z}}^{\hat{\mathfrak{s}}}$, $\hat{\mathfrak{s}} := (0, a_1)$, in Example 4.2 with $T_{\mathcal{C}, \mathcal{Z}}^{(0)} \cong X_{red}$ and $T_{\mathcal{C}, \mathcal{Z}}^{(a_1)} \cong X_{black}$. A simultaneous update of all unknowns of one color is cheap if the underlying operator solely connects black with red and red with black unknowns as it is the case for the discretized Laplacian*

$$\mathbf{L} = \mathbf{L}[\mathcal{A}, \mathfrak{s}] : \mathcal{L}(T_{\mathcal{A}}) \rightarrow \mathcal{L}(T_{\mathcal{A}}), \quad \mathcal{A} = h \begin{bmatrix} 1 & 0 \\ 0 & 1 \end{bmatrix}.$$

The red-black error propagator is then defined as

$$G = (I - L_{black}^\dagger \mathbf{L}[\mathcal{C}, \hat{\mathfrak{s}}])(I - L_{red}^\dagger \mathbf{L}[\mathcal{C}, \hat{\mathfrak{s}}]) : \mathcal{L}(T_{\mathcal{C}, \mathcal{Z}}^{\hat{\mathfrak{s}}}) \rightarrow \mathcal{L}(T_{\mathcal{C}, \mathcal{Z}}^{\hat{\mathfrak{s}}}),$$

where $\mathbf{L}[\mathcal{C}, \hat{\mathfrak{s}}] \cong \mathbf{L}[\mathcal{A}, \mathfrak{s}]$ is simply the Laplacian with respect to $T_{\mathcal{C}, \mathcal{Z}}^{\hat{\mathfrak{s}}}$ and the operators L_{black} and L_{red} have the nonzero multipliers

$$m_{L_{red}}^{(0)} = \begin{bmatrix} 1 & 0 \\ 0 & 0 \end{bmatrix} m_{\mathbf{L}[\mathcal{C}, \hat{\mathfrak{s}}]}^{(0)} \begin{bmatrix} 1 & 0 \\ 0 & 0 \end{bmatrix} \quad \text{and} \quad m_{L_{black}}^{(0)} = \begin{bmatrix} 0 & 0 \\ 0 & 1 \end{bmatrix} m_{\mathbf{L}[\mathcal{C}, \hat{\mathfrak{s}}]}^{(0)} \begin{bmatrix} 0 & 0 \\ 0 & 1 \end{bmatrix}.$$

The spectral radii of the symbols G_k of the red-black error propagator are plotted in Figure 5.3b with $k \in \mathcal{P}(\mathcal{B})$, $\mathcal{B} = \mathcal{C}^{-T}$. Note, that we find 2 eigenvalues per wavevector k . Thus, this plot is not directly comparable with Figure 5.2, where we find 1 eigenvalue per wavevector, cf. Example 4.2.

We summarize how this result can be obtained using the algorithms of Appendix A.

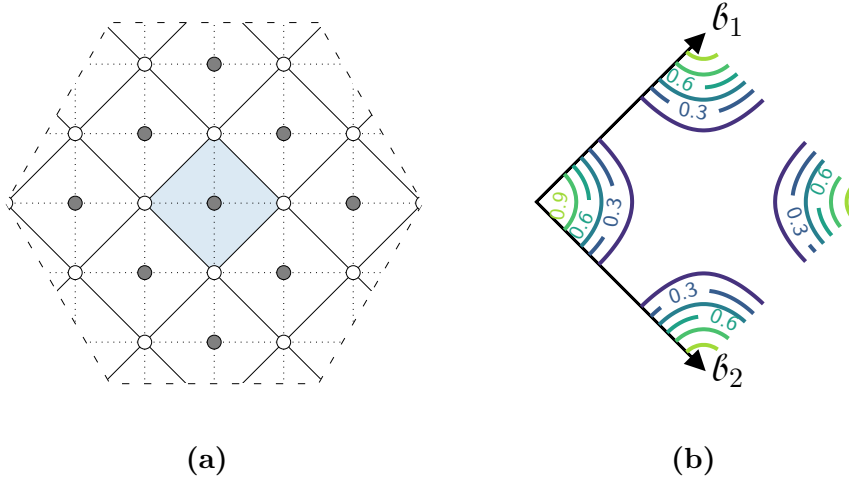


Figure 5.3.: a) Illustration of the red-black splitting, b) The spectral radius of the symbol of the red-black Gauss-Seidel error propagator $G : \mathcal{L}(T_C^{\hat{s}}) \rightarrow \mathcal{L}(T_C^{\hat{s}})$ plotted along $\mathcal{P}(\mathcal{B})$, $\mathcal{B} = C^{-T}$.

Analysis of the red-black method using aLFA:

Define the discretized Laplacian $\mathbf{L} = \mathbf{L}[\mathcal{A}, \mathfrak{s}] : \mathcal{L}(T_{\mathcal{A}}^{\mathfrak{s}}) \rightarrow \mathcal{L}(T_{\mathcal{A}}^{\mathfrak{s}})$ with $\mathcal{A} = [\mathbf{a}_1 \mid \mathbf{a}_2] = \frac{1}{h} \begin{bmatrix} 1 & 0 \\ 0 & 1 \end{bmatrix}$ with the structure element $\mathfrak{s} = (0)$ and nonzero multipliers

$$m_{\mathbf{L}[\mathcal{A}, \mathfrak{s}]}^{(y)} = \begin{cases} -\frac{4}{h^2} & y = 0 \\ \frac{1}{h^2} & y \in \{\pm \mathbf{a}_1, \pm \mathbf{a}_2\}. \end{cases}$$

Obtain the description of the discrete Laplacian w.r.t. the translational invariance of the red-black splitting $\mathcal{C} = [\mathbf{a}_1 + \mathbf{a}_2 \quad \mathbf{a}_1 - \mathbf{a}_2]$ via Algorithm A.4:

$$\mathbf{L}[\mathcal{A}, \tilde{\mathfrak{s}}] \leftarrow \text{LatticeCoarsening}(\mathbf{L}[\mathcal{A}, \mathfrak{s}], \mathcal{C})$$

Make sure that the structure elements of the domain and codomain are ordered as desired, i.e., $\hat{\mathfrak{s}} = (0, \mathbf{a}_1)$, via Algorithm A.7:

$$\mathbf{L}[\mathcal{C}, \hat{\mathfrak{s}}] \leftarrow \text{ChangeStructureElement}(\mathbf{L}[\mathcal{A}, \tilde{\mathfrak{s}}], \hat{\mathfrak{s}}, \hat{\mathfrak{s}})$$

Define the operators $\mathbf{L}_\ell : \mathcal{L}(T_C^{\hat{s}}) \rightarrow \mathcal{L}(T_C^{\hat{s}})$ with nonzero multipliers $m_{L_\ell}^{(0)} =$

$p_{\ell} m_{\mathbf{L}[\mathcal{C}, \widehat{\mathfrak{s}}]}^{(0)} p_{\ell}$, $\ell \in \{\text{black}, \text{red}\}$ and

$$p_{\text{red}} = \begin{bmatrix} 1 & 0 \\ 0 & 0 \end{bmatrix}, \quad p_{\text{black}} = \begin{bmatrix} 0 & 0 \\ 0 & 1 \end{bmatrix}.$$

Compute the spectral radii with Algorithm A.1 via

$$\text{ComputeSpectra}(f, (I, \mathbf{L}, \mathbf{L}_{\text{red}}, \mathbf{L}_{\text{black}})),$$

where f denotes the composition of the error propagators

$$(I, \mathbf{L}, \mathbf{L}_{\text{red}}, \mathbf{L}_{\text{black}}) \xrightarrow{f} (I - (\mathbf{L}_{\text{black}})^{\dagger} \mathbf{L})(I - (\mathbf{L}_{\text{red}})^{\dagger} \mathbf{L}).$$

Example 5.3. We show an example of a four-color overlapping block color method applied to the Laplacian

$$\mathbf{L} = \mathbf{L}[\mathcal{A}, \mathfrak{s}] : \mathcal{L}(T_{\mathcal{A}}) \rightarrow \mathcal{L}(T_{\mathcal{A}}), \quad \mathcal{A} = h \begin{bmatrix} 1 & 0 \\ 0 & 1 \end{bmatrix}.$$

The four colors correspond to the non-disjoint splitting depicted in Figure 5.4. This splitting is chosen in a way, such that each connected set of 9 unknowns of one color does not interact with other unknowns of the same color with respect to the discretized Laplacian. Thus, it is cheap to update all unknowns corresponding to one color at once. The splitting/coloring has a translational invariance of $\mathcal{C} := 4\mathcal{A}$. Rewriting the lattice torus $T_{\mathcal{A}}$ as a crystal torus with respect to the lattice $\mathbb{L}(\mathcal{C})$, i.e., $T_{\mathcal{A}} \cong T_{\mathcal{C}}^{\mathfrak{t}}$, we find that the structure element $\mathfrak{t} = (\mathfrak{t}_1, \dots, \mathfrak{t}_{16}) \cong T_{\mathcal{A}, \mathcal{C}}$ consists of the 16 elements

$$\begin{aligned} \mathfrak{t} &= (i \cdot \mathfrak{a}_1 + j \cdot \mathfrak{a}_2)_{i,j=0,\dots,3} \\ &= (0, \mathfrak{a}_1, \dots, 3\mathfrak{a}_1, \mathfrak{a}_2, \mathfrak{a}_1 + \mathfrak{a}_2, \dots, 3\mathfrak{a}_1 + 3\mathfrak{a}_2). \end{aligned}$$

The non-disjoint splitting is then given by the structure elements

$$\begin{aligned} \mathfrak{s}^{(1)} &= (i \cdot \mathfrak{a}_1 + j \cdot \mathfrak{a}_2)_{i,j=0,\dots,2} = (\mathfrak{t}_1, \mathfrak{t}_2, \mathfrak{t}_3, \mathfrak{t}_5, \mathfrak{t}_6, \mathfrak{t}_7, \mathfrak{t}_9, \mathfrak{t}_{10}, \mathfrak{t}_{11}); \quad \tau^{(1)} := 0 \\ \mathfrak{s}^{(2)} &= \mathfrak{s}^{(1)} + 2\mathfrak{a}_1 =: \mathfrak{s}^{(1)} + \tau^{(2)} \\ \mathfrak{s}^{(3)} &= \mathfrak{s}^{(1)} + 2\mathfrak{a}_2 =: \mathfrak{s}^{(1)} + \tau^{(3)} \\ \mathfrak{s}^{(4)} &= \mathfrak{s}^{(1)} + 2\mathfrak{a}_1 + 2\mathfrak{a}_2 =: \mathfrak{s}^{(1)} + \tau^{(4)}. \end{aligned}$$

such that $T_{\mathcal{C}}^{\mathfrak{s}^{(1)}} \cong \mathbf{1}, T_{\mathcal{C}}^{\mathfrak{s}^{(2)}} \cong \mathbf{2}, T_{\mathcal{C}}^{\mathfrak{s}^{(3)}} \cong \mathbf{3}$ and $T_{\mathcal{C}}^{\mathfrak{s}^{(4)}} \cong \mathbf{4}$.

A simple way to obtain the corresponding error propagator of the splitting method, which updates the unknowns corresponding to $T_{\mathcal{C}}^{\mathfrak{s}^{(\ell)}}$ simultaneously, is to simply derive them from the underlying system operator L as follows. First, we need to find a description $\widehat{\mathbf{L}}$ of the underlying operator, the discretized Laplacian \mathbf{L} , with respect to the translational invariance of the splitting \mathcal{C} . After that the structure element needs to be adjusted such that all unknowns

and their couplings among each other are found within the central multiplier $m_{\widehat{\mathbf{L}}}^{(0)}$. Consider the structure element \mathbf{t} . As can be seen in Figure 5.4, the coupling among the unknowns $\mathbf{s}^{(\ell)}$ which we want to update simultaneously are found in the multipliers:

$$\begin{cases} m_{\widehat{\mathbf{L}}}^{(0)} & \text{if } \ell = 1, \\ m_{\widehat{\mathbf{L}}}^{(0)}, m_{\widehat{\mathbf{L}}}^{(\pm c_1)} & \text{if } \ell = 2, \\ m_{\widehat{\mathbf{L}}}^{(0)}, m_{\widehat{\mathbf{L}}}^{(\pm c_2)} & \text{if } \ell = 3, \\ m_{\widehat{\mathbf{L}}}^{(0)}, m_{\widehat{\mathbf{L}}}^{(\pm c_1)}, m_{\widehat{\mathbf{L}}}^{(\pm c_2)} & \text{if } \ell = 4. \end{cases}$$

Thus, in order to obtain suitable descriptions for $\mathbf{t}^{(\ell)}$, $\ell \in \{2, 3, 4\}$, we need to consider shifted versions $\mathbf{L}[\mathcal{C}, \mathbf{t}^{(\ell)}] \cong \widehat{\mathbf{L}}$ with

$$\mathbf{t}^{(\ell)} := \mathbf{t} + \tau^{(\ell)} \quad (5.2)$$

Then, the error propagator corresponding to a block Jacobi update can be written as

$$G^{(\ell)} = (I - (\mathbf{L}^{(j)})^\dagger \mathbf{L}[\mathcal{C}, \mathbf{t}^{(\ell)}]) : \mathcal{L}(T_e^{\mathbf{t}^{(\ell)}}) \rightarrow \mathcal{L}(T_e^{\mathbf{t}^{(\ell)}})$$

with $(\mathbf{L}^{(\ell)} f)(x) := (m_P m_{\mathbf{L}[\mathcal{C}, \mathbf{t}^{(\ell)}]}^{(0)} m_P) f(x)$ where m_P is the diagonal matrix

$$(m_P)_{ii} = \begin{cases} 1 & i \in \{1, 2, 3, 5, 6, 7, 9, 10, 11\} \\ 0 & \text{else.} \end{cases} \quad (5.3)$$

A plot of the spectral radii of the error propagator which updates all four colors successively ($G = \prod_{\ell=1}^4 G^{(\ell)}$) is given in Figure 5.4b. Note once again that this plot cannot be directly compared with Figure 5.2 or Figure 5.3b, since we are only looking the largest of 16 eigenvalues per wavevector.

We summarize the procedure in which we obtain the error propagators and their spectral radii by making use of the algorithms given in Appendix A.

Analysis of the 4-color overlap method using aLFA:

Denote the discretized Laplacian with $\mathbf{L} = \mathbf{L}[\mathcal{A}, \mathbf{s}]$ and obtain the description of the discretized Laplacian with respect to the translational invariance of the splitting via Algorithm A.4:

$$\widehat{\mathbf{L}} \leftarrow \text{LatticeCoarsening}(\mathbf{L}[\mathcal{A}, \mathbf{s}], \mathcal{C}).$$

Adjust the structure elements, such that the connections among the unknowns updated simultaneously are found within the central multiplier via Algorithm A.7:

$$\mathbf{L}[\mathcal{C}, \mathbf{t}^{(\ell)}] \leftarrow \text{ChangeStructureElement}(\widehat{\mathbf{L}}, \mathbf{t}^{(\ell)}, \mathbf{t}^{(\ell)}),$$

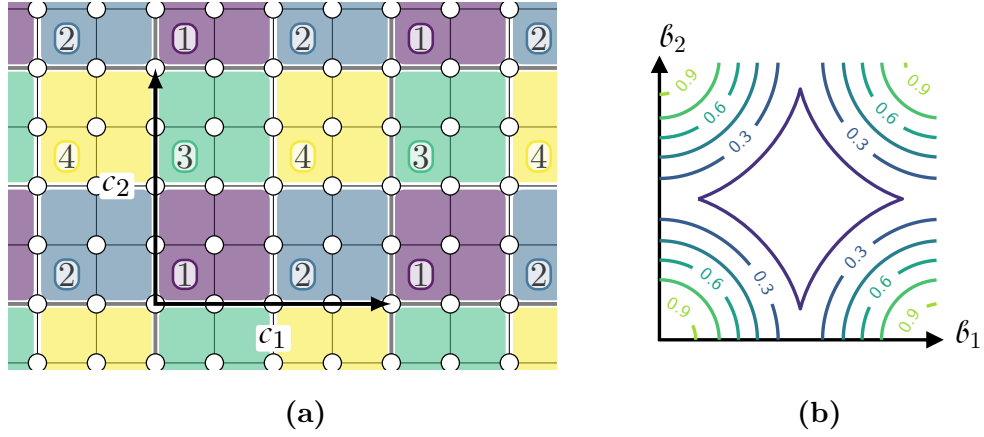


Figure 5.4.: a) Illustration of the domain composition corresponding of the four color overlap method. Each unknown belongs 1, 2 or 4 different colors. The iterative method successively updates unknowns of one color. b) Spectral radii of the symbols of $G = \prod_{\ell=1}^4 G^{(\ell)}$ with $k \in \mathcal{P}(\mathcal{B})$, $\mathcal{B} = (4\mathcal{A})^{-T}$.

where $\mathbf{t}^{(\ell)}$ is defined according to equation (5.2). Use m_P as defined in equation (5.3) to define the operators

$$\mathbf{L}^{(\ell)} : \mathcal{L}(T_C^{\mathbf{t}^{(\ell)}}) \rightarrow \mathcal{L}(T_C^{\mathbf{t}^{(\ell)}}), \quad m_{\mathbf{L}^{(\ell)}}^{(0)} := m_P m_{\mathbf{L}[C, \mathbf{t}^{(\ell)}]}^{(0)} m_P.$$

The computation of the eigenvalues of the error propagator is then carried out with Algorithm A.1 via

$$\text{ComputeSpectra}(f, (I, \mathbf{L}, \mathbf{L}^{(1)}, \mathbf{L}^{(2)}, \mathbf{L}^{(3)}, \mathbf{L}^{(4)}))$$

where the function f denotes the composition of the error propagators

$$(I, \mathbf{L}, \mathbf{L}^{(1)}, \mathbf{L}^{(2)}, \mathbf{L}^{(3)}, \mathbf{L}^{(4)}) \xrightarrow{f} \prod_{\ell=1}^4 (I - (\mathbf{L}^{(\ell)})^\dagger \mathbf{L}) := G.$$

5.3. Multigrid methods

We introduce multigrid methods from a matrix point of view before putting them into the context of Chapter 4 using an example. In Example 5.1 we demonstrated that a splitting method is able to quickly reduce errors in the direction of eigenvectors corresponding to large eigenvalues. Errors in the direction of the eigenvectors corresponding to small eigenvalues, on the other hand, remained virtually unaffected. This behavior showed up as the smoothing of the error. A multigrid method relies on the efficient interplay between a

smoother G , which typically is one of the simple stationary iterative schemes of Chapter 5, and a coarse grid correction that is able to treat error components untouched by the smoother on a coarser scale. In order to formulate the coarse grid correction one first has to specify suitable coarse degrees of freedom. Oftentimes this corresponds to a splitting of the grid points X ($|X| = n$) of the current level into variables which are used on the coarse grid, X^c , and the remainder X^f . Once the choice of coarse degrees of freedom has been made, appropriate *interpolation* and *restriction* operators need to be defined

$$P : \mathbb{R}^{n_c} \rightarrow \mathbb{R}^n \quad \text{and} \quad R : \mathbb{R}^n \rightarrow \mathbb{R}^{n_c},$$

where n_c denotes the number of coarse degrees of freedom, e.g., $n_c = |X^c|$.

Additionally, we need to find a suitable *coarse grid operator*

$$A_c : \mathbb{R}^{n_c} \rightarrow \mathbb{R}^{n_c}.$$

One typical choice is $A_c = RAP$ and in the case of A being symmetric the restriction operator is typically chosen as P^T , which results in a *Galerkin* coarse grid correction. The system matrix A_c should in general be chosen in way such that the solution of $A_c x_c = r_c$ is equal to the coarse representation of the fine grid error. A pseudo-code of the two-grid method is given in Algorithm 5.1.

The (V -cycle) multigrid method is obtained by replacing successively $(A_c)^\dagger$ by (a single iteration of) another two-grid method [47].

Algorithm 5.1: Tentative two-grid method.	
Input: Initial guess $x^{(0)}$	
1	for $m = 2, \dots$
2	$x^{(m)} = G^{\nu_1}(A, x^{(m-1)}, b)$ ▷ pre-smooth ν_1 times
3	$r_c = R(b - Ax^{(m)})$ ▷ coarsen the residual
4	$x_c = (A_c)^\dagger r_c$ ▷ solve the coarse grid problem
5	$x^{(m)} = x^{(m)} + Px_c$ ▷ interpolate and correct
6	$x^{(m)} = G^{\nu_2}(A, x^{(m)}, b)$ ▷ post-smooth ν_2 times

We can write the two-grid and the multigrid method in terms of a linear iterative method $(I - S^{-1}A)$ provided that the initial guess $x_k^{(0)}$ is zero on every grid level k and that the smoother is a consistent linear iterative method.

Lemma 5.12. *The two-grid method is defined by the error propagators,*

$$M = G^{\nu_2} K G^{\nu_1}$$

and

$$K = [I - PA_c^{-1}RA]$$

where G denotes the error propagator of the smoother. These operators are called two-grid operator and coarse grid correction operator, respectively.

Proof. The coarse grid correction of Algorithm 5.1 applied to some $x_{(\text{old})}$ yields

$$\begin{aligned} x_{(\text{new})} &= x_{(\text{old})} + PA_c^{-1}R(b - Ax_{(\text{old})}) \\ &= (I - PA_c^{-1}RA)x_{(\text{old})} + PA_c^{-1}Rb. \end{aligned}$$

Thus, the method is a consistent linear iterative method with the associated error propagator $K = [I - PA_c^{-1}RA]$. Since G is an error propagator itself, the product $M = G^{\nu_2}KG^{\nu_1}$ is again an error propagator. \square

Lemma 5.13. *The m -grid multigrid method is defined by the error propagators*

$$M_\ell = G_\ell^{\nu_2}K_\ell G_\ell^{\nu_1}$$

and

$$K_\ell = (I_\ell - P_\ell[I_{\ell+1} - M_{\ell+1}]A_{\ell+1}^{-1}R_\ell A_\ell),$$

for $\ell = 0, \dots, m-1$ and $M_m = 0$. The operators G_ℓ , I_ℓ , P_ℓ , A_ℓ and R_ℓ denote smoother, identity, prolongation, grid operator and the restriction on grid level ℓ .

Proof (by induction). Let $m \in \mathbb{N}$ be arbitrary. We obviously have that the formula is correct for M_{m-1} and thus we only need to prove the statement for M_0 while assuming that the formula is correct for M_1, \dots, M_m . One iteration of the multigrid method is given by Algorithm 5.1 where solving the coarse grid problem in line 5 is replaced by a single iteration of the iterative method defined by the error propagator M_1 . As the initial guess $x_1^{(0)}$ of the coarse grid problem

$$A_1 x_1 = R_0(b_0 - A_0 x_{(\text{old})})$$

is equal to zero we can apply Lemma 5.6 and find

$$x_1 = (I_1 - M_1^\gamma)A_1^{-1}R_0(b_0 - A_0 x_{(\text{old})}).$$

Thus, for the coarse grid correction we find

$$\begin{aligned} x_{(\text{new})} &= x_{(\text{old})} + P_0 x_1 \\ &= x_{(\text{old})} + P_0(I_1 - M_1)A_1^{-1}R_0(b_0 - A_0 x_{(\text{old})}) \\ &= (I_0 - P_0(I_1 - M_1)A_1^{-1}R_0 A_0)x_{(\text{old})} + P_0(I_1 - M_1)A_1^{-1}R_0 b_0. \end{aligned}$$

This implies the error propagator

$$K_0 = (I_0 - P_0(I_1 - M_1)A_1^{-1}R_0 A_0)$$

and hence $M_0 = G_0^{\nu_2}K_0 G_0^{\nu_1}$. \square

In this thesis we restrict ourselves to a single pre-smoothing step ($\nu_1 = 1$) and fully neglect post-smoothing ($\nu_2 = 0$) and thus only consider the simple two-grid error propagator given by

$$M = KG.$$

Analysis of a multigrid method via aLFA

We already demonstrated how to use the algorithms in Appendix A in order to analyze smoother G in Section 5.2. In order to extract the spectrum of a two-grid method

$$M = KG,$$

we further have to specify the coarse grid correction operator K . As an example we consider the full coarsening strategy with the full weighting (Galerkin) scheme which is commonly used for scalar elliptic discretized PDEs on rectangular grids. A schematic stencil of the *full weighting* restriction and prolongation is given in Figure 5.5. The restriction operator is a multiplication operator

$$R : \mathcal{L}(T_{2\mathcal{A}}^{\mathfrak{t}}) \rightarrow \mathcal{L}(T_{2\mathcal{A}}^{(0)}),$$

where $T_{2\mathcal{A}}^{\mathfrak{t}}$, $\mathcal{A} = [a_1 \mid a_2] = \frac{1}{h} \begin{bmatrix} 1 & 0 \\ 0 & 1 \end{bmatrix}$, $\mathfrak{t} = (0, a_1, a_2, a_1 + a_2) \cong T_{\mathcal{A}, 2\mathcal{A}}$, denotes the fine crystal rewritten with respect to the translational invariance $2\mathcal{A}$ and $T_{2\mathcal{A}}^{(0)}$ denotes the coarse crystal. The nonzero multipliers of R are given by

$$\begin{aligned} m_R^{(-a_1)} &= \begin{bmatrix} 0 & 2 & 0 & 1 \end{bmatrix} & m_R^{(0)} &= \begin{bmatrix} 4 & 2 & 2 & 1 \end{bmatrix} \\ m_R^{(-a_1 - a_2)} &= \begin{bmatrix} 0 & 0 & 2 & 1 \end{bmatrix} & m_R^{(-a_2)} &= \begin{bmatrix} 0 & 0 & 0 & 1 \end{bmatrix} \end{aligned}$$

The spectral radii of the two-grid correction operator can be obtained with Algorithm A.1 via

$$\text{ComputeSpectra}(f, I, R, L, G),$$

where the function f denotes the composition of the error propagators

$$(R, L, G) \xrightarrow{f} (I - R^T(RLR^T)^\dagger RL)G = KG = M.$$

Numerical results

In this section we show results for the Galerkin multigrid method with the previously introduced full weighting scheme applied to the Laplacian on the rectangular grid.

As a smoother G we consider the four different methods introduced in Section 5.2, namely

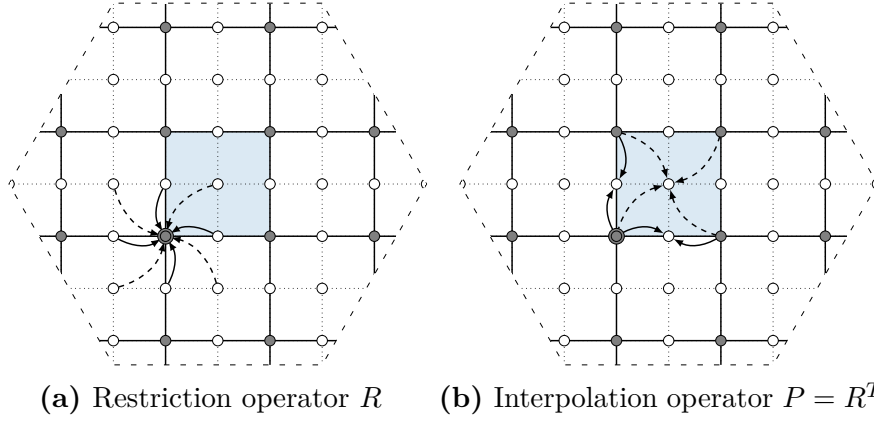


Figure 5.5.: Schematic stencil of the full weighting intergrid operators.

1. the relaxed Jacobi ($\omega = \frac{4}{5}$),
2. (unrelaxed) lexicographic Gauss-Seidel,
3. (unrelaxed) red-black Gauss-Seidel and
4. the (unrelaxed) four-color overlap block method.

In Figure 5.6 the plots of the spectral radii of the two-grid error propagators

$$M = KG$$

for the first three smoothers are given with respect to $2^{-1}\mathcal{B} = (2\mathcal{A})^{-T}$ whereas the analysis in case of the overlap smoother is given with respect to $4^{-1}\mathcal{B} = (4\mathcal{A})^{-T}$. In Figure 5.7 a plot of the measured asymptotic convergence rate of an actual implementation of the multigrid method with respect to the discretization parameter h is given. It can be seen that the convergence estimate mostly coincides with the measured rate. In the case of the Jacobi smoother the estimate is exact as long as the tested torus size $T_{\mathcal{A},\mathcal{Z}}^s$ is large enough, i.e., the resolution of the dual space is fine enough. To be more precise, the estimate is exact iff $k \in (T_{\mathcal{A},\mathcal{Z}}^s)^*$, where k is the wavevector corresponding to the largest eigenvalue $\rho = \rho((KG)_k)$ (cf. Remark 4.21). The convergence estimate in the case of the lexicographic Gauss-Seidel smoother is only asymptotically ($h \rightarrow 0$) exact due to the fact that the representation as a multiplication operator is only correct for the unknowns that are not located at the bottom or left boundary due to the lexicographical ordering (cf. Section 5.2).

Remark 5.14. *In the case of the four-color overlap block method we used the ordering (cf. Figure 5.4a)*

$$\mathfrak{s}^{(1)} \rightarrow \mathfrak{s}^{(4)} \rightarrow \mathfrak{s}^{(2)} \rightarrow \mathfrak{s}^{(3)}$$

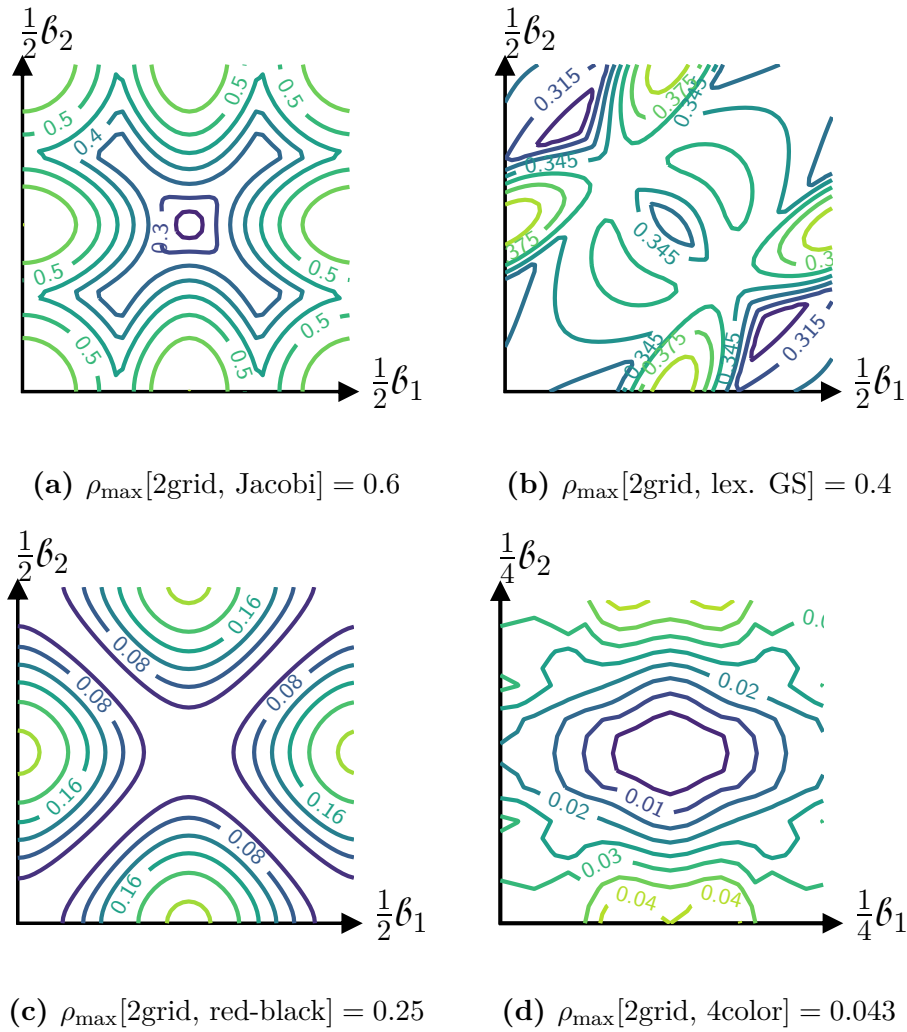


Figure 5.6.: Spectral radii of the symbols of the two-grid error propagator M , $B = \mathcal{A}^{-T}$. (a) relaxed Jacobi, (b) Gauss-Seidel, (c) red-black Jacobi, (d) four color overlap block

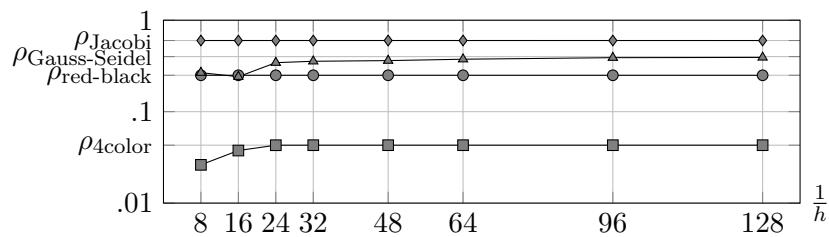


Figure 5.7.: Measured two-grid asymptotic convergence rate with respect to different smoother: \blacklozenge relaxed Jacobi, \blacktriangle Gauss-Seidel, \bullet red-black Gauss-Seidel, \blacksquare four color block overlap.

to obtain the convergence estimate of $\rho = \rho(KG_1G_4G_2G_3) = 0.043$.

Out of the 24 possible permutations, we obtain a total of 3 different convergence estimates. The other two convergence rates are for example found using the orderings 1, 2, 3, 4 and 1, 2, 4, 3 and the corresponding two-grid convergence rates are

$$\rho(KG_1G_2G_3G_4) = 0.0625 \text{ and } \rho(KG_1G_2G_4G_3) = 0.11.$$

We are going to study symmetries of the two-grid method for this smoother in detail in Section 5.4.

In Figure 5.8 we also show results of the m -grid analysis, $m = 3, 4$, for the Gauss-Seidel and the relaxed Jacobi ($\omega = \frac{4}{5}$) method. It can be seen that the asymptotic convergence rate only changes very slightly from 2 to 4 grid. This means that the convergence rates of the two-grid method can be maintained without solving the coarse grid problems exactly.

5.4. Symmetries in colored smoothers

As mentioned in the numerical results of Section 5.3, out of the $4! = 24$ possible permutations

$$\sigma \in \mathbf{Sym}_4 := \{\sigma : \{1, 2, 3, 4\} \rightarrow \{1, 2, 3, 4\}, \text{ bijective}\}$$

of the four color overlap smoother we only obtain 3 different convergence rates when it is used in the two-grid method using full-coarsening:

$$\{\rho(K \prod_{i=1}^4 G_{\sigma(i)}) : \sigma \in \mathbf{Sym}_4\} = \{0.043, 0.0625, 0.11\}.$$

In this section we discuss how to systematically work out the symmetries of a two-grid error propagator. As the number of permutations grows factorial with the number of different colors, it can be useful (or even necessary) to reduce the number of orderings to be analyzed beforehand instead of testing them all.

On the one hand, there is a simple algebraic argument which lets us reverse the order of the smoother without changing the convergence rate, i.e.,

$$\rho(KG_1G_2 \dots G_m) = \rho(KG_mG_{m-1} \dots G_1).$$

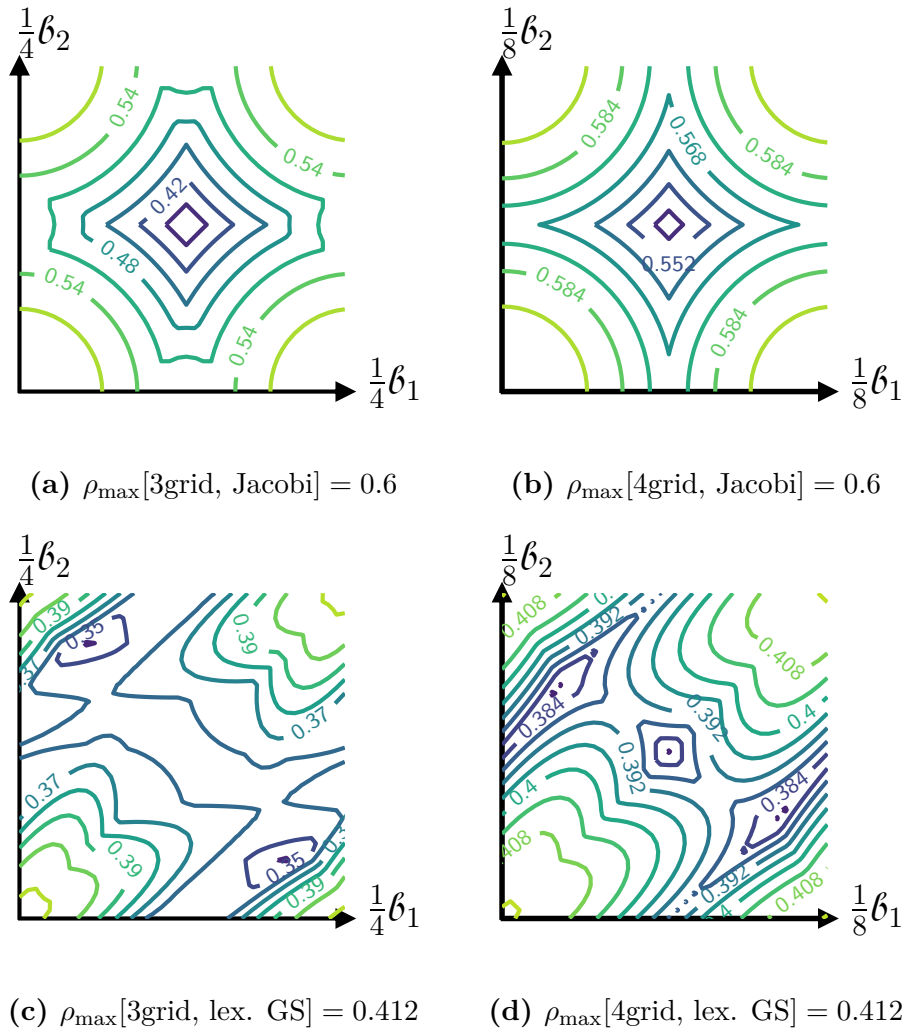


Figure 5.8.: Spectral radii of the symbols of the m -grid error propagator, $\mathcal{B} = \mathcal{A}^{-T}$. (a) Relaxed Jacobi, $\omega = \frac{4}{5}$, $m = 3$, (b) Relaxed Jacobi, $\omega = \frac{4}{5}$, $m = 4$ (c) Gauss-Seidel, $m = 3$, (d) Gauss-Seidel, $m = 4$.

Theorem 5.15 (Algebraic symmetry). *Consider the operator*

$$(I - L_1L)(I - L_2L) \cdots (I - L_mL) \in \mathbb{C}^{n \times n}$$

where $I \in \mathbb{C}^{n \times n}$ denotes the identity, $L_1, L_2, \dots, L_m \in \mathbb{C}^{n \times n}$ are symmetric, i.e., $L_i = L_i^T$, and $L \in \mathbb{C}^{n \times n}$ is nonsingular and symmetric. Then we have

$$\begin{aligned} & \text{spec}((I - L_1L)(I - L_2L) \cdots (I - L_mL)) \\ &= \text{spec}((I - L_1L)(I - L_mL)(I - L_{m-1}L) \cdots (I - L_2L)). \end{aligned}$$

Proof. A straightforward calculation yields:

$$\begin{aligned} & \text{spec}((I - L_1L)(I - L_2L) \cdots (I - L_mL)) \\ &= \text{spec}([(I - L_1L)(I - L_2L) \cdots (I - L_mL)]^T) \\ &= \text{spec}(L^{-1}(I - LL_m)LL^{-1}(I - LL_{m-1}) \cdots (I - LL_1)L) \\ &= \text{spec}((I - L_mL)(I - L_{m-1}L) \cdots (I - L_1L)) \\ &= \text{spec}((I - L_1L)(I - L_mL)(I - L_{m-1}L) \cdots (I - L_2L)) \quad \square \end{aligned}$$

On the other hand, the coarse grid correction operator K usually fulfills several geometric symmetries which can potentially be applied to the smoother in order to work out equivalent orderings. These symmetries can simply be worked out by making use of the so-called two-dimensional space groups also known as the wallpaper groups [1], which are mathematical classifications of two-dimensional repetitive patterns. For our purpose, a repetitive pattern simply corresponds to a crystal. Besides its translational invariance there can be the following *elementary symmetric operations* which map a crystal to itself:

- n -fold rotations, ($n = 2, 3, 4, 6$),
- reflections and
- glide reflections.

As there are only 17 different wallpaper groups in total, one can quickly work out to what wallpaper group a given crystal corresponds.

Remark 5.16. *In this section we restrict ourselves to the 2-dimensional case. A generalization to any dimension is possible, but more complicated [29].*

As an example we consider the four-color smoother introduced in Example 5.3 in combination with the full-coarsening scheme. The fine crystal with respect to the lattice basis $2\mathcal{A}$, given by

$$\mathbb{L}^t(2\mathcal{A}), \quad \mathcal{A} = \frac{1}{h} \left[\begin{array}{c|c} 1 & 0 \\ \hline 0 & 1 \end{array} \right], \quad \mathfrak{t} = (0, a_1, a_2, a_1 + a_2),$$

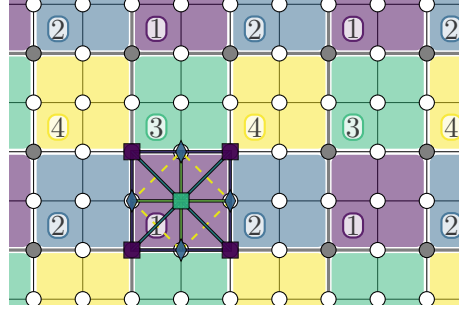


Figure 5.9.: The coarse crystal corresponds to the wallpaper group $p4mm$.

corresponds to the wallpaper group $p4mm$.¹ This wallpaper group consists of the following elementary symmetries:

rotations				reflections	
2	3	4	6	mirror-	glide-
1	-	2	-	3	1

An illustration of the coloring of the smoother, the crystal $\mathbb{L}^t(2\mathcal{A})$ and its symmetries is given in Figure 5.9. Here, the n -fold rotational centers are depicted with diamonds ($n = 2$) and squares ($n = 4$), whereas solid lines correspond to reflections and dashed lines to glide reflections. Each single operator of the coarse grid correction $K = (I - PL_c^{-1}RL)$ and thus the coarse grid correction operator itself fulfills these symmetries as well. The application of the geometric symmetry operations of $p4mm$ to the coloring yields the following permutations $\sigma_i \in \mathbf{Sym}_4$:

i	symmetry operation	σ_i
1	2-fold rotation \blacklozenge	$(1, 3)(2, 4)$
2	4-fold rotation \blacksquare	$(1, 2, 4, 3)$
3	4-fold rotation \blacksquare	$(2, 3)$
4	reflection —	$(1, 3)(2, 4)$
5	reflection —	$(2, 3)$
6	reflection —	$()$
7	glide-reflection - - - -	$(1, 2, 4, 3)$

In here, we use the cycle notation, i.e., a permutation $\sigma = (s_1, s_2, \dots, s_k)$ corresponds to the mapping $s_1 \mapsto s_2 \mapsto \dots \mapsto s_{k-1} \mapsto s_k \mapsto s_1$.

These 7 permutations σ_i are generators of a permutation group

$$H = \langle \sigma_1, \dots, \sigma_7 \rangle := \{ \sigma : \sigma = \sigma_{j_1} \sigma_{j_2} \dots \sigma_{j_k}, j_i \in \{1, \dots, 7\} \}.$$

¹This wallpaper group is also known as $p4m$.

²This group H is actually isomorphic to the dihedral group \mathbf{D}_4 .

This group H is a subgroup of the symmetric group \mathbf{Sym}_4 and splits it into 3 different cosets $Hg = \{hg : h \in H\}$, $g \in \mathbf{Sym}_4$, of size 8, i.e.,

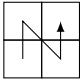
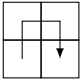
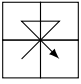
$$H \setminus \mathbf{Sym}_4 = \{Hg : g \in \mathbf{Sym}_4\} =: \{H_1, H_2, H_3\} \text{ with:}$$

H_1	H_2	H_3
()	(3,4)	(2,3,4)
(2,3)	(2,4,3)	(2,4)
(1,2)(3,4)	(1,2)	(1,3,2)
(1,2,4,3)	(1,2,3)	(1,3)
(1,3,4,2)	(1,4,2)	(1,4,3,2)
(1,3)(2,4)	(1,4,2,3)	(1,4,3)
(1,4)	(1,3,4)	(1,2,3,4)
(1,4)(2,3)	(1,3,2,4)	(1,2,4)

These cosets can for example be computed with GAP, a system for computational discrete algebra [16]. For each $j \in \{1, 2, 3\}$ we have

$$\left| \left\{ \rho\left(K \prod_{i=1}^4 G_{\sigma_j(i)}\right) : \sigma_j \in H_j \right\} \right| = 1$$

and each H_j corresponds to a specific shape:

j	1	2	3
Shape of H_j			
$\rho\left(K \prod_{i=1}^4 G_{\sigma_j(i)}\right)$	0.0625	0.11	0.043

For this two-grid method the algebraic symmetry (cf. Theorem 5.15) does not further reduce the number of distinct orderings, but, for example, the fact that the convergence rates of full-coarsening in combination with either red-black or black-red smoothing are equal, i.e., $\rho(KG_{\text{red}}G_{\text{black}}) = \rho(KG_{\text{black}}G_{\text{red}}) = 0.25$, is a consequence of this algebraic symmetry and not due to geometric reasons (cf. Section 5.3).

5.5. Smoothing analysis

In the analysis and construction of multigrid methods a so-called *smoothing analysis* is very common. An introduction to this type of analysis is for example given in [47]. Such an analysis assumes an idealized coarse grid correction

which completely eliminates smooth errors. We start by reviewing some of the examples already discussed, before presenting a general approach to smoothing analysis in the aLFA framework.

Recall, that we computed the spectrum of the Jacobi method via its symbols G_k , $k \in T_{\mathcal{A},\mathcal{Z}}^*$ in Example 5.1. In here, the wavevectors $k \in T_{\mathcal{A},\mathcal{Z}}^*$ near $\mathbb{L}(\mathcal{A}^{-T})$ correspond to *smooth* functions $e^{2\pi i\langle k, \cdot \rangle_2} : T_{\mathcal{A},\mathcal{Z}}^{(0)} \rightarrow \mathbb{C}$. Thus, a smoothing analysis is done by discarding certain wavevectors, i.e., the smoothing analysis corresponds to the computation of the quantity

$$\sup\{\rho(G_k) : k \in T_{\mathcal{A},\mathcal{Z}}^* \text{ not near } \mathbb{L}(\mathcal{A}^{-T})\}.$$

We specify this statement by considering the coarse crystal $T_{2\mathcal{A},\mathcal{Z}}^{(0)}$ we used in Section 5.3. For reasons of dimensionality, i.e., $|T_{\mathcal{A},2\mathcal{A}}| = 4$, at most a quarter of all wavefunctions $e^{2\pi i\langle k, x \rangle_2}$, $k \in T_{\mathcal{A},\mathcal{Z}}^*$, can be eliminated. For each $k \in \mathcal{P}(\mathcal{A}^{-T})$ the idealized coarse grid correction with respect to this coarse crystal is assumed to remove exactly the *smoothest* out of the four wavefunctions $e^{2\pi i\langle k+k_j, \cdot \rangle_2} : T_{\mathcal{A},\mathcal{Z}}^{(0)} \rightarrow \mathbb{C}$, $(k_1, k_2, k_3, k_4) \cong T_{\mathcal{A},2\mathcal{A}}^*$, that is

$$j = \arg \min_{j \in \{1,2,3,4\}} \{\|k + k_j - \hat{k}\|_2 : \hat{k} \in \mathbb{L}(\mathcal{A}^{-T})\}. \quad (5.4)$$

In Figure 5.10a a plot of the smoothing analysis for the relaxed Jacobi method is given, where the areas corresponding to equation (5.4) are greyed out.

However, the smoother to be analyzed may have a coarser translational invariance $\hat{\mathcal{A}}$, $\mathbb{L}(\hat{\mathcal{A}}) \subset \mathbb{L}(\mathcal{A})$, than the underlying system operator and thus mixes wavefunctions $e^{2\pi i\langle k, \cdot \rangle_2} : T_{\mathcal{A},\mathcal{Z}}^{(0)} \rightarrow \mathbb{C}$. If this translational invariance is smaller than the coarse crystal, i.e., $\mathbb{L}(2\mathcal{A}) \subset \mathbb{L}(\hat{\mathcal{A}})$, which is the case for Jacobi, lexicographic Gauss-Seidel and red-black Gauss-Seidel, we can analyze the smoother with respect to the translational invariance $\mathbb{L}(2\mathcal{A})$. That is, we compute the symbols $G_k \in \mathbb{C}^{4 \times 4}$ of $G : \mathcal{L}(T_{\mathcal{C},\mathcal{Z}}^u) \rightarrow \mathcal{L}(T_{\mathcal{C},\mathcal{Z}}^u)$, $\mathbf{u} \cong T_{\mathcal{A},2\mathcal{A}}^{(0)}$, with respect to the standard ordered basis $[e_{1,k} \ e_{2,k} \ \cdots \ e_{4,k}]$, cf. Theorem 4.4.

Next, we transform these symbols according to Remark 4.22 in order to obtain the transformation matrix $\hat{G}_k = E^{-1}G_kE$ with respect to the ordered basis E given by Theorem 4.8. This ordered basis E consists of the four basis functions $\frac{1}{4}(\eta e^{2\pi i\langle k+k_j, \cdot \rangle_2})$, $j = 1, 2, 3, 4$, where $\eta : \mathcal{L}(T_{\mathcal{A},\mathcal{Z}}^{(0)}) \rightarrow \mathcal{L}(T_{\mathcal{C},\mathcal{Z}}^u)$ is the natural isomorphism between the fine crystal representations, cf. Definition 4.6. The smoothing analysis now amounts to the computation of $\sup\{\rho(Z_k \hat{G}_k) : k \in \mathcal{P}((2\mathcal{A})^{-T})\}$, where Z_k corresponds to the filter which discards smooth wavefunctions. Thus, $Z_k \in \mathbb{C}^{4 \times 4}$ is a diagonal matrix, where $(Z_k)_{j,j}$ is either 1 or 0 depending on whether the wavevector $k + k_j$ corresponds to a low or high frequency mode, cf. equation (5.4). In case the smoother does not mix frequencies, i.e., it can be analyzed with respect to the translational invariance

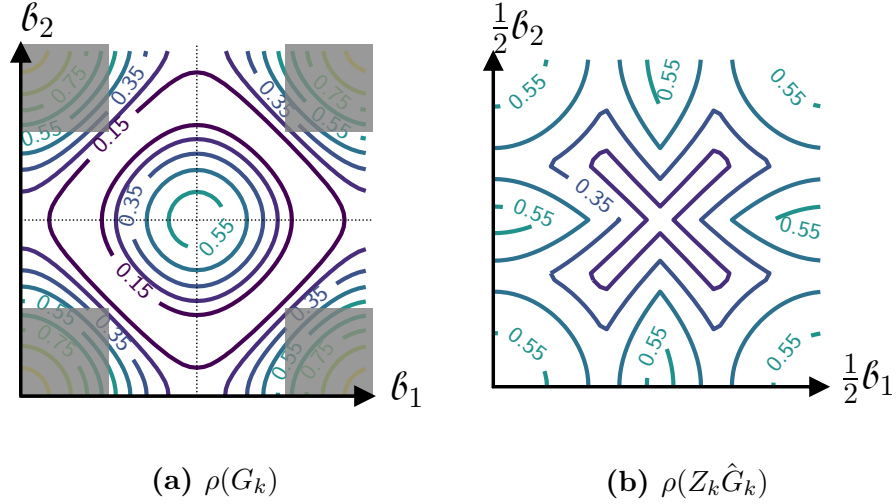


Figure 5.10.: Smoothing analysis of the relaxed ($\omega = \frac{4}{5}$) Jacobi iteration, $\rho_{\max} = 0.6$, $\mathcal{B} = \mathcal{A}^{-T}$. (a) A plot of the spectral radii G_k with respect to the spaces of harmonics \hat{H}_k of $\mathcal{L}(T_{\mathcal{A}, \mathcal{Z}}^{(0)})$. The areas corresponding to smooth wavefunctions are greyed out. (b) A plot of $\rho(Z_k \hat{G}_k)$ with respect to the spaces of harmonics H_k of $\mathcal{L}(T_{2\mathcal{A}, \mathcal{Z}}^u)$, $u \cong T_{\mathcal{A}, 2\mathcal{A}}$, where Z_k corresponds to the filter which discards smooth wavefunctions. The plot in (b) can be obtained from (a) by taking the maximum of the superimposition of its four quarters.

\mathcal{A} of the underlying system operator, a connection from the simple smoothing analysis, where certain areas of $\mathcal{P}(\mathcal{A}^{-T})$ are discarded, to this general analysis is apparent due to the fact that the transition from $\mathcal{L}(T_{\mathcal{A}, \mathcal{Z}}^{(0)})$ to $\mathcal{L}(T_{2\mathcal{A}, \mathcal{Z}}^u)$ is a superimposition in frequency space, cf. Theorem 4.8. For example, the plot of $\rho(Z_k \hat{G}_k)$ in Figure 5.10b, where G corresponds to relaxed Jacobi, can be obtained from Figure 5.10a by taking the maximum of the superimposition of the four quarters (excluding the grey zones). Plots of $\rho(Z_k \hat{G}_k)$ for lexicographic Gauss-Seidel and red-black Gauss-Seidel are given in Figures 5.12a and 5.12b.

In case the translational invariance of the smoother is coarser than the translational invariance of the coarse grid as it is the case for the four-color overlap smoother ($4\mathcal{A}$ vs. $2\mathcal{A}$), we lift the analysis to the function space $\mathcal{L}(T_{4\mathcal{A}, \mathcal{Z}}^u)$, $\hat{u} \cong T_{\mathcal{A}, 4\mathcal{A}}^{(0)}$. Due to a coarsening ratio of a quarter, Z_k now has to eliminate the smoothest 4 of the 16 basis functions.

The predictions obtained by the smoothing analysis coincide with the actual convergence rate using the full-weighting Galerkin scheme in case of relaxed Jacobi (.6) and red-black Gauss-Seidel (.25). The predictions of lexicographic Gauss-Seidel (smoothing analysis: .5, two-grid analysis: .4) and the four-color overlap scheme (smoothing analysis: .057, two-grid analysis: .043) are slightly off, cf. Figure 5.6.

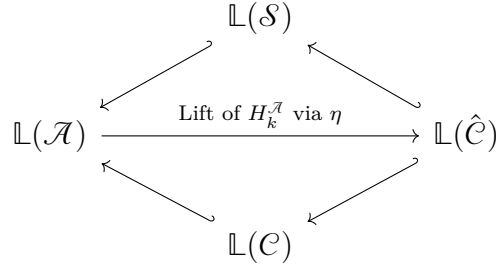


Figure 5.11.: Arrangement of translational invariances ($\mathbb{L}(\mathcal{A})$ system operator, $\mathbb{L}(\mathcal{S})$ smoother, $\mathbb{L}(\mathcal{C})$ coarse grid) in the general smoothing analysis, where $\mathbb{L}(\hat{\mathcal{C}})$ denotes the least common sublattice of all translational invariances.

General smoothing analysis As already seen, the smoothing analysis via the basis lifting of Theorem 4.8 is particularly simple if the translational invariances of the system operator \mathcal{A} , of the smoother \mathcal{S} and the coarse grid \mathcal{C} are nested. That is, in case $\mathbb{L}(\mathcal{C}) \subset \mathbb{L}(\mathcal{S}) \subset \mathbb{L}(\mathcal{A})$ the basis of $H_k^{\mathcal{A}}$ is lifted to $\mathcal{L}(T_{\mathcal{C}, \mathcal{Z}}^{T_s^{\mathcal{A}, \mathcal{C}}})$ and the smoothest $|\mathfrak{s}|$ of the $|T_{\mathcal{A}, \mathcal{C}}| \cdot |\mathfrak{s}|$ basis functions need to be discarded by Z_k .

If on the other hand $\mathbb{L}(\mathcal{S}) \subset \mathbb{L}(\mathcal{C}) \subset \mathbb{L}(\mathcal{A})$, the basis of $H_k^{\mathcal{A}}$ is lifted to $\mathcal{L}(T_{\mathcal{S}, \mathcal{Z}}^{T_s^{\mathcal{A}, \mathcal{S}}})$ and the $|T_{\mathcal{A}, \mathcal{S}}| \cdot |T_{\mathcal{A}, \mathcal{C}}|^{-1} \cdot |\mathfrak{s}|$ smoothest of the $|T_{\mathcal{A}, \mathcal{S}}^*| \cdot |\mathfrak{s}|$ basis functions are discarded by Z_k .

This leaves the case, where both $\mathbb{L}(\mathcal{S}) \subset \mathbb{L}(\mathcal{A})$ and $\mathbb{L}(\mathcal{C}) \subset \mathbb{L}(\mathcal{A})$, but neither $\mathbb{L}(\mathcal{S}) \subset \mathbb{L}(\mathcal{C})$ nor $\mathbb{L}(\mathcal{C}) \subset \mathbb{L}(\mathcal{S})$. In that case a smallest common sublattice $\mathbb{L}(\hat{\mathcal{C}})$ can be found according to Theorem 3.6 such that $\mathbb{L}(\hat{\mathcal{C}}) \subset \mathbb{L}(\mathcal{S})$ and $\mathbb{L}(\hat{\mathcal{C}}) \subset \mathbb{L}(\mathcal{C})$. Lifting the basis of $H_k^{\mathcal{A}}$ to $\mathcal{L}(T_{\hat{\mathcal{C}}, \mathcal{Z}}^{T_s^{\mathcal{A}, \hat{\mathcal{C}}}})$ the smoothing analysis discards the $|T_{\mathcal{A}, \hat{\mathcal{C}}}| \cdot |T_{\mathcal{A}, \mathcal{C}}|^{-1} \cdot |\mathfrak{s}|$ smoothest of the $|T_{\mathcal{A}, \hat{\mathcal{C}}}| \cdot |\mathfrak{s}|$ basis functions. The arrangement of translational invariances of this most general case is illustrated in Figure 5.11.

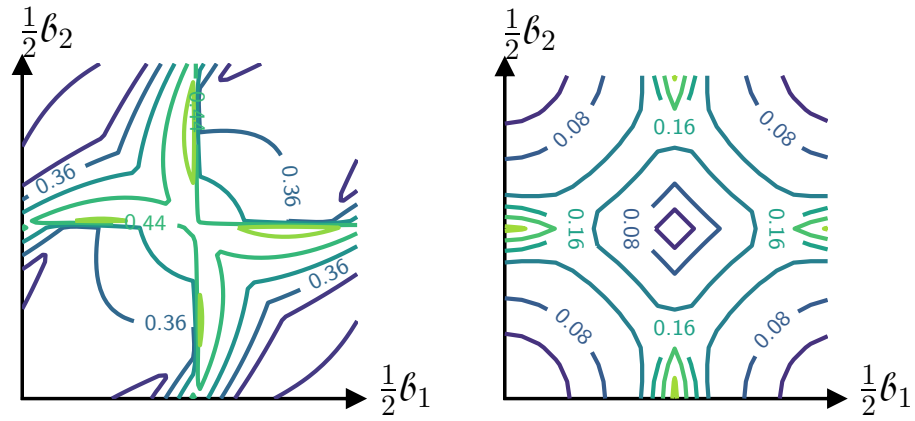
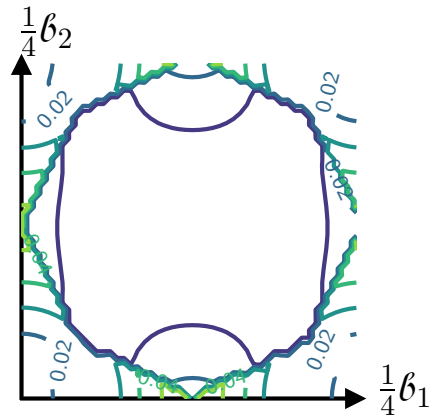
(a) $\rho_{\max}[\text{lex. GS}] = 0.5$ (b) $\rho_{\max}[\text{red-black}] = 0.25$ (c) $\rho_{\max}[\text{4color}] = 0.057$

Figure 5.12.: Spectral radii of the symbols $Z_k \hat{G}_k$ which correspond to the smoothing analysis for different choices of G . (a) lexicographic Gauss-Seidel, (b) red-black Gauss-Seidel, (c) four color overlap block smoother.

Chapter 6

Graphene

In this chapter we study the geometric structure of graphene, the tight-binding Hamiltonian operator L and finally construct and analyze a multigrid method for linear systems of equations originating from this operator. As already mentioned in the introduction, several results of this chapter are already published in [23]. In this article the results are obtained using conventional LFA. Due to the hexagonal structure of graphene, the lexicographic ordering of Kaczmarz and the mixing analysis of the coarse grid correction which involves a mixing of eight frequencies, the analysis turned out to be quite lengthy. In this chapter we stick to the terminology of Chapters 3 and 4 and make use of the algorithms of Appendix A to analyze the problem and the method even though we do not explicitly state the function calls as we did in Section 5.2. We furthermore present some additional results, such as an in-depth analysis of the coarse grid correction and a parallelizable block smoother which are not contained in [23].

6.1. Crystal structure of graphene

Carbon materials occur in many different allotropes. Besides the well-known forms of graphite and diamond, researchers recently isolated graphene, a single layer of carbon atoms bonded in a hexagonal or honeycomb structure. The distance a of two neighboring carbon atoms in graphene is approximately $1.42\text{\AA} = 1.42 \cdot 10^{-10}\text{m}$. Graphene is the basic element of fullerenes, which are molecules of carbons in the form of a sphere (Buckminsterfullerene C_{60}), tubes (carbon nanotubes) and many other shapes [14, 20].

The graphene structure can be described as a crystal $\mathbb{L}^s(\mathcal{A})$ where the underlying lattice is triangular. This means that each three nearby lattice points

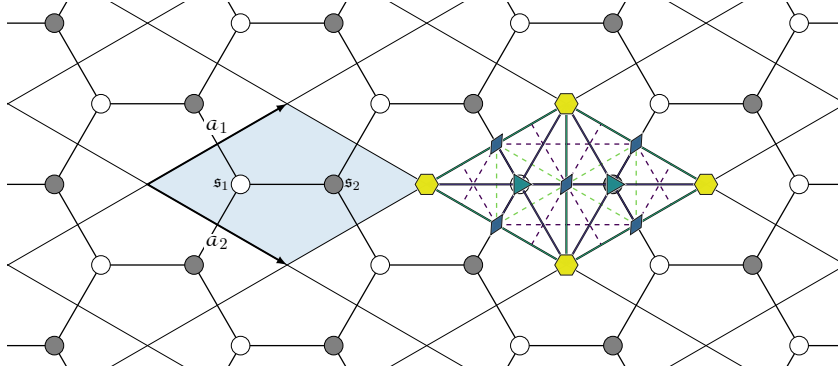


Figure 6.1.: The graphene crystal $\mathbb{L}^s(\mathcal{A})$ and all its elementary symmetry operations. (\circ atom of type A , \bullet atom of type B)

form an equilateral triangle. We have

$$\mathbb{L}^s(\mathcal{A}), \quad a_1 = \left(\frac{3}{2}, \frac{\sqrt{3}}{2}\right)a, \quad a_2 = \left(\frac{3}{2}, -\frac{\sqrt{3}}{2}\right)a,$$

with the structure element

$$\mathfrak{s} = (\mathfrak{s}_1, \mathfrak{s}_2), \quad \mathfrak{s}_1 = (a, 0) = \frac{1}{3}(a_1 + a_2), \quad \mathfrak{s}_2 = (2a, 0) = \frac{2}{3}(a_1 + a_2).$$

To distinguish the atoms we denote $\mathbb{L}(\mathcal{A}) + \mathfrak{s}_1$ by type A and $\mathbb{L}(\mathcal{A}) + \mathfrak{s}_2$ by type B . As illustrated in Figure 6.1, this crystal $\mathbb{L}^s(\mathcal{A})$ possesses several symmetries besides the translational invariance. In here n -fold rotational symmetry centers are depicted with diamonds ($n = 2$), triangles ($n = 3$) and hexagons ($n = 6$), whereas solid lines correspond to reflections and dashed lines to glided reflections. It is well-known that the crystal symmetries correspond to the wallpaper group $p6mm$,¹ i.e., the following elementary symmetry operations map the crystal to itself:

rotations				reflections	
2	3	4	6	mirror-	glide-
1	1	–	1	2	2

6.2. Tight-binding Hamiltonian

In order to calculate the electronic band structure of graphene a tight-binding Hamiltonian approach can be used which considers electrons hopping between

¹This wallpaper group is also known as $p6m$.

atoms with a hopping energy t that only depends on the distance of the atoms. Such an operator is defined by

$$L_t : \mathcal{L}(T_{\mathcal{A}, \mathcal{Z}}^s) \rightarrow \mathcal{L}(T_{\mathcal{A}, \mathcal{Z}}^s), \quad (L_t f)(x) := \sum_{y \in T_{\mathcal{A}, \mathcal{Z}}} m_{L_t}^{(y)} f(x + y)$$

with

$$m_{L_t}^{(y)} = \begin{bmatrix} t(\|y\|_2) & t(\|y + \mathfrak{s}_1\|_2) \\ t(\|y - \mathfrak{s}_1\|_2) & t(\|y\|_2) \end{bmatrix}$$

for some function $t : \{\|x + \mathfrak{s}_\ell\|_2 : x \in \mathbb{L}(\mathcal{A}), \ell = 1, 2\} \rightarrow \mathbb{R}$. The hopping energy t decreases exponentially with distance. Thus, good approximations are already achieved by considering only couplings to the nearest, next-nearest and next-to-next nearest-neighbors. To simplify the notation, let $n_0, n_1, \dots, \in \mathbb{R}$ denote the ordering of the distances $\{\|x + \mathfrak{s}_\ell\|_2 : x \in \mathbb{L}(\mathcal{A}), \ell = 1, 2\} = \cup_j \{n_j\}$, i.e.,

$$n_i < n_j \Leftrightarrow i < j.$$

We then denote the tight-binding Hamiltonian L_t with the hopping energies

$$t(n_i) = \begin{cases} t_i & \text{for } i = 0, 1, \dots, M \\ 0 & \text{else.} \end{cases}$$

by $L_{[t_0, t_1, \dots, t_M]}$. For example, in the case of $L = L_{[t_0, t_1]}$ we have

$$(L f)(x) := \sum_{y \in T_{\mathcal{A}}} m_L^{(y)} f(x + y)$$

for all $x \in T_{\mathcal{A}}$ with nonzero multipliers

$$\begin{aligned} m_L^{(-a_2)} &= \begin{bmatrix} 0 & t_1 \\ 0 & 0 \end{bmatrix} & m_L^{(a_1)} &= \begin{bmatrix} 0 & 0 \\ t_1 & 0 \end{bmatrix} \\ m_L^{(0)} &= \begin{bmatrix} t_0 & t_1 \\ t_1 & t_0 \end{bmatrix} \\ m_L^{(-a_1)} &= \begin{bmatrix} 0 & t_1 \\ 0 & 0 \end{bmatrix} & m_L^{(a_2)} &= \begin{bmatrix} 0 & 0 \\ t_1 & 0 \end{bmatrix} \end{aligned}$$

as illustrated in Figure 6.2. Values $[t_0, t_1, \dots]$ for the hopping energies found in the literature [34] are approximately

$$t^{(1)} = [0, -2.7]eV \quad (t^{(3)} = [-.36, -2.78, -.12, -.068]eV)$$

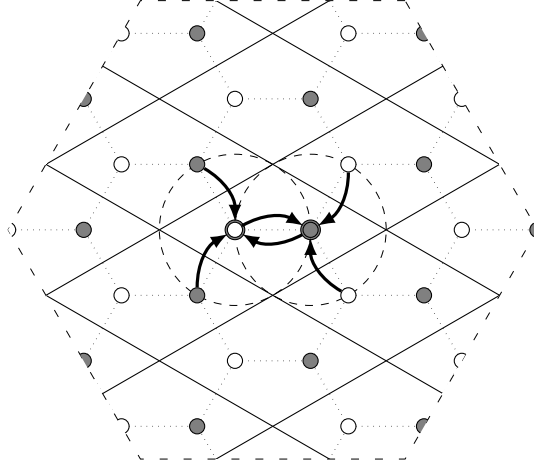


Figure 6.2.: Schematic stencil of the tight-binding Hamiltonian $L_{[t_0, t_1]}$ of graphene (nearest-neighbor (NN) description).

in the nearest-neighbor NN (third-nearest-neighbor 3NN) description.

The eigenvalues (of the symbols) of the tight-binding Hamiltonians $L_{t^{(1)}}$ (NN) and $L_{t^{(3)}}$ (3NN) are plotted in Figure 6.3 along $\mathcal{P}(\mathcal{B})$, where the dual lattice basis is given by

$$\mathcal{B} = \mathcal{A}^{-T} = \frac{1}{3a} \begin{bmatrix} 1 & 1 \\ \sqrt{3} & -\sqrt{3} \end{bmatrix}.$$

The wavevectors

$$K_1 = \frac{1}{3}\mathfrak{b}_1 + \frac{2}{3}\mathfrak{b}_2, \quad K_2 = \frac{2}{3}\mathfrak{b}_1 + \frac{1}{3}\mathfrak{b}_2$$

are called *Dirac points* and correspond to the kernel of the tight-binding Hamiltonian, i.e., $\text{spec}[(L_{[0, -1]})_{K_j}] = \text{spec}[(L_{[-.36, -2.78, -.12, -.068]})_{K_j}] = \{0\}$, $j = 1, 2$. Thus, the kernel of the tight-binding Hamiltonian is four-dimensional and a basis is given by

$$E_{K_1} \cup E_{K_2} = \text{span} \left\{ \begin{bmatrix} e^{2\pi i \langle K_j, x + \mathfrak{s}_1 \rangle_2} \\ 0 \end{bmatrix}, \begin{bmatrix} 0 \\ e^{2\pi i \langle K_j, x + \mathfrak{s}_2 \rangle_2} \end{bmatrix} : j = 1, 2 \right\}. \quad (6.1)$$

The nearest-neighbor and third-nearest-neighbor Hamiltonians are obviously very similar. The spectra basically only differ far away from the Dirac points. Thus, if a multigrid method performs well in the nearest-neighbor case, it certainly is a suitable preconditioner for the third-nearest-neighbor case. Due to this fact we simply stick to the nearest-neighbor model for the remainder of this chapter.

Remark 6.1. *In fact, the off-diagonal elements of*

$$(L_t)_{K_j} = \sum_y \begin{bmatrix} t(\|y\|_2) & t(\|y + \mathfrak{s}_1\|_2) \\ t(\|y - \mathfrak{s}_1\|_2) & t(\|y\|_2) \end{bmatrix} e^{2\pi i \langle K_j, y \rangle_2},$$

which correspond to the interaction between the two sublattices $\mathbb{L}(\mathcal{A}) + \mathfrak{s}_1$ and $\mathbb{L}(\mathcal{A}) + \mathfrak{s}_2$, for an arbitrary t are always equal to zero. This is due to the fact, that this sum can be grouped in triplets, each corresponding to the 3-fold symmetry of the crystal. For each $y = j_1 \mathfrak{a}_1 + j_2 \mathfrak{a}_2 \in \mathbb{L}(\mathcal{A})$ we have

$$C_{\pm} = t(\|y \pm \mathfrak{s}_1\|_2) = t(\|R_{\frac{2\pi}{3}}(y \pm \mathfrak{s}_1)\|_2) = t(\|R_{\frac{4\pi}{3}}(y \pm \mathfrak{s}_1)\|_2),$$

where $R_{\frac{2\pi}{3}}$ denotes the (counter clockwise) rotation matrix. Due to

$$R_{\frac{2\pi}{3}} \mathfrak{s}_1 = \mathfrak{s}_1 - \mathfrak{a}_2 \quad \text{and} \quad R_{\frac{4\pi}{3}} \mathfrak{s}_1 = \mathfrak{s}_1 - \mathfrak{a}_1$$

the corresponding coefficients of C_{\pm} are given by

$$e^{2\pi i \langle K_j, y \rangle_2}, \quad e^{2\pi i \langle K_j, R_{\frac{2\pi}{3}} y \rangle_2} e^{2\pi i \langle K_j, -\mathfrak{a}_2 \rangle_2} \quad \text{and} \quad e^{2\pi i \langle K_j, R_{\frac{4\pi}{3}} y \rangle_2} e^{2\pi i \langle K_j, -\mathfrak{a}_1 \rangle_2}.$$

Using the equality $e^{2\pi i \langle K_j, R_{\theta} y \rangle_2} = e^{2\pi i \langle R_{-\theta} K_j, y \rangle_2}$ and the fact that $R_{m \frac{2\pi}{3}} K_j \in \mathbb{L}(\mathcal{B}) + K_j$, $m \in \mathbb{Z}$, we find

$$e^{2\pi i \langle K_j, R_m \frac{2\pi}{3} y \rangle_2} = e^{2\pi i \langle K_j, R_n \frac{2\pi}{3} y \rangle_2} \quad \text{for all } m, n \in \mathbb{Z}.$$

Thus, the sum is equal to the sum over all three 3rd roots of unity which is 0.

The diagonal entries of $(L_t)_{K_j}$, corresponding to the intra-action of the A and B sublattices, are in general not equal to zero. In the third-nearest-neighbor description we have $t_0 = 3 \cdot t_2$ and, because the six coefficients of t_2 , given by

$$e^{2\pi i \langle K_j, \pm \mathfrak{a}_1 \rangle_2}, \quad e^{2\pi i \langle K_j, \pm \mathfrak{a}_2 \rangle_2}, \quad e^{2\pi i \langle K_j, \pm (\mathfrak{a}_1 - \mathfrak{a}_2) \rangle_2},$$

sum up to -3 , we find $\text{spec}[(L_{[3t_2, t_1, t_2, t_3]})_{K_j}] = \{0\}$.

Remark 6.2. The wavefunctions on a graphene torus $T_{\mathcal{A}, \mathcal{Z}}^{\mathfrak{s}}$ corresponding to the Dirac points K_1 and K_2 are well defined, i.e., the tight-binding Hamiltonian system is singular iff there are integer $\alpha, \beta \in \mathbb{Z}$ as well as unimodular $U, V \in \mathbb{Z}^{2 \times 2}$ such that

$$U \mathcal{A}^{-1} \mathcal{Z} V = 3 \begin{bmatrix} \alpha & 0 \\ 0 & \beta \end{bmatrix}.$$

6.3. Components of the geometric multigrid method

As already mentioned in Section 6.2 we restrict ourselves to the nearest-neighbor Hamiltonian $L := L_{[0, -1]}$. In this section we present the components of a geometric multigrid method to solve the linear system

$$Ax = b, \quad A = \eta L \eta^{-1} : \mathcal{L}(T_{\mathcal{Z}, \mathcal{Z}}^{T_{\mathcal{A}, \mathcal{Z}}^{\mathfrak{s}}}) \rightarrow \mathcal{L}(T_{\mathcal{Z}, \mathcal{Z}}^{T_{\mathcal{A}, \mathcal{Z}}^{\mathfrak{s}}}).$$

As we use the Galerkin-approach, we only have to describe the smoother and the interpolation operator.

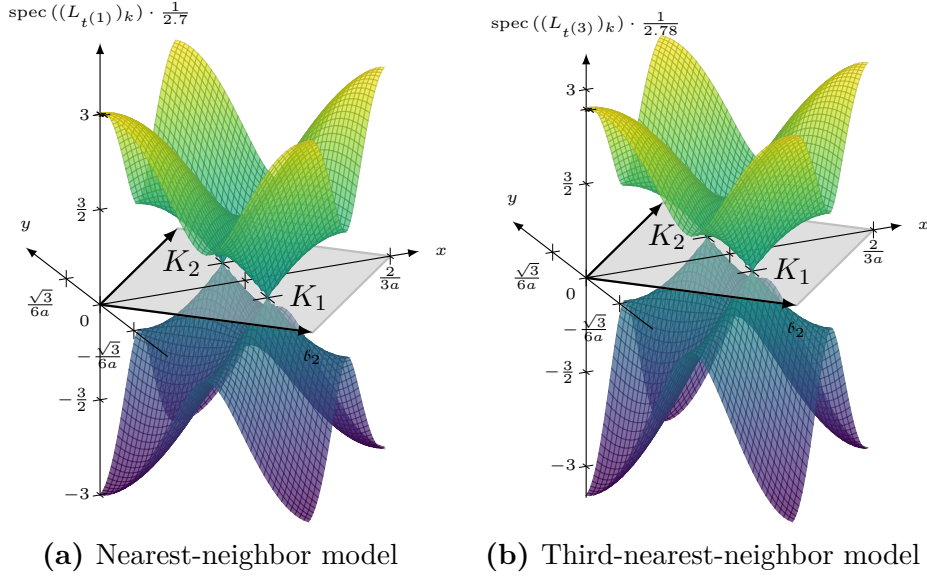


Figure 6.3.: The eigenvalues of the tight-binding Hamiltonian plotted along $\mathcal{P}(\mathcal{B})$, $\mathcal{B} = \mathcal{A}^{-T}$.

Smoother

Due to the fact that the underlying system is (maximally) indefinite, many splitting methods perform poorly or not at all. We found the following two strategies which can be used as a smoother as part of a multigrid method.

Remark 6.3. *The name smoother should not be taken literally in this context. Eigenfunctions corresponding to eigenvalues nearby the Dirac points K_1, K_2 are highly oscillating. Such errors remain nearly unaffected by the methods presented in the following.*

Kaczmarz-method

The *Kaczmarz* iteration can be viewed as the (scalar) Gauss-Seidel iteration on the normal equations $A^T A x = A^T b$ [22]. For the nearest-neighbor model ($t = [0, -1]$) we find

$$L_t^T \cdot L_t = L_{[3,0,1]} = \tilde{L} : \mathcal{L}(T_{\mathcal{A}, \mathcal{Z}}^5) \rightarrow \mathcal{L}(T_{\mathcal{A}, \mathcal{Z}}^5),$$

which is a system without any interaction between the two triangular lattices consisting solely of atoms of type A and B .² We assume that the crystal points are lexicographically numbered from bottom to top and left to right as depicted

²In the third-nearest-neighbor model such a decoupling does not occur.

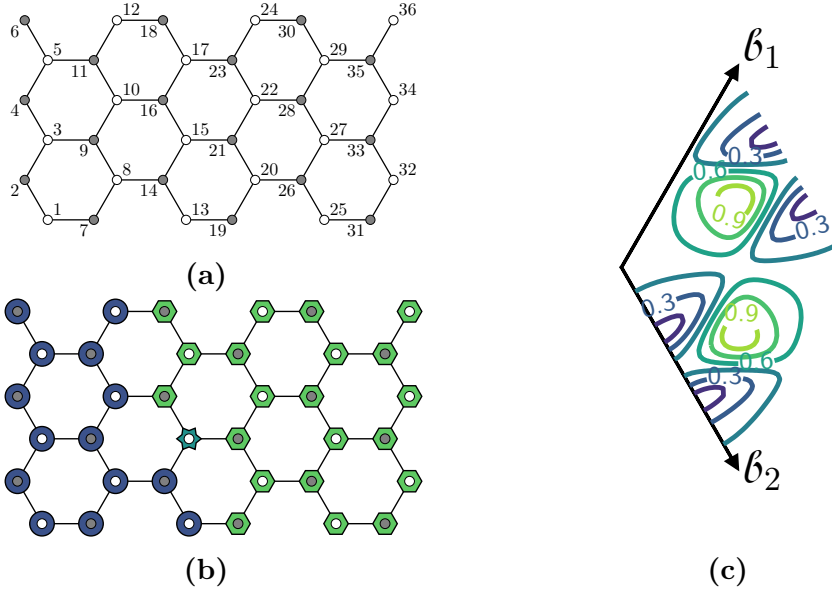


Figure 6.4.: a) Lexicographic ordering of the graphene crystal. b) Status of unknowns within a Kaczmarz iteration. Unknowns already updated \bullet ; current unknown to be updated \star ; remaining unknowns not yet updated \hexagon . c) Spectral radii $\rho(G_K)_k$ of the error propagator $G_K = (I - L_K^{-1}L_{[3,0,1]})$ of the Kaczmarz method plotted along $\mathcal{P}(\mathcal{B})$, $\mathcal{B} = \mathcal{A}^{-T}$. We have $\rho(G_K) = 1$.

in Figures 6.4a and 6.4b. Due to that ordering, we describe the Kaczmarz-method with respect to the shifted structure element (cf. Section 4.3)

$$\mathbf{t} = (\mathbf{t}^{(1)}, \mathbf{t}^{(2)}), \quad \mathbf{t}^{(1)} = \mathbf{s}^{(1)}, \quad \mathbf{t}^{(2)} = \mathbf{s}^{(2)} - \mathbf{a}_2.$$

The error propagator of the Kaczmarz method is given by

$$G_K = (I - L_K^{-1}\hat{L}) : \mathcal{L}(T_{\mathcal{A},\mathcal{Z}}^{\mathbf{t}}) \rightarrow \mathcal{L}(T_{\mathcal{A},\mathcal{Z}}^{\mathbf{t}}),$$

where $\hat{L} \cong \tilde{L}$. The operator L_K is a multiplication operator with

$$(L_K f)(x) = \sum_{y \in T_{\mathcal{A},\mathcal{Z}}} m_{L_K}^{(y)} f(x+y), \quad m_{L_K}^{(y)} = \begin{cases} 0 & \text{if } y_1 > 0 \text{ or } y_2 > 0 \\ \text{tril}(m_{\tilde{L}}^{(0)}) & \text{for } y = 0 \\ m_{\tilde{L}}^{(y)} & \text{else.} \end{cases}$$

This is the (block) Gauss-Seidel operator L_{GS} defined in Chapter 5 with the difference that we use the lower triangular part of the central multiplier $m_{\tilde{L}}^{(0)}$ instead of the complete 2×2 block. A plot of $\rho((G_K)_k)$ is given in Figure 6.4c.

Overlapping Hexagons

Consider the non-disjoint splitting/coloring of the graphene crystal into hexagons as depicted in Figure 6.5. This splitting has a translational invariance of

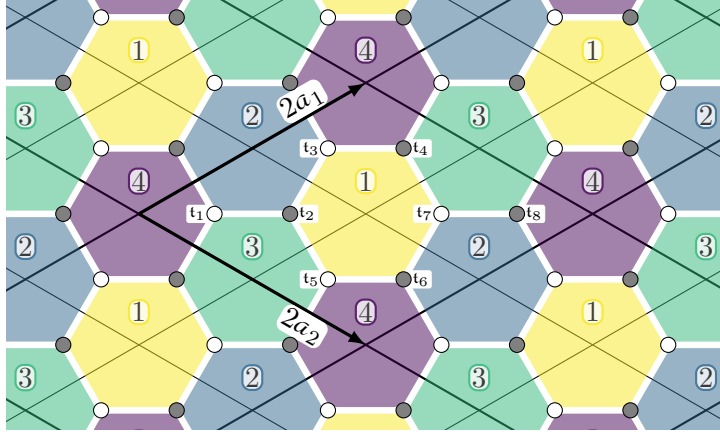


Figure 6.5.: Illustration of the domain decomposition into hexagons. Each unknown belongs to 3 different colors.

$\mathcal{C} = 2\mathcal{A}$. Rewriting the graphene crystal $T_{\mathcal{A}}^{\mathfrak{s}}$ with respect to this coarser lattice $\mathbb{L}(\mathcal{C})$, we find $T_{\mathcal{A}}^{\mathfrak{s}} \cong T_{\mathcal{C}}^{\mathfrak{t}}$ with the structure element

$$\mathfrak{t} = (\mathfrak{t}_1, \dots, \mathfrak{t}_8) = (\mathfrak{s}, \mathfrak{s} + \mathbf{a}_1, \mathfrak{s} + \mathbf{a}_2, \mathfrak{s} + \mathbf{a}_1 + \mathbf{a}_2). \quad (6.2)$$

The splitting is then given by the structure elements

$$\begin{aligned} \mathfrak{t}^{(1)} &= (\mathfrak{t}_2, \mathfrak{t}_3, \mathfrak{t}_4, \mathfrak{t}_5, \mathfrak{t}_6, \mathfrak{t}_7) \\ \mathfrak{t}^{(2)} &= \mathfrak{t}^{(1)} + \mathbf{a}_2 \\ \mathfrak{t}^{(3)} &= \mathfrak{t}^{(1)} + \mathbf{a}_1 \\ \mathfrak{t}^{(4)} &= \mathfrak{t}^{(1)} + \mathbf{a}_1 + \mathbf{a}_2 \end{aligned}$$

such that $T_{\mathcal{C}}^{\mathfrak{s}^{(1)}} \cong \mathbf{1}, T_{\mathcal{C}}^{\mathfrak{s}^{(2)}} \cong \mathbf{2}, T_{\mathcal{C}}^{\mathfrak{s}^{(3)}} \cong \mathbf{3}$ and $T_{\mathcal{C}}^{\mathfrak{s}^{(4)}} \cong \mathbf{4}$. Note, that the restriction of the tight-binding formulation to a hexagon is a *nonsingular* linear system of equations of size 6×6 . For Hamiltonians of the type $L_{[t_0, t_1]}$ as in the case of the nearest-neighbor description each two different hexagons of the same color do not interact. Thus, a Jacobi sweep on the unknowns of one color is cheap and additionally yields a good degree of parallelism. For operators with greater interaction range one has to use more colors. For example, for operators of type $L_{[t_0, \dots, t_4]}$ as it is the case in the third-nearest-neighbor description, one has to use at least 7 colors to decouple the system as depicted in Figure 6.6. Plots of the spectral radii of the error propagators corresponding to the four-color overlap smoother

$$(G_{1,2,3,4}^{\text{hex4}})_k = \prod_{m=1}^4 (I - L_{J,\omega}^{(m)} L)_k$$

using a relaxation of $\omega \in \{\frac{1}{2}, 1\}$ are given in Figures 6.7a and 6.7b. Additionally, in Figure 6.7c a plot of the spectral radii of $(G_{1,2,3,4}^{\text{hex4}})$ in dependence of the

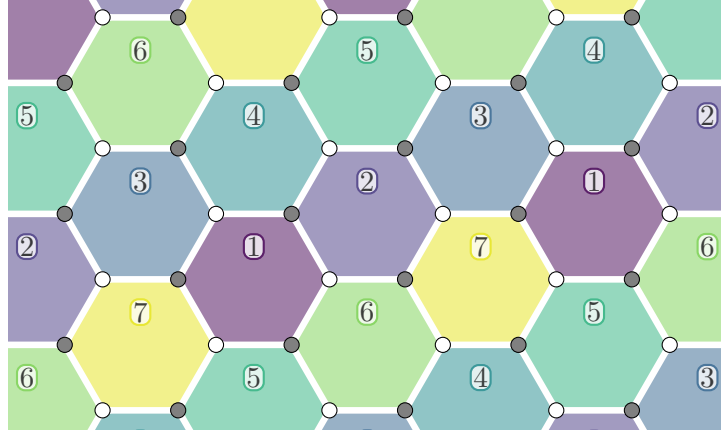


Figure 6.6.: Illustration of the domain decomposition into 7 hexagons. Each unknown belongs to 3 different colors.

relaxation parameter $\omega \in [0, 1]$ is depicted. It can be seen that the spectral radius is greater than 1 for any choice of ω . Thus, this method cannot be used as a standalone solver.

Remark 6.4. *The spectrum of G^{hex4} does not depend on the ordering at all due to the geometric symmetries of the graphene crystal (cf. Figure 6.1). Nevertheless, the ordering has an impact when used as part of a multigrid method as we will discuss in more detail in Section 6.5.*

Intergrid transfer

We choose a coarsening of the graphene crystal in analogy to full-coarsening of a rectangular grid depicted in Figure 6.8. The coarse crystal without the fine grid points is simply given by

$$T_{2\mathcal{A}}^{2\mathfrak{s}}$$

which is again a honeycomb structure and a subset of the fine graphene crystal. The latter is meant in the following sense. Recall from equation (6.2) that we have $T_{\mathcal{A}}^{\mathfrak{s}} \cong T_{2\mathcal{A}}^{\mathfrak{t}}$ with the structure element

$$\mathfrak{t} = (\mathfrak{t}_1, \dots, \mathfrak{t}_8) = (\mathfrak{s}, \mathfrak{s} + \mathfrak{a}_1, \mathfrak{s} + \mathfrak{a}_2, \mathfrak{s} + \mathfrak{a}_1 + \mathfrak{a}_2).$$

The structure element $2\mathfrak{s}$ of the coarse crystal $T_{2\mathcal{A}}^{2\mathfrak{s}}$ corresponds to

$$2(\mathfrak{s}_1, \mathfrak{s}_2) = (\mathfrak{s}_2, \mathfrak{s}_1 + \mathfrak{a}_1 + \mathfrak{a}_2) = (\mathfrak{t}_2, \mathfrak{t}_7).$$

Thus, an atom of type A_c (B_c) on the coarse crystal is of type B (A) on the fine lattice.

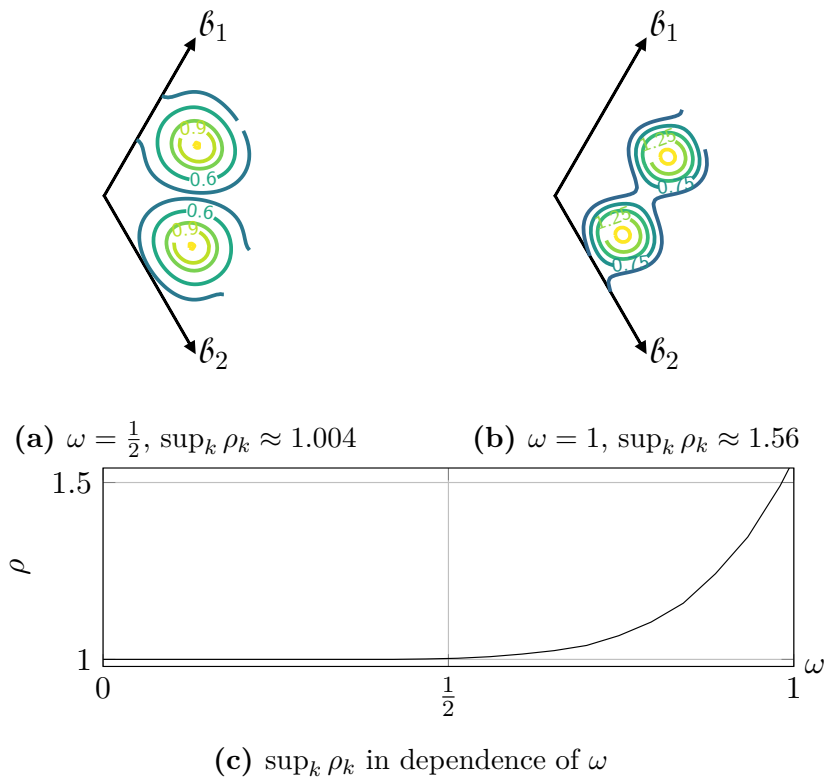


Figure 6.7.: Plots of the spectral radii of the four-color block smoother $G = \prod_m (I - L_{J,\omega}^{(m)} L)$.

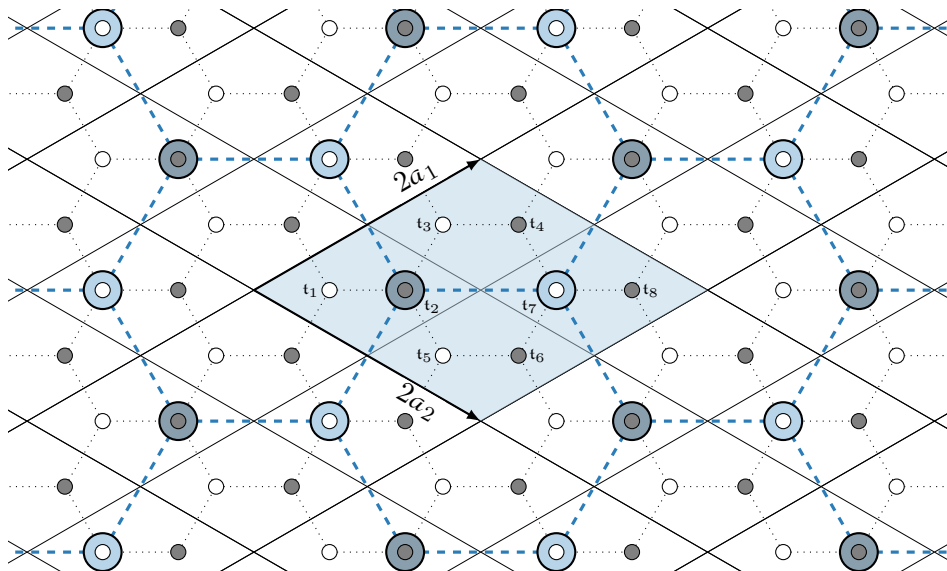


Figure 6.8.: Coarsening strategy of the graphene crystal.

The main idea in the construction of the interpolation operator

$$P = \hat{P} \circ I : \mathcal{L}(T_{2\mathcal{A}}^{2s}) \xrightarrow{I} \mathcal{L}(T_{2\mathcal{A}}^t) \xrightarrow{\hat{P}} \mathcal{L}(T_{2\mathcal{A}}^t) \cong \mathcal{L}(T_{\mathcal{A}}^s),$$

is the exact preservation of the kernel modes of the tight-binding Hamiltonian. Recall from equation (6.1) that the kernel is four dimensional and corresponds to the two Dirac points $K_1 = \frac{1}{3}\mathbf{b}_1 + \frac{2}{3}\mathbf{b}_2$, $K_2 = \frac{2}{3}\mathbf{b}_1 + \frac{1}{3}\mathbf{b}_2$, $\mathcal{B} = \mathcal{A}^{-T}$. A kernel function on the fine graphene crystal $T_{\mathcal{A}}^s$ is of the form

$$\Psi_f(x) = \sum_{j=1,2} \begin{bmatrix} \alpha_j \cdot e^{2\pi i \langle K_j, x+s_1 \rangle_2} \\ \beta_j \cdot e^{2\pi i \langle K_j, x+s_2 \rangle_2} \end{bmatrix} \in \mathcal{L}(T_{\mathcal{A}}^s), \quad \alpha_j, \beta_j \in \mathbb{R}, \quad x \in T_{\mathcal{A}}.$$

The application of the natural isomorphism $\eta : \mathcal{L}(T_{\mathcal{A}}^s) \rightarrow \mathcal{L}(T_{2\mathcal{A}}^t)$ yields

$$[\eta\Psi_f](x) = \sum_{j=1,2} \begin{bmatrix} \alpha_j \cdot e^{2\pi i \langle K_j, x+t_1 \rangle_2} \\ \beta_j \cdot e^{2\pi i \langle K_j, x+t_2 \rangle_2} \\ \alpha_j \cdot e^{2\pi i \langle K_j, x+t_3 \rangle_2} \\ \beta_j \cdot e^{2\pi i \langle K_j, x+t_4 \rangle_2} \\ \alpha_j \cdot e^{2\pi i \langle K_j, x+t_5 \rangle_2} \\ \beta_j \cdot e^{2\pi i \langle K_j, x+t_6 \rangle_2} \\ \alpha_j \cdot e^{2\pi i \langle K_j, x+t_7 \rangle_2} \\ \beta_j \cdot e^{2\pi i \langle K_j, x+t_8 \rangle_2} \end{bmatrix} \in \mathcal{L}(T_{2\mathcal{A}}^t), \quad \text{for all } x \in T_{2\mathcal{A}}.$$

Now, consider such a function consisting of the same frequencies on the coarse crystal

$$\Psi_c(x) = \sum_{j=1,2} \begin{bmatrix} \tilde{\beta}_j \cdot e^{2\pi i \langle K_j, x+2s_1 \rangle_2} \\ \tilde{\alpha}_j \cdot e^{2\pi i \langle K_j, x+2s_2 \rangle_2} \end{bmatrix} \in \mathcal{L}(T_{2\mathcal{A}}^{2s}), \quad \tilde{\alpha}_j, \tilde{\beta}_j \in \mathbb{R}, \quad x \in T_{2\mathcal{A}}.$$

The natural injection of this function into the function space $\mathcal{L}(T_{2\mathcal{A}}^t)$ yields

$$(I\Psi_c)(x) = \sum_{j=1,2} \begin{bmatrix} 0 \\ \tilde{\beta}_j \cdot e^{2\pi i \langle K_j, x+t_2 \rangle_2} \\ 0 \\ 0 \\ 0 \\ \tilde{\alpha}_j \cdot e^{2\pi i \langle K_j, x+t_7 \rangle_2} \\ 0 \end{bmatrix} \in \mathcal{L}(T_{2\mathcal{A}}^t), \quad \text{for all } x \in T_{2\mathcal{A}}.$$

Thus, by choosing $\tilde{\alpha}_j = \alpha_j$ and $\tilde{\beta}_j = \beta_j$, we preserve the kernel modes if \hat{P}

fulfills the following linear system of equations

$$\hat{P} \sum_{j=1,2} \begin{bmatrix} 0 \\ \beta_j \cdot e^{2\pi i \langle K_j, x+t_2 \rangle_2} \\ 0 \\ 0 \\ 0 \\ \alpha_j \cdot e^{2\pi i \langle K_j, x+t_7 \rangle_2} \\ 0 \end{bmatrix} = \sum_{j=1,2} \begin{bmatrix} \alpha_j \cdot e^{2\pi i \langle K_j, x+t_1 \rangle_2} \\ \beta_j \cdot e^{2\pi i \langle K_j, x+t_2 \rangle_2} \\ \alpha_j \cdot e^{2\pi i \langle K_j, x+t_3 \rangle_2} \\ \beta_j \cdot e^{2\pi i \langle K_j, x+t_4 \rangle_2} \\ \alpha_j \cdot e^{2\pi i \langle K_j, x+t_5 \rangle_2} \\ \beta_j \cdot e^{2\pi i \langle K_j, x+t_6 \rangle_2} \\ \alpha_j \cdot e^{2\pi i \langle K_j, x+t_7 \rangle_2} \\ \beta_j \cdot e^{2\pi i \langle K_j, x+t_8 \rangle_2} \end{bmatrix} \quad (6.3)$$

for all $x \in T_{2\mathcal{A}}$, $\alpha_1, \alpha_2, \beta_1, \beta_2 \in \mathbb{R}$. In order to fulfill these equations, the value at a point located at $x + \mathbf{t}_j$, $j = 1, 3, 5, 7$ ($j = 2, 4, 6, 8$), $x \in T_{2\mathcal{A}}$, needs to be interpolated from the values at the coarse crystal points positioned at $y + \mathbf{t}_7$ ($y + \mathbf{t}_2$), $y \in T_{2\mathcal{A}}$. This means that a point of type A (B) need to interpolate from coarse crystal points of the other species B_c (A_c).

The 2nd and 7th row of equation (6.3) are obviously fulfilled if we simply carry over the values, thus we choose the identity on the fine crystal points which make up the coarse crystal, i.e.,

$$P|_{\mathcal{L}(T_{2\mathcal{A}}^{2s})} = \text{id}.$$

The other equations can be fulfilled by interpolating from at least two coarse crystal points. For reasons which become clear in the theoretical analysis in Section 6.4 we opt to use the four, instead of only two, closest coarse crystal points of the opposite species. This choice is depicted in Figure 6.9. Consider for example row 3 of equation (6.3). Here, the four interpolation points are located at $x \pm a_2$ and $x \pm (2a_1 - a_2)$. The corresponding four interpolation weights $\omega = (\omega_s, \tilde{\omega}_s, \omega_\ell, \tilde{\omega}_\ell)$ are obtained by solving

$$\begin{aligned} & \begin{bmatrix} e^{2\pi i \langle K_1, a_2 \rangle_2} & e^{2\pi i \langle K_1, -a_2 \rangle_2} & e^{2\pi i \langle K_1, 2a_1 - a_2 \rangle_2} & e^{2\pi i \langle K_1, -2a_1 + a_2 \rangle_2} \\ e^{2\pi i \langle K_2, a_2 \rangle_2} & e^{2\pi i \langle K_2, -a_2 \rangle_2} & e^{2\pi i \langle K_2, 2a_1 - a_2 \rangle_2} & e^{2\pi i \langle K_2, -2a_1 + a_2 \rangle_2} \end{bmatrix} \omega = \begin{bmatrix} 1 \\ 1 \end{bmatrix} \\ \Leftrightarrow & \begin{bmatrix} e^{\frac{4}{3}\pi i} & e^{-\frac{4}{3}\pi i} & e^{0\pi i} & e^{-0\pi i} \\ e^{\frac{2}{3}\pi i} & e^{-\frac{2}{3}\pi i} & e^{2\pi i} & e^{-2\pi i} \end{bmatrix} \omega = \begin{bmatrix} 1 \\ 1 \end{bmatrix} \\ \Leftrightarrow & \begin{bmatrix} -\frac{1}{2} - \frac{\sqrt{3}}{2}i & -\frac{1}{2} + \frac{\sqrt{3}}{2}i & 1 & 1 \\ -\frac{1}{2} + \frac{\sqrt{3}}{2}i & -\frac{1}{2} - \frac{\sqrt{3}}{2}i & 1 & 1 \end{bmatrix} \omega = \begin{bmatrix} 1 \\ 1 \end{bmatrix}. \end{aligned}$$

In order to fulfill these equations the shortrange interpolation weights need to be equal, i.e., $\tilde{\omega}_s = \omega_s$. The linear system of equations results in the relation

$$\omega_s = \omega_\ell + \tilde{\omega}_\ell - 1. \quad (6.4)$$

Note, that this choice is also valid for the other fine crystal points due to the three-fold rotational symmetry of the crystal. Finally, the representation as a

multiplication operator of our prolongation

$$(Pf)(x) = \sum_{y \in T_{2,\mathcal{A}}} m_P^{(y)} f(x+y), \quad m_P^{(y)} \in \mathbb{R}^{8 \times 2},$$

is illustrated in Figure 6.9 and its nonzero multipliers are given by (0 is replaced by \cdot for the sake of readability):

$$\begin{array}{c}
 m_P^{(-2a_1-2a_2)} = \begin{bmatrix} \cdot & \omega_\ell \\ \cdot & \cdot \\ \cdot & \cdot \\ \cdot & \cdot \\ \cdot & \cdot \\ \cdot & \cdot \\ \cdot & \cdot \\ \cdot & \cdot \end{bmatrix} \\
 m_P^{(-2a_2)} = \begin{bmatrix} \cdot & \omega_s \\ \cdot & \cdot \\ \cdot & \omega_s \\ \cdot & \cdot \\ \cdot & \tilde{\omega}_\ell \\ \cdot & \cdot \\ \cdot & \cdot \\ \cdot & \cdot \end{bmatrix} \\
 m_P^{(-2a_1)} = \begin{bmatrix} \cdot & \omega_s \\ \cdot & \cdot \\ \cdot & \tilde{\omega}_\ell \\ \cdot & \cdot \\ \cdot & \omega_s \\ \cdot & \cdot \\ \cdot & \cdot \\ \cdot & \cdot \end{bmatrix} \\
 m_P^{(-2a_1+2a_2)} = \begin{bmatrix} \cdot & \cdot \\ \cdot & \cdot \\ \cdot & \cdot \\ \cdot & \cdot \\ \cdot & \omega_\ell \\ \cdot & \cdot \\ \cdot & \cdot \\ \cdot & \cdot \end{bmatrix} \\
 m_P^{(2a_1-2a_2)} = \begin{bmatrix} \cdot & \cdot \\ \cdot & \cdot \\ \cdot & \omega_\ell \\ \cdot & \cdot \\ \cdot & \cdot \\ \cdot & \cdot \\ \cdot & \cdot \\ \cdot & \cdot \end{bmatrix} \\
 m_P^{(0)} = \begin{bmatrix} \cdot & \tilde{\omega}_\ell \\ \cdot & \cdot \\ \cdot & \omega_s \\ \cdot & \omega_s \\ \cdot & \omega_s \\ \cdot & \cdot \\ \cdot & \tilde{\omega}_\ell \\ \cdot & \cdot \end{bmatrix} \\
 m_P^{(2a_1)} = \begin{bmatrix} \cdot & \cdot \\ \cdot & \cdot \\ \cdot & \cdot \\ \omega_s & \cdot \\ \cdot & \cdot \\ \tilde{\omega}_\ell & \cdot \\ \cdot & \cdot \\ \omega_s & \cdot \end{bmatrix} \\
 m_P^{(2a_2)} = \begin{bmatrix} \cdot & \cdot \\ \cdot & \cdot \\ \cdot & \cdot \\ \cdot & \cdot \\ \tilde{\omega}_\ell & \cdot \\ \cdot & \cdot \\ \omega_s & \cdot \\ \omega_s & \cdot \end{bmatrix} \\
 m_P^{(2a_1+2a_2)} = \begin{bmatrix} \cdot & \cdot \\ \cdot & \cdot \\ \cdot & \cdot \\ \cdot & \cdot \\ \cdot & \cdot \\ \cdot & \cdot \\ \omega_\ell & \cdot \\ \cdot & \cdot \end{bmatrix}
 \end{array}$$

6.4. Analysis of the coarse grid correction

In this section we analyze the influence of the interpolation weight combination (cf. equation (6.4)) to the coarse grid correction. (Due to the fact that the coarse grid correction operator is a projection, we do not get any insight by extracting its eigenvalues. Thus, we instead proceed as follows.)

Recall that the derived interpolation weights ensure that the Dirac modes $e^{2\pi i \langle K_\ell, x \rangle_2}$ are exactly preserved. We not only want to preserve the Kernel, we especially want that wave functions nearby are preserved as accurately as possible due to the fact that any smoother performs poorly on errors in the direction of eigenfunctions corresponding to small eigenvalues. Reconsider for example row 3 of equation (6.3) which can be written as $f(K_1) = 0$ with

$$f(k) = (e^{2\pi i \langle k, a_2 \rangle_2} + e^{2\pi i \langle k, -a_2 \rangle_2}) \omega_s + e^{2\pi i \langle k, 2a_1 - a_2 \rangle_2} \omega_\ell + e^{2\pi i \langle k, -2a_1 + a_2 \rangle_2} \tilde{\omega}_\ell - 1,$$

where $\omega_s = \omega_\ell + \tilde{\omega}_\ell - 1$. Now, using polar coordinates for the wavevector k , i.e., $k = K_1 + p(r, \phi)$, $p(r, \phi) = r[\cos(\phi), \sin(\phi)]$, an error measure of the prolongation of wavefunctions in proximity to a Dirac point is given by

$$E(\omega_\ell, \tilde{\omega}_\ell) := \sup_{\phi} \left\{ \left\| \frac{\partial}{\partial r} f(K_1 + p(r, \phi)) \Big|_{r=0} \right\|_2 \right\}. \quad (6.5)$$

(For symmetry reasons it is sufficient to consider a single row of equation (6.3) around one Dirac point.) A plot of equation (6.5) is shown in Figure 6.10. As one can see, the error E is constant along the distance to $(\frac{1}{2}, \frac{1}{2})$ in the 1-norm. Regarding this result, the best interpolation weight combination is given by $(\omega_\ell, \tilde{\omega}_\ell) = (\frac{1}{2}, \frac{1}{2})$, and $\omega_s = 0$. Unfortunately, for this choice, the spectrum of the coarse grid operator $L_c = P^T L_{[0,-1]} P$ has additional kernel functions at $\hat{k} \notin \{K_1, K_2\}$ as can be seen in Figure 6.11. As a result, the two-grid method amplifies errors in the direction $e^{2\pi i \langle \hat{k} + \varepsilon, x \rangle}$ for some small $\varepsilon \in \mathbb{R}^2$ which causes divergence of the method. We now study which interpolation weights are allowed with respect to the spectrum of L_c .

Lemma 6.5. *Given an interpolation operator P with interpolation weights $\omega_\ell, \tilde{\omega}_\ell$ and ω_s the Galerkin coarse grid operator*

$$L_c = P^T L_{[0,-1]} P : \mathcal{L}(T_{2\lambda}^{2s}) \rightarrow \mathcal{L}(T_{2\lambda}^{2s})$$

is given by

$$L_c = L_{[t_0, t_1, t_2, t_3, t_4]}$$

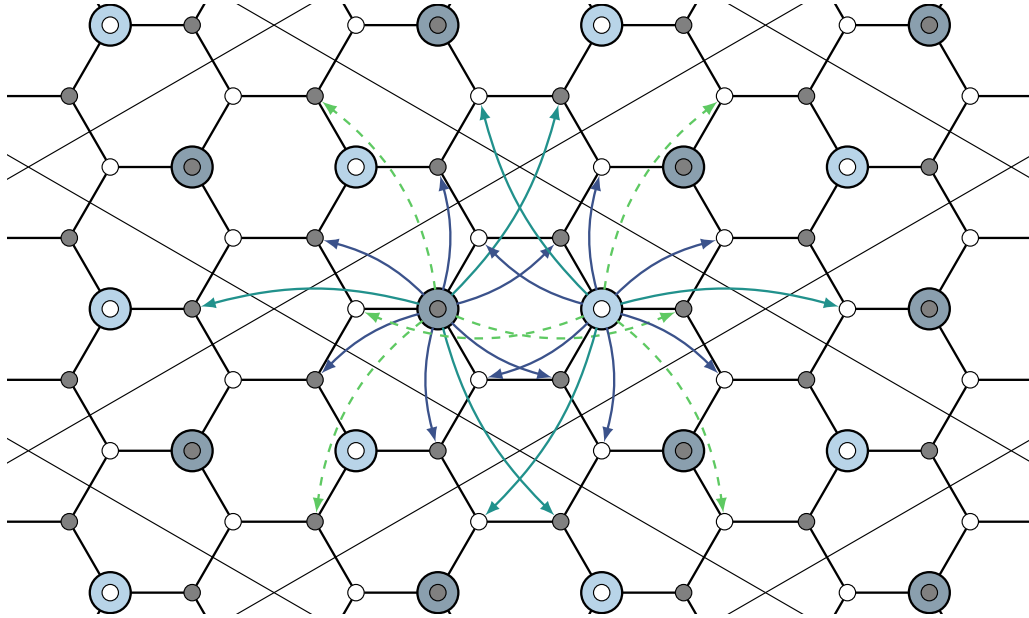


Figure 6.9.: Illustration of interpolation using weights $\rightarrow \omega_s$, $\rightarrow \omega_\ell$ and $\dashrightarrow \tilde{\omega}_\ell$.

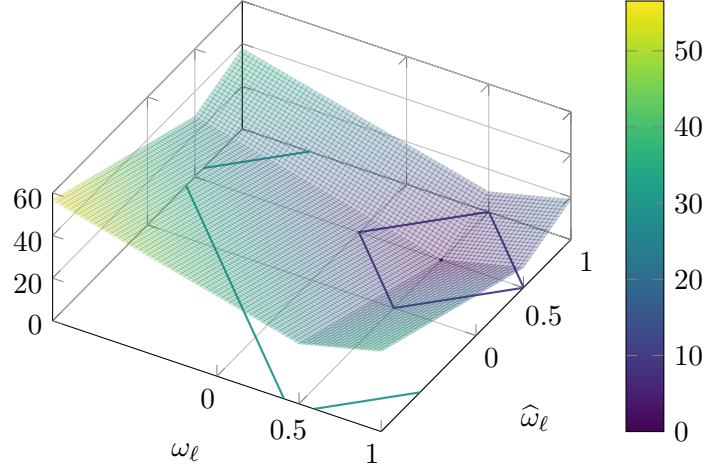


Figure 6.10.: Error measure of the prolongation of wavefunctions in proximity to a Dirac point in dependence of the interpolation weight combination $(\omega_\ell, \widehat{\omega}_\ell)$.

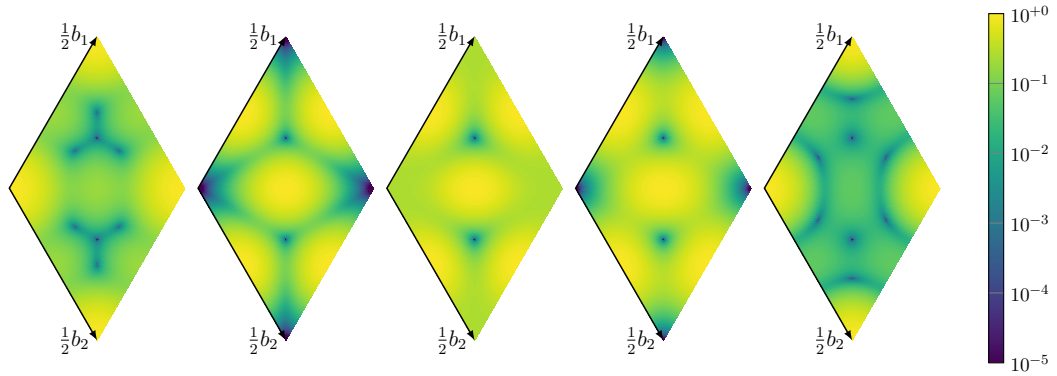


Figure 6.11.: Logarithmic plots of the spectra of $L_c = P^T L_{[0,-1]} P$ for different choices of the interpolation weights $\omega_\ell = \widehat{\omega}_\ell$ and $\omega_s = 2\omega_\ell - 1$; color indicates $\rho((L_c)_k)$. (From left to right: $\omega_\ell = 0$, $\omega_\ell = \frac{1}{6}$, $\omega_\ell = \frac{1}{4}$, $\omega_\ell = \frac{1}{3}$ and $\omega_\ell = \frac{1}{2}$).

with $t_0 = t_2 = 0$ and

$$\begin{aligned} t_1 &= -6\omega_s^2 - 4\omega_s - 4\omega_s(\omega_\ell + \widehat{\omega}_\ell) - 2\omega_\ell^2 - 2\widehat{\omega}_\ell, \\ t_3 &= -2\omega_s^2 - 2\omega_\ell - 4\omega_s\omega_\ell - 2\widehat{\omega}_\ell^2, \\ t_4 &= -2\omega_s\omega_\ell - 2\omega_\ell\widehat{\omega}_\ell. \end{aligned}$$

Proof. This result directly follows from Lemma 4.23. □

The symbol of this coarse grid operator is in general given by

$$(L_c)_k = \begin{bmatrix} 0 & \gamma_{\omega_\ell, \widehat{\omega}_\ell}(k) \\ \gamma_{\omega_\ell, \widehat{\omega}_\ell}(k) & 0 \end{bmatrix}.$$

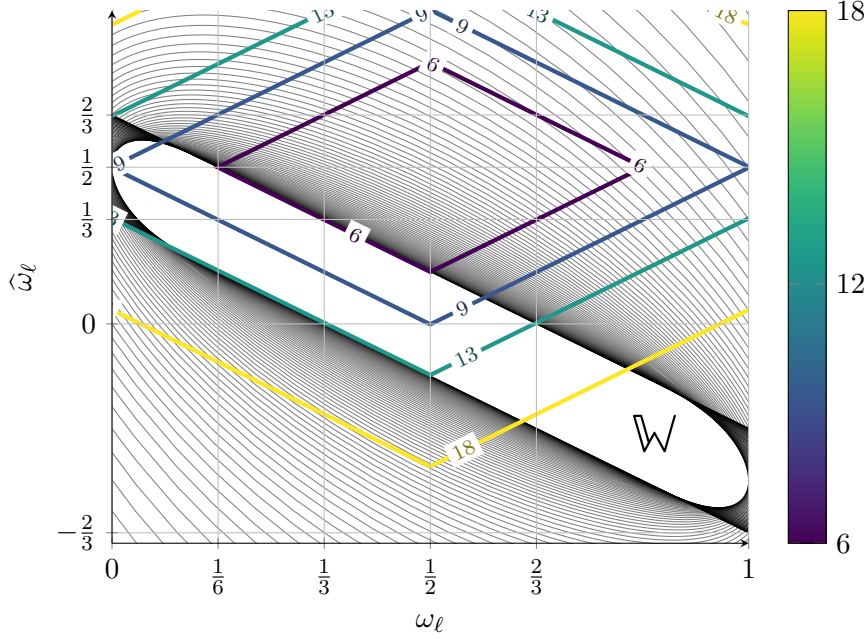


Figure 6.12.: Plot of the area $\mathbb{W} \subset \{(x, y - x) : x \in (0, 1), y \in (\frac{1}{3}, \frac{2}{3})\}$ from which one can chose interpolation weight combination $(\omega_\ell, \widehat{\omega}_\ell)$ as well as several contour lines of the error measure $E(\omega_\ell, \widehat{\omega}_\ell)$.

Using the result of Lemma 6.5 we found³ the contour lines of $\gamma_{\omega_\ell, \widehat{\omega}_\ell}(k) = 0$ for fixed $k \neq \{K_1, K_2\}$. Each contour line correspond to one ellipse and all ellipses fill up \mathbb{R}^2 except a small area $\mathbb{W} \subset \{(x, y - x) : x \in (0, 1), y \in (\frac{1}{3}, \frac{2}{3})\}$ plotted in Figure 6.12. This plot also includes the contour lines of the error measure $E(\omega_\ell, \widehat{\omega}_\ell)$ (cf. equation (6.5)). We have

$$[0 \in \text{spec}((L_c)_k) \Leftrightarrow k \in \{K_1, K_2\}] \iff (\omega_\ell, \widehat{\omega}_\ell) \in \mathbb{W},$$

which means that the two-grid method diverges if $(\omega_\ell, \widehat{\omega}_\ell) \notin \mathbb{W}$.

Thus, the best convergence rate of a two-grid method for any smoother is most certainly found in the *top-right* region of \mathbb{W} , i.e., near the line segment $(\omega_\ell, \widehat{\omega}_\ell) \in \{(x - \varepsilon, \frac{2}{3} - x - \varepsilon) : x \in [\frac{1}{6}, \frac{1}{2}]\}$ for some small $\varepsilon > 0$. Using only 2 interpolation weights is not allowed as both corresponding points $(0, 0)$ and $(\frac{1}{2}, \frac{1}{2})$ are outside of \mathbb{W} . Three instead of four interpolation weights can be used due to $(\frac{1}{3}, \frac{2}{3}) \times \{0\} \in \mathbb{W}$. Here, the weight combination $(\omega_\ell, \omega_s) = (\frac{1}{2}, -\frac{1}{2})$ yields the best preservation of the wavefunctions close to the Dirac modes.

³Using a Computer Algebra System.

6.5. Convergence rates of the multigrid method

In this section we present spectral radii of the derived two-grid method

$$M = KG$$

for the tight-binding formulation of graphene, where G corresponds to one pre-smoothing iteration, with respect to various degrees of freedom. First, we consider Kaczmarz smoothing and show the influence of the interpolation weights on the actual convergence rate of the method (cf. Section 6.4). After that, we analyze the overlapping hexagon smoother with four and seven colors.

Kaczmarz

We first consider the two-grid method with the error propagator $M = KG$, where G corresponds to a single iteration of Kaczmarz. A plot of the spectral radii $\rho(M)$ of the two-grid error propagators for varying interpolation weights $(\omega_\ell, \tilde{\omega}_\ell) \in \mathbb{W}$ is shown in Figure 6.13. We have a relatively large stable plateau of a convergence rate of $[\.75, \.77]$. Furthermore a connection to the standalone analysis of the coarse grid correction (cf. Section 6.4) can be seen. As predicted, the best convergence rate of $\rho \approx \.749$ is obtained for a choice $(\omega_\ell, \tilde{\omega}_\ell)$ on the line segment $\{(x - \varepsilon, \frac{2}{3} - x - \varepsilon) : x \in [\frac{1}{6}, \frac{1}{2}]\}$ which corresponds to the best preservation of the wavefunctions nearby the Dirac modes. However, the minimum along the line $(\omega_\ell, 0)$ is not exactly found at $(\frac{1}{2}, 0)$. Instead, a marginally better choice for this particular smoother can be found at approximately $(.545, 0)$.

In Figure 6.14 we show the spectral radii of the multigrid V -cycle error propagator using $m = 2, \dots, 6$ levels of the multigrid hierarchy in combination with a single pre-smoothing iteration of Kaczmarz. In here we used the interpolation weights $\omega_\ell = .5$, $\tilde{\omega}_\ell = 0$ and $\omega_s = \omega_\ell + \tilde{\omega}_\ell - 1$ on each level. The convergence rate decays only slightly from 2 to 3 grid, but stays constant for $m \geq 3$ which proves the robustness of multigrid method.

Overlapping Hexagons

In this section we analyze the two-grid method using the four and seven color overlapping hexagon smoother introduced in Section 6.3.

For this two-grid method we have several additional degrees of freedom besides the choice of the interpolation weights. We can furthermore freely choose

- the relaxation parameter $\omega \in (0, 1)$ and
- the ordering in which we update the blocks.

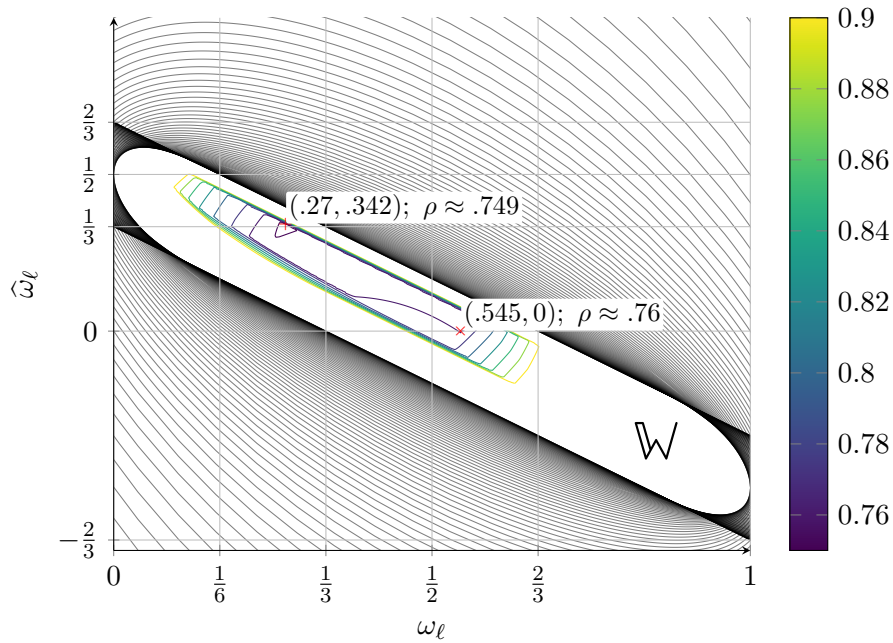


Figure 6.13.: Plot of the spectral radii of the two-grid error propagator $M = KG$ using Kaczmarz smoothing with respect to the choice of the interpolation weights $(\omega_\ell, \tilde{\omega}_\ell)$, $\omega_s = \omega_\ell + \tilde{\omega}_\ell - 1$ (NN description).



Figure 6.14.: Spectral radii of the m -grid error propagator with a single pre-smoothing iteration of Kaczmarz.

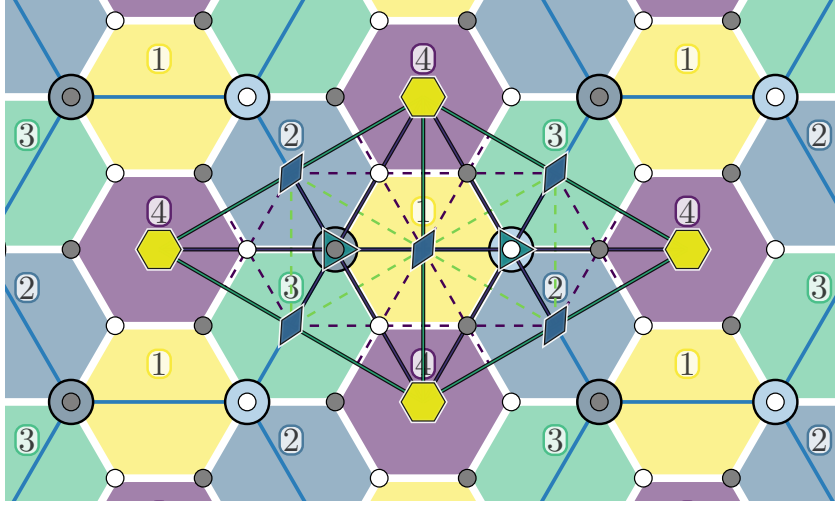


Figure 6.15.: The four color overlap splitting, the coarse graphene crystal $\mathbb{L}^t(2\mathcal{A})$ and all its elementary symmetries.

Using four colors

First, we reduce the number of $4! = 24$ different orderings in which one can update four colors analogously to Section 5.4. The coarse grid correction operator K fulfills the crystal symmetries of the wallpaper group $p6mm$ as depicted in Figure 6.15. Due to the fact that most of these elementary symmetry operations yield the same permutations, it is sufficient to consider for example the six-fold symmetry $\sigma_1 := (1, 3, 2) \in \mathbf{Sym}_4$ and the horizontal reflection $\sigma_2 := (2, 3) \in \mathbf{Sym}_4$ as generators for the permutation group $H := \langle \sigma_1, \sigma_2 \rangle$. This group H splits \mathbf{Sym}_4 into 4 different cosets $Hg = \{hg : h \in H\}$, $g \in \mathbf{Sym}_4$, i.e.,

$$H \setminus \mathbf{Sym}_4 = \{Hg : g \in \mathbf{Sym}_4\} = \{H_1, H_2, H_3, H_4\},$$

where $H_i := \{\sigma \in \mathbf{Sym}_4 : \sigma(4) = i\}$. Using the algebraic symmetry (cf. Theorem 5.15), we can further merge H_1 with H_4 and H_2 with H_3 . Thus, we end up with two different orderings, for example

$$\mathfrak{A} := (1, 2, 3, 4) \text{ and } \mathfrak{B} := (1, 2, 4, 3).$$

In Figure 6.16 a contour plot of the spectral radii of the two-grid error propagator KG is shown, where we use the ordering $\mathfrak{A} = (1, 2, 3, 4)$ and no relaxation, i.e., $\omega = 1$. As can be seen, for the interpolation weight combination $\omega_\ell = .5$, $\tilde{\omega}_\ell = 0$ and $\omega_s = \omega_\ell + \tilde{\omega}_\ell - 1$, we have a convergence rate below 10^{-15} , i.e., it is a direct solver. A plot of the (absolute part of the) sorted spectrum of the error propagator G of the four-color overlap smother is given in Figure 6.17,

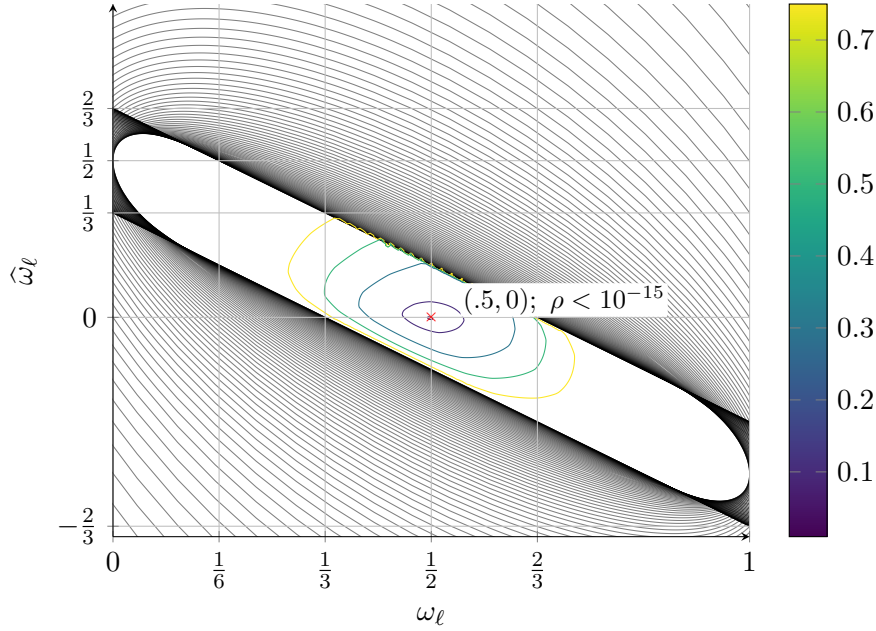


Figure 6.16.: Plot of the spectral radii of the two-grid error propagator KG using the four color overlap smoother with the ordering $\mathfrak{A} = (1, 2, 3, 4)$ with respect to the choice of the interpolation weights with respect to the choice of the interpolation weights $(\omega_\ell, \tilde{\omega}_\ell)$, $\omega_s = \omega_\ell + \tilde{\omega}_\ell - 1$.

i.e., $\text{spec}(G) = \{\lambda_1, \dots, \lambda_n\}$ with $|\lambda_1| \leq |\lambda_2| \leq \dots \leq |\lambda_n|$ where we used $G : \mathcal{L}(T_{2\mathcal{A}, 100\mathcal{A}}^t) \rightarrow \mathcal{L}(T_{2\mathcal{A}, 100\mathcal{A}}^t)$ resulting in $n = 20000$ eigenvalues. One can see that exactly 75% of the eigenvalues are below 10^{-17} .⁴ Due to the fact that the coarsening factor is 25%, the coarse grid correction can at most eliminate 25% of these eigenvalues. As this is exactly the case, we have found an example of a perfect interplay of smoother and coarse grid correction using a sparse/local interpolation which makes it an exceptional result. Usually, such an optimal interpolation turns out to be a dense matrix [12].

From here on we restrict ourselves to exactly these interpolation weights.

Figure 6.18 shows the convergence rates in dependence of the relaxation parameter ω for both orderings \mathfrak{A} and \mathfrak{B} for the fixed interpolation weight combination $(\omega_\ell, \tilde{\omega}_\ell, \omega_s) = (.5, 0, -.5)$. The ordering $\mathfrak{B} = (1, 2, 4, 3)$ is far inferior to ordering \mathfrak{A} as this smoother only works with under-relaxation and we can only obtain a convergence rate of $\rho \approx .35$ for $\omega \approx .7$ at best.

⁴These eigenvalues are probably only > 0 for numerical reasons.

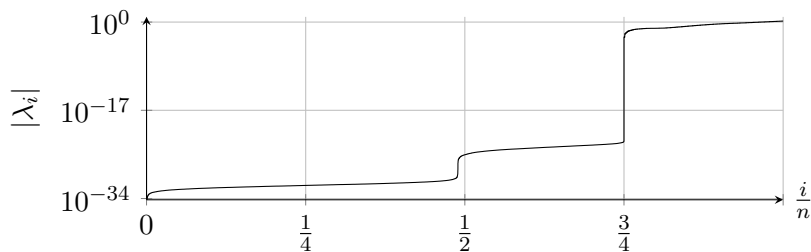


Figure 6.17.: Plot of the sorted spectrum $|\lambda_1| < \dots < |\lambda_n|$ of the error propagator G of the four-color smoother.

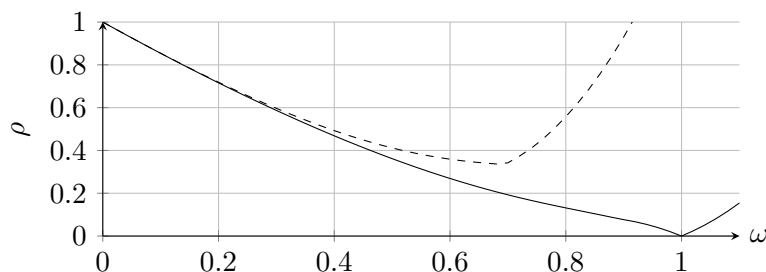


Figure 6.18.: Plot of the spectral radii of the two-grid error propagator KG using the four color overlap smoother with interpolation weights $(\omega_\ell, \tilde{\omega}_\ell, \omega_s) = (.5, 0, -.5)$ in dependence of the relaxation parameter ω . — ordering $\mathfrak{A} = (1, 2, 3, 4)$; - - - ordering $\mathfrak{B} = (1, 2, 4, 3)$.

Using seven colors

When using the third-nearest-neighbor Hamiltonian or when solving the Galerkin coarse grid problem one has to use more than four colors to decouple the system. Thus, we briefly show results for a seven color smoother applied to the nearest-neighbor Hamiltonian.

Again, we can reduce the number of $7! = 5040$ different permutations using the elementary symmetry operations of the coarse grid operator (cf. Figure 6.19). Note, that the mirror symmetries of the wallpaper group $p6mm$ are not compatible with the seven color splitting: For example, a reflection along the horizontal axis does not yield a well defined generator as this reflection for example yields the inconsistent permutations $3 \mapsto 3$ and $3 \mapsto 7$. Thus, we restrict ourselves to the permutations of the wallpaper group $p6$, a sub-group of $p6mm$ without any reflections. Then, we can reduce the $7! = 5040$ permutations to 120 distinct orderings. Using the algebraic symmetry (cf. Theorem 5.15), this number can further be reduced to 64, i.e., we have $5040 = 8$ cosets of size 42 + 56 cosets of size 84.

Figure 6.20 shows the convergence rates with respect to the relaxation parameter ω for two selected orderings \mathfrak{A} and \mathfrak{B} using the interpolation weight combination $(\omega_\ell, \tilde{\omega}_\ell, \omega_s) = (.5, 0, -.5)$. These two orderings correspond to the best and the worst possible choice. For the best possible ordering we find

$$\arg \min_{\sigma \in \mathbf{Sym}_7} \left(\min_{\omega} \rho \left(K \prod_{i=1}^7 G_{\sigma(i), \omega} \right) \right) \hat{=} \mathfrak{A} = (1, 2, 4, 6, 3, 7, 5) \hat{=} \img alt="Diagram of a 2D hexagonal lattice with seven nodes highlighted in a specific pattern corresponding to ordering A." data-bbox="688 475 750 526"/>$$

with a convergence rate of $\rho(K \prod_{i=1}^7 G_{\mathfrak{A}(i), 7}) \approx 0.23$ and for the worst possible ordering we have

$$\arg \max_{\sigma \in \mathbf{Sym}_7} \left(\min_{\omega} \rho \left(K \prod_{i=1}^7 G_{\sigma(i), \omega} \right) \right) \hat{=} \mathfrak{B} = (1, 2, 3, 4, 5, 6, 7) \hat{=} \img alt="Diagram of a 1D chain of seven hexagons corresponding to ordering B." data-bbox="648 580 780 642"/>$$

with a convergence rate of $\rho(K \prod_{i=1}^7 G_{\mathfrak{B}(i), 4}) \approx 0.68$. Thus, the number of colors and the ordering can have a big influence on the convergence rate of the method. Furthermore, a lexicographic ordering can be the worst possible choice.

6.5.1. Open boundaries

In this section we study the multigrid performance applied to non-periodic graphene samples. At first, we introduce the graphene samples to which the multigrid method is applied.

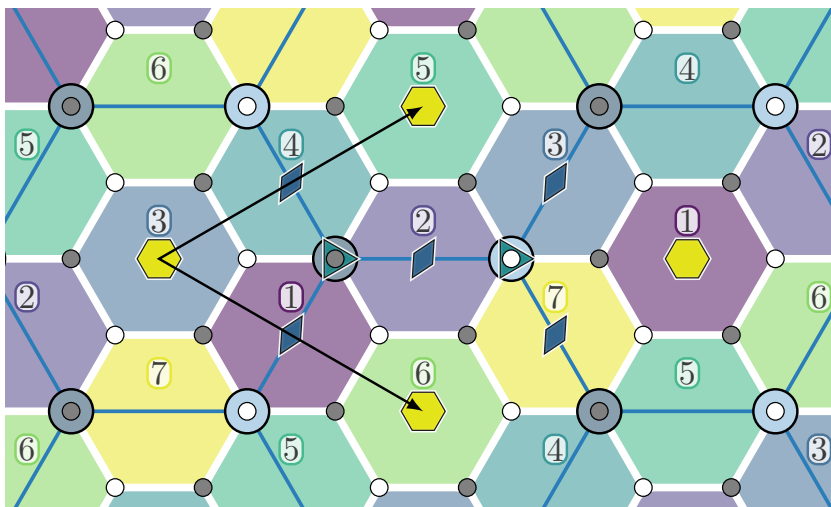


Figure 6.19.: The four color overlap splitting, the coarse graphene crystal $\mathbb{L}^t(2\mathcal{A})$ and all its elementary symmetries.

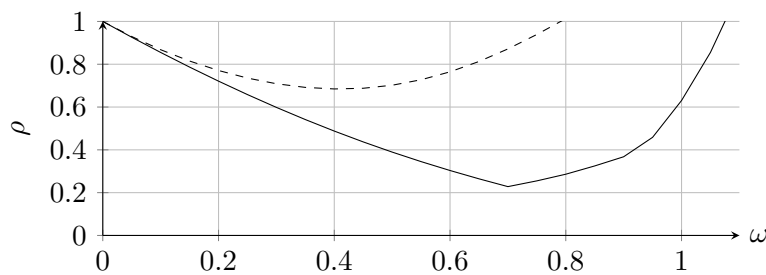


Figure 6.20.: Plot of the spectral radii of the two-grid error propagator KG using the seven color overlap smoother with interpolation weights $(\omega_\ell, \tilde{\omega}_\ell, \omega_s) = (.5, 0, -.5)$ in dependence of the relaxation parameter ω . — ordering $\mathfrak{A} = (1, 2, 4, 6, 3, 7, 5)$; ---- ordering $\mathfrak{B} = (1, 2, 3, 4, 5, 6, 7)$.

Rectangular Graphene sheets

For numerical simulations we implemented the presented multigrid method for finite rectangular subsection of the graphene crystal.

Definition 6.6. Define a rectangular graphene patch $\mathbb{G}_{n,m,\ell}$ with $n, m, \ell \in \mathbb{N}$ by

$$\mathbb{G}_{n,m,\ell} := \mathbb{L}^s(\mathcal{A}) \cap \mathcal{P}(\mathcal{A} \cdot \mathcal{C}),$$

with

$$\mathcal{C} = \begin{bmatrix} n & \ell \frac{2m+n}{N_r} \\ m & -\ell \frac{2n+m}{N_r} \end{bmatrix}$$

where $N_r = \text{gcd}(2n+m, 2m+n)$. One easily checks that $(\mathcal{A}c_1)$ is orthogonal to $(\mathcal{A}c_2)$. Its chiral angle is given by $\theta = -\frac{\pi}{6} + \tan^{-1}\left(\frac{\sqrt{3}m}{m+2n}\right)$; cf. Figure 6.21a.

Remark 6.7. Due to symmetries of the crystal, all possible rectangular patches $\mathbb{G}_{n,m,\ell}$ are defined by

$$n, m, \ell \in \mathbb{N} \setminus 0 \quad \text{and} \quad n \geq m,$$

which restricts the chiral angle to $0^\circ \leq \theta < 30^\circ$.

- For $n = m$ ($\theta = 0^\circ$), we obtain an armchair boundary in the direction of $(\mathcal{A}c_1)$ and a zigzag boundary in the direction of $(\mathcal{A}c_2)$, as illustrated by the horizontal and vertical boundary in Figure 6.21a.
- The number of atoms in $\mathbb{G}_{n,m,\ell}$ is

$$|\mathbb{G}_{n,m,\ell}| = 2 \frac{|(\mathcal{A}c_1) \times (\mathcal{A}c_2)|}{|a_1 \times a_2|} = \frac{4\ell(n^2 + nm + m^2)}{N_r},$$

where \times denotes the vector product operator.

Typical boundary conditions for rectangular graphene sheets $\mathbb{G}_{n,m,\ell}$ are *open* and *periodic*. Open boundary conditions are realized by simply omitting the terms of the tight-binding Hamiltonian which would belong to off-lattice points. Carbon nanotubes correspond to periodic boundary conditions in one direction and are obtained from $\mathbb{G}_{n,m,\ell}$ by rolling it up along $(\mathcal{A}c_1)$ such that $x \in \mathbb{G}_{n,m,\ell}$ is identified with $x + (\mathcal{A}c_1)$; cf. Figure 6.21b. Periodic boundary conditions along both basis vectors correspond to the graphene torus

$$T_{\mathcal{A},\mathcal{A} \cdot \mathcal{C}}^s = \mathbb{L}^s(\mathcal{A}) / \mathbb{L}(\mathcal{A} \cdot \mathcal{C}).$$

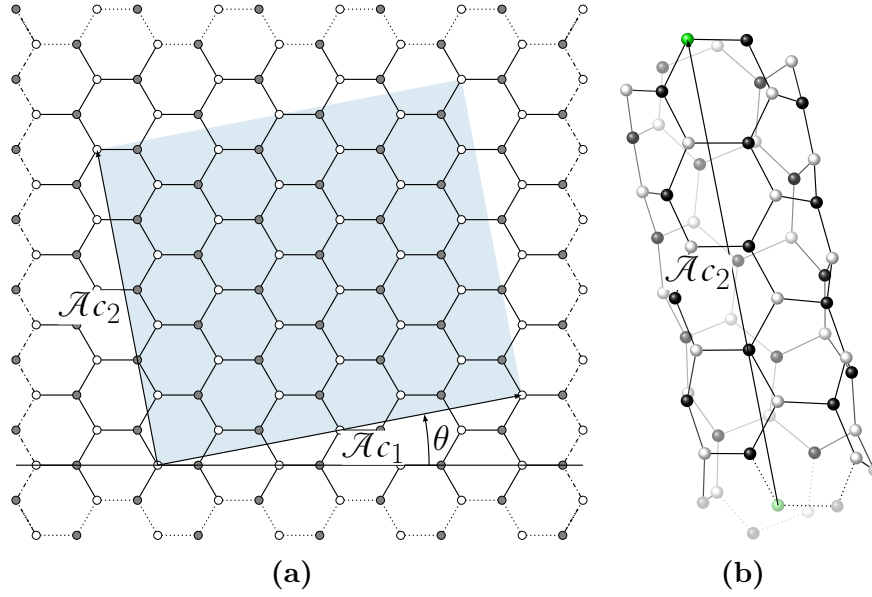


Figure 6.21.: (a) An example of a finite graphene sample $G_{4,2,1}$, - - - - zigzag boundary; ····· armchair boundary. (b) The corresponding nanotube when periodic boundary conditions in the direction of \mathcal{A}_{c1} are applied.

Numerical results

In the following we used a single iteration of Kaczmarz smoothing in our multigrid method in combination with the interpolation weight combination $(\omega_\ell, \tilde{\omega}_\ell, \omega_s) = (.5, 0, -.5)$.

In accordance to Figure 6.21a, we denote the boundary at \mathcal{A}_{c1} by x_1 and the one at \mathcal{A}_{c2} by x_2 . Further o refers to an open and p to a periodic boundary condition. Thus, in short-hand notation we describe the different cases by the tuple (x_1, x_2) , where $x_1, x_2 \in \{p, o\}$.

In the first set of tests, we consider a graphene sample with chiral angle $\theta = 0^\circ$, which results in a pure armchair boundary at \mathcal{A}_{c1} and a pure zigzag boundary at \mathcal{A}_{c2} . In terms of the multigrid construction, we simply remove any interpolation across an open boundary. That is, fine grid points near the open boundary interpolate from fewer than 3 coarse grid points, but use the same weights as interior points. As it can be seen in Figure 6.22, the convergence of the multigrid method remains unchanged in the case (o, p) , i.e., when using open boundary conditions at the armchair boundary. In contrast convergence stagnates in the cases (p, o) and (o, o) .

As it has been observed experimentally and shown analytically in [14, 49], the presence of open boundary conditions along a zigzag edge, as it is the case in (p, o) and (o, o) , leads to *edge states* Ψ_{ES} . These are eigenmodes which are damped exponentially towards the inner sites perpendicular to the zigzag edge.

The number of edge states scales linearly with the length of the zigzag edge $\|c_2\|_2$.

In our experiments, we found that an error composed of edge states can neither be resolved efficiently by further relaxation at the boundary nor by different choices of the coarse grid correction. Thus, we tried to fix the method in the following way. In order to prevent the presence of edge states on the coarse grid, we interpolate periodically across the open zigzag boundary, despite the open boundary condition, such that the interpolation in the cases (x_1, o) is now identical to the interpolation in the cases (x_1, p) . With that choice, the coarse grid operator $A_c = P^T A P$ is periodic at the zigzag boundary and it does not contain any edge states. As can be seen in the left plot of Figure 6.23, this approach does improve convergence in the (p, o) case, but leads to stagnation at the level of the largest eigenvalue corresponding to an edge state. Thus, we additionally apply deflation on the finest level using the analytical description of the edge states Ψ_{ES} given in [49]. That means that we remove from the current iterate the part in the direction of the edge states via

$$x \leftarrow x - \frac{\langle \Psi_{\text{ES}}, x \rangle_2}{\langle \Psi_{\text{ES}}, \Psi_{\text{ES}} \rangle_2} \Psi_{\text{ES}}.$$

The resulting method shows a convergence similar to the theoretical prediction, as illustrated in the right plot of Figure 6.23. The case (o, o) is very similar to the case (p, o) and the multigrid method can be fixed in a similar way.

Rotated graphene samples with chiral angle $0^\circ < \theta < 30^\circ$ have boundaries with a mixture of armchair and zigzag sites. According to [28], already a very small number of zigzag sites lead to edge states. In Figure 6.24 we apply the above construction of periodic interpolation, despite open boundary conditions, combined with deflation to rotated graphene samples. The results are similar to the $\theta = 0^\circ$ case and it stands to reason that a convergence rate close to the theoretical bound can be achieved with further adjustments at the boundary. However, to our knowledge, no analytical description of the edge states in the general case $G_{n,m,\ell}$ exists so that they have to be calculated numerically beforehand in order to use them in the deflation procedure.

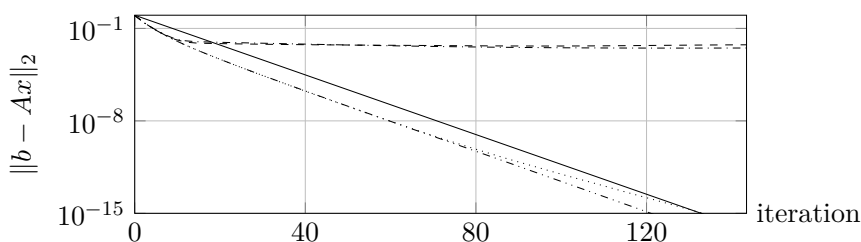


Figure 6.22.: Convergence of the multigrid method (5 level V -cycle) on $\mathbb{G}_{64,64,64}$ using different combinations of boundary conditions. (— theor. bound, ---- (o,o) , (o,p) , -.-.- (p,o) and - - - - (p,p))

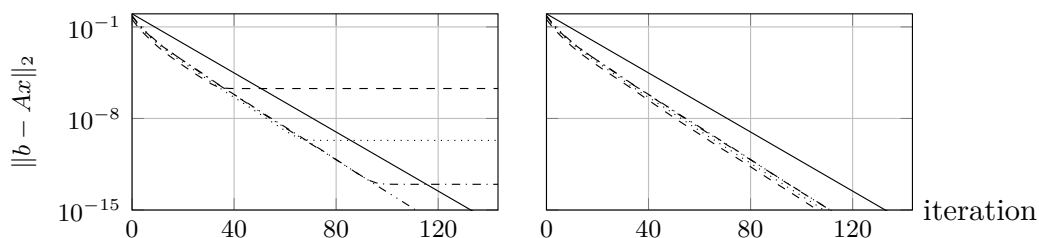


Figure 6.23.: Convergence of the multigrid method (5 level V -cycle) on different graphene patches $\mathbb{G}_{n,n,16}$ using (p,o) boundary conditions. *Left:* periodic interpolation across the open boundary; *right:* periodic interpolation and deflation. (— theor. bound, ---- $n = 16$, $n = 32$, -.-.- $n = 48$ and - - - - $n = 64$)

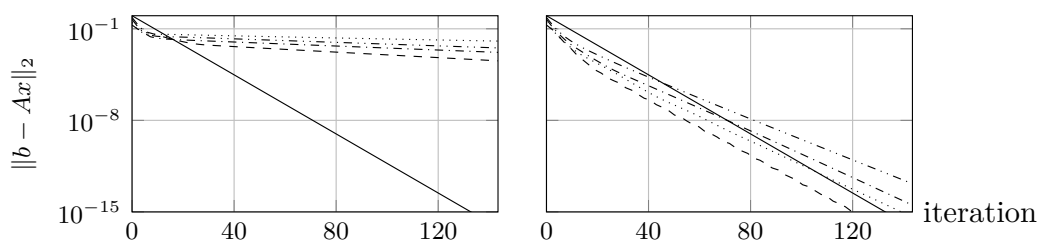


Figure 6.24.: Convergence of the two-grid method on rotated graphene patches $\mathbb{G}_{n,n-1,2}$ using (o,p) boundary conditions. *Left:* periodic interpolation across the open boundary; *right:* periodic interpolation and deflation. (— theor. bound, ---- $n = 4$, $n = 6$, -.-.- $n = 10$ and - - - - $n = 14$)

Conclusion

In this thesis we studied translationally invariant operators on crystals using techniques from integer linear algebra and crystallography. Upon these results we showed connections to iterative splitting methods using multicolor (or domain decomposition type) block Jacobi and Gauss-Seidel type methods, as well as geometric multigrid methods. The outcome of the theoretical study are several algorithms which make up a practical framework to analyze multigrid methods with minimal effort, i.e., the description of the occurring operators. Furthermore, we have shown how a general smoothing analysis can be carried out within this framework. A Python3 implementation of this framework is publicly available on GitLab [24].

We applied the framework to several smoother and multigrid methods for the discretized Laplacian operator for demonstrative purposes and to validate the framework. Even though this framework and the theory does not necessarily enlarge the set of methods that are analyzable by LFA, it enables the reliable, quick and easy-to-use analysis of complex methods on complicated structures.

The automation presented in this paper does have some limitation. Each individual operator in the analysis is only allowed to change each value of the value distribution at most once. This limitation solely restricts the class of smoothers that can be analyzed with this approach. Any sequential, i.e., lexicographic, smoother with overlapping update regions changes values in the overlap multiple times in one application. This cannot be easily translated to a corresponding local multiplication operator, but it can be dealt with in frequency space (cf. [26, 27, 43]). This particular treatment of sequential overlap is momentarily not covered in our framework. Note, that the mere presence of overlap is not the problem here. By introducing a coloring, such that the complete sweep can be split into a sequence of updates where each one of them only changes values at most once, automated LFA can be applied (cf. Section 5.2). Due to the fact that a coloring in overlapping approaches

also favors parallelism over their sequential counterparts, this limitation is relatively minor when targeting actual applications.

We furthermore have shown how to construct a scalable multigrid method with optimal complexity for the maximally indefinite system of equations arising in the tight-binding formulation of graphene. Besides the sequential Kaczmarz smoother, we developed a parallelizable block overlap method with superior performance. For this multigrid method we furthermore did a standalone analysis of the coarse grid correction which provides deeper insight into the behavior of the method. This led to the discovery of a two-grid method with an optimal *local* interpolation which is surprising as the optimal interpolation is usually a dense matrix (cf. [12]). In addition, we have shown that the ordering of a colored smoother can have a great influence on the convergence speed of a multigrid method. By exploiting the geometric and algebraic symmetries of a (colored) smoother, we illustrated how to reduce the factorial number of different orderings to be analyzed. Finally, we provide an ansatz for how the edge states induced by open boundary conditions at zigzag boundaries can be treated efficiently. By a combination of periodic interpolation over the open boundary, to prevent edge states on the coarser grids, and deflation of the edge states on the finest grid, the multigrid method converges according to the theoretically predicted rate.

Appendix A

Algorithms

A comprehensive list of the algorithms used within the automated local Fourier analysis.

Algorithm A.1: Spectra of a composition of multiplication operators.

Input: $L^{(j)} : T_{\mathcal{A}^{(j)}}^{\mathfrak{s}^{(j)}} \rightarrow T_{\mathcal{A}^{(j)}}^{\mathfrak{t}^{(j)}}$, $m_{L^{(j)}}^{(x)} \in \mathbb{C}^{|\mathfrak{t}^{(j)}| \times |\mathfrak{s}^{(j)}|}$, $x \in \mathbb{L}(\mathcal{A}^{(j)})$, composition function f and (optionally) a sublattice $\mathbb{L}(\mathcal{Z}) \subset \mathbb{L}(\mathcal{A})$.

Output: Spectrum $X := \{\text{spec}(f(L^{(1)}, \dots, L^{(K)})_k) : k \in \mathcal{P}(\mathcal{A}^{-T}) \cap \mathbb{L}(\mathcal{Z}^{-T})\}$ of the operator composition $f(L^{(1)}, \dots, L^{(K)}) : \mathcal{L}(T_{\mathcal{A}, \mathcal{Z}}^{\mathfrak{s}}) \rightarrow \mathcal{L}(T_{\mathcal{A}, \mathcal{Z}}^{\mathfrak{s}})$

- 1 **Function** $X = \text{ComputeSpectrum}(f, (L^{(1)}, \dots, L^{(K)}), \mathcal{Z})$
- 2 $(\hat{L}^{(1)}, \dots, \hat{L}^{(K)}) = \text{MakeOperatorsCompatible}(L^{(1)}, \dots, L^{(K)})$ ▷ See Algorithm A.5
- 3 **if** \mathcal{Z} is not None **then**
- 4 $\mathcal{Z} = 20\mathcal{A}$ ▷ Use an equidistant sampling of 20^n points.
- 5 Sample the dual lattice to obtain $k \in \mathcal{P}(\mathcal{A}^{-T}) \cap \mathbb{L}(\mathcal{Z}^{-T})$ ▷ See Remark 4.21
- 6 Compute the spectrum of the composition operator of symbols
 $f(L_k^{(1)}, \dots, L_k^{(K)})$ ▷ See Theorem 4.24

Algorithm A.2: Normalize a multiplication operator.

Input: $L : T_{\mathcal{A}}^{\mathfrak{s}} \rightarrow T_{\mathcal{A}}^{\mathfrak{t}}$, $m_L^{(x)} \in \mathbb{C}^{|\mathfrak{t}| \times |\mathfrak{s}|}$, $x \in \mathbb{L}(\mathcal{A})$.

Output: $G \cong L$ in normal form with $G : T_{\mathcal{A}}^{\mathfrak{u}} \rightarrow T_{\mathcal{A}}^{\mathfrak{v}}$, $m_G^{(x)} \in \mathbb{C}^{|\mathfrak{v}| \times |\mathfrak{u}|}$, $x \in \mathbb{L}(\mathcal{A})$.

- 1 **Function** $G = \text{Normalize}(L)$ ▷ See Definition 4.27
- 2 $\mathfrak{u}_j = \mathfrak{s}_j - \mathcal{A} \lfloor \mathcal{A}^{-1} \mathfrak{s}_j \rfloor$ for all $j = 1, \dots, |\mathfrak{s}|$ ▷ Shift into $\mathcal{P}(\mathcal{A}) = \mathcal{A}[0, 1)^n$
- 3 $\mathfrak{v}_j = \mathfrak{t}_j - \mathcal{A} \lfloor \mathcal{A}^{-1} \mathfrak{t}_j \rfloor$ for all $j = 1, \dots, |\mathfrak{t}|$ ▷ Shift into $\mathcal{P}(\mathcal{A}) = \mathcal{A}[0, 1)^n$
- 4 Sort \mathfrak{u} and \mathfrak{v} lexicographically
- 5 $G = \text{ChangeStructureElement}(L, \mathfrak{u}, \mathfrak{v})$ ▷ See Algorithm A.7

Algorithm A.3: Find all elements in the quotient space of two lattices.	
Input: Two n -dimensional lattices with $\mathbb{L}(\mathcal{C}), \mathbb{L}(\mathcal{A})$ with $\mathbb{L}(\mathcal{C}) \subset \mathbb{L}(\mathcal{A})$.	
Output: Structure element $\mathfrak{s} \cong T_{\mathcal{A}, \mathcal{C}} = \mathbb{L}(\mathcal{A}) / \mathbb{L}(\mathcal{C})$	
1	Function $\mathfrak{s} = \text{ElementsInQuotientSpace}(\mathcal{A}, \mathcal{C})$ ▷ See Theorem 3.16
2	$H =$ Hermite normal form of $\mathcal{A}^{-1}\mathcal{C}$ ▷ See Theorem 2.5
3	$m = \prod_{i=1}^n h_{i,i}$ ▷ Size of \mathfrak{s}
4	$\mathfrak{s}_i = 0$ for all $i = 0, \dots, m$ ▷ Initialize \mathfrak{s}
5	for $i = 1, 2, \dots, m$
6	$k = i - 1$
7	for $j = 1, 2, \dots, n$
8	$t = \text{mod}(k, h_{j,j})$ ▷ Shift in direction a_j
9	$k = \frac{k-t}{h_{j,j}}$
10	$\mathfrak{s}_i = \mathfrak{s}_i + ta_j$

Algorithm A.4: Rewrite a multiplication operator w.r.t. a coarser lattice.	
Input: $L : T_{\mathcal{A}}^{\mathfrak{s}} \rightarrow T_{\mathcal{A}}^{\mathfrak{t}}, m_L^{(x)} \in \mathbb{C}^{ \mathfrak{t} \times \mathfrak{s} }, x \in \mathbb{L}(\mathcal{A})$, and a sublattice $\mathbb{L}(\mathcal{C}) \supset \mathbb{L}(\mathcal{A})$	
Output: $G \cong L$ with $G : T_{\mathcal{C}}^{\mathfrak{u}} \rightarrow T_{\mathcal{C}}^{\mathfrak{v}}, m_G^{(x)} \in \mathbb{C}^{ \mathfrak{v} \times \mathfrak{u} }, x \in \mathbb{L}(\mathcal{C})$.	
1	Function $G = \text{LatticeCoarsening}(L, \mathcal{C})$ ▷ See Theorem 4.25
2	$\mathfrak{e} = \text{ElementsInQuotientSpace}(\mathcal{A}, \mathcal{C})$ ▷ See Algorithm A.3
3	$\mathfrak{u} = (\mathfrak{e}_1 + \mathfrak{s}, \dots, \mathfrak{e}_{ \mathfrak{e} } + \mathfrak{s}), \mathfrak{v} = (\mathfrak{e}_1 + \mathfrak{t}, \dots, \mathfrak{e}_{ \mathfrak{e} } + \mathfrak{t})$ ▷ Define structure elements
4	$(m_G^{(y)}) = 0 \in \mathbb{C}^{ \mathfrak{v} \times \mathfrak{u} }$ for all $y \in \mathbb{L}(\mathcal{C})$ ▷ Initialize new multipliers
5	for $m_L^{(y)} \neq 0$
6	for $(i, j) \in \{1, \dots, \mathfrak{e} \}^2$
7	$(m_G^{(\mathfrak{e}[\mathfrak{C}^{-1}(y + \mathfrak{e}_i - \mathfrak{e}_j)])})_{i,j} = m_L^{(y)}$ ▷ Define multipliers block-wise

Algorithm A.5: Rewriting multiplication operators w.r.t. a single lattice.	
Input: $L^{(j)} : T_{\mathcal{A}^{(j)}}^{\mathfrak{s}^{(j)}} \rightarrow T_{\mathcal{A}^{(j)}}^{\mathfrak{t}^{(j)}}, m_{L^{(j)}}^{(x)} \in \mathbb{C}^{ \mathfrak{t}^{(j)} \times \mathfrak{s}^{(j)} }, x \in \mathbb{L}(\mathcal{A}^{(j)})$	
Output: $\hat{L}^{(j)} \cong L^{(j)}$ in normal form, $\hat{L}^{(j)} : T_{\mathcal{A}}^{\mathfrak{u}^{(j)}} \rightarrow T_{\mathcal{A}}^{\mathfrak{v}^{(j)}}, m_{\hat{L}^{(j)}}^{(x)} \in \mathbb{C}^{ \mathfrak{v}^{(j)} \times \mathfrak{u}^{(j)} }, x \in \mathbb{L}(\mathcal{A})$.	
1	Function $(\hat{L}^{(1)}, \dots, \hat{L}^{(K)}) = \text{MakeOperatorsCompatible}(L^{(1)}, \dots, L^{(K)})$
2	$\mathcal{A} = \mathcal{A}^{(1)}$
3	for $j = 2, \dots, K$
4	$\mathcal{A} = \text{LeastCommonMultiple}(\mathcal{A}, \mathcal{A}^{(j)})$ ▷ See Algorithm A.6
5	for $j = 1, \dots, K$
6	$\hat{L}^{(j)} = \text{LatticeCoarsening}(L^{(j)}, \mathcal{A})$ ▷ See Algorithm A.4
7	$\hat{L}^{(j)} = \text{Normalize}(\hat{L}^{(j)})$ ▷ See Algorithm A.2

Algorithm A.6: Find a least common multiple of two lattices.

Input: Lattice basis $\mathcal{B}, \mathcal{A} \in \mathbb{R}^{n \times n}$

Output: Lattice basis \mathcal{C} , s.t. $\mathbb{L}(\mathcal{C}) \subset \mathbb{L}(\mathcal{A})$ and $\mathbb{L}(\mathcal{C}) \subset \mathbb{L}(\mathcal{B})$

- 1 **Function** $\mathcal{C} = \text{LeastCommonMultiple}(\mathcal{A}, \mathcal{B})$ ▷ See Theorem 3.6
- 2 Find an integer r , s.t. $M = r\mathcal{A}^{-1}\mathcal{B}$ is integral
- 3 Compute Smith normal form $S = V^{-1}MT^{-1}$ of M ▷ See Theorem 2.9
- 4 $(N_{\mathcal{B}})_{i,i} = r \cdot \gcd(r, s_{i,i})^{-1}$, $\mathcal{C} = \mathcal{B}T^{-1}N_{\mathcal{B}}$ ▷ Define the lattice basis

Algorithm A.7: Changing the structure elements.

Input: Structure elements $\mathbf{u} \cong \mathfrak{s}$, $\mathbf{v} \cong \mathfrak{t}$ w.r.t. $\mathbb{L}(\mathcal{A})$ and

$$L : T_{\mathcal{A}}^{\mathfrak{s}} \rightarrow T_{\mathcal{A}}^{\mathfrak{t}}, m_L^{(x)} \in \mathbb{C}^{|\mathfrak{t}| \times |\mathfrak{s}|}, x \in \mathbb{L}(\mathcal{A}).$$

Output: $\hat{L} \cong L$ with $\hat{L} : T_{\mathcal{A}}^{\mathfrak{u}} \rightarrow T_{\mathcal{A}}^{\mathfrak{v}}, m_{\hat{L}}^{(x)} \in \mathbb{C}^{|\mathfrak{v}| \times |\mathfrak{u}|}, x \in \mathbb{L}(\mathcal{A})$.

- 1 **Function** $\hat{L} = \text{ChangeStructureElement}(L, \mathbf{u}, \mathbf{v})$ ▷ See Theorems 4.28 and 4.29
- 2 $m_{\pi} = 0 \in \{0, 1\}^{|\mathfrak{s}| \times |\mathfrak{s}|}$, $m_{\sigma} = 0 \in \{0, 1\}^{|\mathfrak{t}| \times |\mathfrak{t}|}$ ▷ Initialize permutation matrices
- 3 **for** $(i, j) \in \{1, \dots, |\mathfrak{s}|\}^2$ ▷ Compute changes in \mathfrak{d}
- 4 **if** $\mathcal{A}^{-1}(\mathfrak{s}_i - \mathbf{u}_j)$ is integral **then**
- 5 $\mathfrak{c}_i = \mathfrak{s}_i - \mathbf{u}_j$ ▷ Save shift
- 6 $(m_{\pi})_{j,i} = 1$ ▷ Save permutation
- 7 **for** $(i, j) \in \{1, \dots, |\mathfrak{t}|\}^2$ ▷ Compute changes in \mathfrak{c}
- 8 **if** $\mathcal{A}^{-1}(\mathfrak{t}_i - \mathbf{v}_j)$ is integral **then**
- 9 $\mathfrak{f}_i = \mathfrak{t}_i - \mathbf{v}_j$ ▷ Save shift
- 10 $(m_{\sigma})_{j,i} = 1$ ▷ Save permutation
- 11 $(m_{\hat{L}}^{(y)}) = 0 \in \mathbb{C}^{|\mathfrak{t}| \times |\mathfrak{s}|}$ for all $y \in \mathbb{L}(\mathcal{A})$ ▷ Initialize new multipliers
- 12 **for** $m_L^{(y)} \neq 0$
- 13 **for** $(i, j) \in \{1, \dots, |\mathfrak{t}|\} \times \{1, \dots, |\mathfrak{s}|\}$
- 14 $(m_{\hat{L}}^{(y - \mathfrak{c}_j + \mathfrak{f}_i)})_{i,j} = (m_L^{(y)})_{i,j}$ ▷ Incorporate shifts \mathfrak{c} and \mathfrak{f} , see Theorem 4.28
- 15 $m_{\hat{L}}^{(y)} = m_{\sigma} \cdot m_L^{(y)} \cdot m_{\pi}^{-1}$ for all $y \in \mathbb{L}(\mathcal{A})$ ▷ Incorporate permutations, see Theorem 4.29

Nomenclature

- X^* The adjoint operator of X .
- $\text{cof}(A)$ The cofactor matrix of A .
- X^\dagger The Moore-Penrose pseudoinverse of X .
- $\det(A)$ The determinant of A .
- $e_{\ell,k}$ A wavefunction $(0, \dots, 0, e^{2\pi i \langle k, \cdot + \mathfrak{s}_\ell \rangle / 2}, 0, \dots, 0)$ on the function space $\mathcal{L}(T_{\mathcal{A}, \mathfrak{z}}^{\mathfrak{s}})$ of a crystal torus (see Theorem 4.4).
- η The natural isomorphism $\eta : \mathcal{L}(T_{\mathcal{A}, \mathfrak{z}}) \rightarrow \mathcal{L}(T_{\mathcal{C}, \mathfrak{z}}^{T_{\mathcal{A}, \mathfrak{z}}}), \mathbb{L}(\mathcal{Z}) \subset \mathbb{L}(\mathcal{C}) \subset \mathbb{L}(\mathcal{A})$ (see Definition 4.6).
- $\lfloor x \rfloor$ The floor function applied to x .
- $\text{gcd}(a, b)$ The greatest common divisor of a and b .
- X_k Either the symbol of a multiplication operator X w.r.t. the wavevector k (see Definition 4.19) or the space of Harmonics if $X = H$ (see Definition 4.5).
- $\mathbb{L}(\mathcal{A})$ The n -dimensional Bravais lattice $\mathcal{A}\mathbb{Z}^n$, $\mathcal{A} \in \mathbb{R}^{n \times n}$ (see Definition 3.1).
- $\mathbb{L}^{\mathfrak{s}}(\mathcal{A})$ The crystal $\{(x + \mathfrak{s}_1, x + \mathfrak{s}_2, \dots, x + \mathfrak{s}_m) : x \in \mathbb{L}(\mathcal{A})\}$, where $\mathfrak{s} \in \Xi(\mathcal{A})^m$ (see Definition 3.11).
- $\mathbb{L}(\mathcal{A})^*$ The dual lattice of $\mathbb{L}(\mathcal{A})$ defined by $\mathbb{L}(\mathcal{A}^{-T})$ (see Definition 3.19).
- $\text{lcm}(a, b)$ The least common multiple of two integers a and b .
- $\text{lcm}(\mathbb{L}(\mathcal{A}), \mathbb{L}(\mathcal{B}))$ The sublattice $\mathbb{L}(\mathcal{C}) \subset \mathbb{L}(\mathcal{A})$, $\mathbb{L}(\mathcal{C}) \subset \mathbb{L}(\mathcal{B})$, with $|\det(\mathcal{C})|$ as small as possible (see Theorem 3.6).

- $\mathcal{L}(X, Y)$ The set of functions $\{f : X \rightarrow Y\}$ (see Definition 4.1).
- $\mathcal{L}(X)$ The set of functions $\{f : X \rightarrow \mathbb{C}\}$ (see Definition 4.1).
- $\mathcal{L}(T_{\mathcal{A}, \mathcal{Z}}^s)$ The set of functions $\mathcal{L}(T_{\mathcal{A}, \mathcal{Z}}, \mathbb{C}^m)$ (see Definition 4.1).
- $a \mid b$ a divides b without remainder.
- $m_L^{(y)}$ A multiplier of a multiplication operator $L : \mathcal{L}(T_{\mathcal{A}}^s) \rightarrow \mathcal{L}(T_{\mathcal{A}}^t)$ such that $Lf(x) = \sum_y m_L^{(y)} f(x + y)$ (see Definition 4.17).
- $\mathcal{P}(\mathcal{A})$ The parallelotope $\mathcal{A}[0, 1)^n$ (see Definition 3.8).
- $\rho(X)$ The spectral radius of X .
- $\text{spec}(X)$ The set of all eigenvalues of X .
- Sym_N The symmetric group of degree N (see Section 5.4).
- $T_{\mathcal{A}, \mathcal{C}}$ The lattice torus or quotient space $\mathbb{L}(\mathcal{A}) / \mathbb{L}(\mathcal{C})$ (see Definition 3.13).
- $T_{\mathcal{A}, \mathcal{C}}^s$ The crystal torus or quotient space $\mathbb{L}^s(\mathcal{A}) / \mathbb{L}(\mathcal{C})$ (see Definition 3.13).
- $T_{\mathcal{A}, \mathcal{Z}}^*$ The lattice torus defined by the dual lattices $\mathbb{L}(\mathcal{Z})^* / \mathbb{L}(\mathcal{A})^*$ (see Remark 3.21).
- $T_{\mathcal{A}}$ An arbitrary large but finite lattice torus $T_{\mathcal{A}, \mathcal{Z}}, \mathbb{L}(\mathcal{Z}) \subset \mathbb{L}(\mathcal{A})$ (see Chapter 4).
- $T_{\mathcal{A}}^s$ An arbitrary large but finite crystal torus $T_{\mathcal{A}, \mathcal{Z}}^s, \mathbb{L}(\mathcal{Z}) \subset \mathbb{L}(\mathcal{A})$ (see Chapter 4).
- X^T The transpose of X .
- $\Xi(\mathcal{A})$ A primitive cell of $\mathbb{L}(\mathcal{A})$ (see Definition 3.8).

Bibliography

- [1] M. Armstrong, *Groups and Symmetry*, Springer, New York, NY, USA, 1988.
- [2] N. Ashcroft and N. Mermin, *Solid State Physics*, Saunders College, Philadelphia, 1976.
- [3] R. Babich, J. Brannick, R. C. Brower, M. A. Clark, T. A. Manteuffel, S. F. McCormick, J. C. Osborn, and C. Rebbi, *Adaptive multigrid algorithm for the lattice wilson-dirac operator*, Phys. Rev. Lett. 105 (20 Nov. 2010), p. 201602.
- [4] R. Bank, *A comparison of two multilevel iterative methods for nonsymmetric and indefinite elliptic finite element equations*, SIAM J. Numer. Anal. 18.4 (1981), pp. 724–743.
- [5] A. Bayliss, C. Goldstein, and E. Turkel, *The numerical solution of the helmholtz equation for wave propagation problems in underwater acoustics*, Comput. Math. Appl. 11.7 (1985), Special Issue Computational Ocean Acoustics, pp. 655–665.
- [6] M. Bolten and H. Rittich, *Fourier analysis of periodic stencils in multigrid methods*, SIAM J. Sci. Comput. 40.3 (2018), A1642–A1668.
- [7] T. Boonen, J. Van lent, and S. Vandewalle, *Local fourier analysis of multigrid for the curl-curl equation*, SIAM J. Sci. Comput. 30.4 (2008), pp. 1730–1755.
- [8] J. Bramble, J. Pasciak, and J. Xu, *The analysis of multigrid algorithms for nonsymmetric and indefinite elliptic problems*, Math. Comp. 51.184 (1988), pp. 389–414.
- [9] J. H. Bramble, D. Y. Kwak, and J. E. Pasciak, *Uniform convergence of multigrid V-cycle iterations for indefinite and nonsymmetric problems*, SIAM J. Numer. Anal. 31.6 (1994), pp. 1746–1763.
- [10] A. Brandt, *Multi-level adaptive solutions to boundary-value problems*, Math. Comp. 31.138 (1977), pp. 333–390.

- [11] A. Brandt, *Rigorous quantitative analysis of multigrid, I. constant coefficients two-level cycle with L_2 -norm*, SIAM J. Numer. Anal. 31.6 (1994), pp. 1695–1730.
- [12] J. Brannick, F. Cao, K. Kahl, R. Falgout, and X. Hu, *Optimal interpolation and compatible relaxation in classical algebraic multigrid*, SIAM J. Sci. Comput. 40.3 (2018), A1473–A1493.
- [13] P. V. Buividovich and M. I. Polikarpov, *Monte-Carlo study of the electron transport properties of monolayer graphene within the tight-binding model*, Phys. Rev. B 86 (Feb. 2012), p. 245117.
- [14] A. H. Castro Neto, F. Guinea, N. M. R. Peres, K. S. Novoselov, and A. K. Geim, *The electronic properties of graphene*, Rev. Mod. Phys. 81 (Jan. 2009), pp. 109–162.
- [15] A. Frommer, K. Kahl, S. Krieg, B. Leder, and M. Rottmann, *Adaptive aggregation-based domain decomposition multigrid for the lattice wilson-dirac operator*, SIAM J. Sci. Comput. 36.4 (2014), A1581–A1608.
- [16] *GAP – Groups, Algorithms, and Programming, Version 4.10.1*, The GAP Group, 2019.
- [17] F. Gaspar, J. Gracia, and F. Lisbona, *Fourier analysis for multigrid methods on triangular grids*, SIAM J. Sci. Comput. 31.3 (2009), pp. 2081–2102.
- [18] J. Grabmeier, E. Kaltofen, and V. Weispfenning, eds., *Computer Algebra Handbook*, Springer Berlin Heidelberg, 2003.
- [19] R. Gross and A. Marx, *Festkörperphysik*, Oldenbourg Wissenschaftsverlag, 2012.
- [20] A. Hirsch, *The era of carbon allotropes*, Nat. Mater. 9.11 (2010), pp. 868–871.
- [21] T. Huckle, *Compact fourier analysis for designing multigrid methods*, SIAM J. Sci. Comput. 31.1 (2008), pp. 644–666.
- [22] S. Kaczmarz, *Angenäherte Auflösung von Systemen linearer Gleichungen*, Bull. Pol. Acad. Sci. Math. 35 (1937), pp. 355–357.
- [23] K. Kahl and N. Kintscher, *Geometric multigrid for the tight-binding hamiltonian of graphene*, SIAM J. Numer. Anal. 56.1 (2018), pp. 499–519.
- [24] K. Kahl and N. Kintscher, *aLFA: automated local Fourier analysis*, <https://gitlab.com/NilsKintscher/alfa>, 2019.
- [25] M. Lüscher, *Local coherence and deflation of the low quark modes in lattice QCD*, JHEP 07(2007)081 (2007).

-
- [26] S. P. MacLachlan and C. W. Oosterlee, *Local fourier analysis for multigrid with overlapping smoothers applied to systems of pdes*, Numer. Linear Algebra Appl. 18.4 (2011), pp. 751–774.
- [27] J. Molenaar, *A two-grid analysis of the combination of mixed finite elements and Vanka-type relaxation*, in: *Multigrid Methods III*, ed. by W. Hackbusch and U. Trottenberg, Birkhäuser Basel, Basel, 1991, pp. 313–323.
- [28] K. Nakada, M. Fujita, G. Dresselhaus, and M. S. Dresselhaus, *Edge state in graphene ribbons: Nanometer size effect and edge shape dependence*, Phys. Rev. B 54 (24 Dec. 1996), pp. 17954–17961.
- [29] J. Neubüser, H. Wondratschek, and R. Bülow, *On crystallography in higher dimensions. I. General definitions*, Acta Cryst. A 27.6 (Nov. 1971), pp. 517–520.
- [30] M. Newman, *Integral Matrices*, Academic Press, 1972.
- [31] J. C. Osborn, R. Babich, J. Brannick, R. C. Brower, M. A. Clark, S. D. Cohen, and C. Rebbi, *Multigrid solver for clover fermions*, PoS LATTICE2010, 037 (2010).
- [32] *PARI/GP version 2.9.5*, available from <http://pari.math.u-bordeaux.fr/>, The PARI Group, Univ. Bordeaux, 2018.
- [33] R. Penrose, *A generalized inverse for matrices*, Mathematical Proceedings of the Cambridge Philosophical Society 51.3 (1955), pp. 406–413.
- [34] S. Reich, J. Maultzsch, C. Thomsen, and P. Ordejón, *Tight-binding description of graphene*, Phys. Rev. B 66.3 (2002), p. 035412.
- [35] H. Rittich, *Extending and Automating Fourier Analysis for Multigrid Methods*, PhD thesis, University of Wuppertal, June 2017.
- [36] H. Rittich, *LFA Lab*, <https://github.com/hrittich/lfa-lab>, 2018.
- [37] C. Rodrigo, P. Salinas, F. Gaspar, and F. Lisbona, *Local fourier analysis for cell-centered multigrid methods on triangular grids*, J. Comput. Appl. Math. 259 (Mar. 2014), pp. 35–47.
- [38] C. Rodrigo, F. J. Gaspar, and L. T. Zikatanov, *On the validity of the local Fourier analysis*, J. Comput. Math. 37.3 (2019), pp. 340–348.
- [39] C. Rodrigo, F. Sanz, F. J. Gaspar, and F. J. Lisbona, *Local fourier analysis for edge-based discretizations on triangular grids*, Numer. Math. Theory Me. 8.1 (2015), pp. 78–96.
- [40] Y. Saad, *Iterative methods for sparse linear systems* (2003).
- [41] A. Schrijver, *Theory of Linear and Integer Programming*, John Wiley & Sons, Inc., New York, NY, USA, 1986.
- [42] Y. Shapira, *Multigrid techniques for highly indefinite equations*, in: *8th Copper Mountain Conference on Multigrid Methods*, 1995, pp. 689–705.

- [43] S. Sivaloganathan, *The use of local mode analysis in the design and comparison of multigrid methods*, Comput. Phys. Commun. 65.1 (1991), pp. 246–252.
- [44] E. Stein and G. Weiss, *Introduction to Fourier Analysis on Euclidean Spaces*, Princeton University Press, Princeton, N.J., 1971.
- [45] R. Stevenson, *On the Validity of Local Mode Analysis of Multi-Grid Methods*, PhD thesis, Utrecht University, Dec. 1990.
- [46] L. N. Trefethen and D. Bau, *Numerical Linear Algebra*, SIAM, 1997.
- [47] U. Trottenberg, C. W. Oosterlee, and A. Schüller, *Multigrid*, vol. 33, Texts in Applied Mathematics. Bd. With contributions by A. Brandt, P. Oswald and K. Stüben, Academic Press, San Diego, 2001.
- [48] M. Ulybyshev, P. Buividovich, M. Katsnelson, and M. Polikarpov, *Monte Carlo study of the semimetal-insulator phase transition in monolayer graphene with a realistic interelectron interaction potential*, Phys. Rev. Lett. 111.5 (2013), p. 056801.
- [49] K. Wakabayashi, K.-i. Sasaki, T. Nakanishi, and T. Enoki, *Electronic states of graphene nanoribbons and analytical solutions*, Sci. Technol. Adv. Mater. 11.5 (2010), p. 054504.
- [50] R. Wienands and C. Oosterlee, *On three-grid fourier analysis for multigrid*, SIAM J. Sci. Comput. 23.2 (2001), pp. 651–671.
- [51] R. Wienands and W. Joppich, *Practical Fourier Analysis for Multigrid Methods*, CRC press, 2004.
- [52] H. Yserentant, *On the multilevel splitting of finite element spaces for indefinite elliptic boundary value problems*, SIAM J. Numer. Anal. 23.3 (1986), pp. 581–595.
- [53] G. Zhou and S. Fulton, *Fourier analysis of multigrid methods on hexagonal grids*, SIAM J. Sci. Comput. 31.2 (2009), pp. 1518–1538.